

Train Tribometer Design and Feasibility

Wheel-rail adhesion measurement for train operations and predictive
maintenance

Sebastian Jonathan Schipper

Graduation Committee:

EngD Programme Director

Dr. J.T. Voordijk

University of Twente

Supervisors

Prof.dr.ir. M.B. de Rooij

University of Twente

Dr.ir. E.R.M. Gelinck

ProRail

External member

Prof.dr.ir. R.P.B.J. Dollevoet

Delft University of Technology / ProRail

This research was financially supported by ProRail and carried out at the Surface Technology and Tribology (STT) group, Faculty of Engineering Technology, University of Twente, the Netherlands.

Colophon

ISBN: 978-94-6421-834-3

Printed by: Ipskamp Printing, Enschede

Copyright ©2022, Sebastian Jonathan Schipper, the Netherlands.

Train Tribometer Design and Feasibility

EngD Thesis

To obtain the degree of

Engineering Doctorate (EngD)

At the University of Twente,

On the authority of the rector magnificus,

Prof. dr. ir. A. Veldkamp,

On account of the decision of the graduation committee,

To be defended

On Friday 16 September 2022 at 13:00 hours

By

Sebastian Jonathan Schipper

Born on the 22nd of June 1996

in Enschede, the Netherlands

This EngD Thesis has been approved by:

Prof.dr.ir. M.B. de Rooij

Summary

Friction, often called adhesion in the railway sector, in the wheel-rail interface is a complex phenomenon and remains largely unknown within the railroad industry. The desire to improve the efficiency (transport capacity, punctuality and so on) of the transportation by train calls for the development of railway systems such as European Rail Traffic Management System (ERTMS) and Automatic Train Operations (ATO).

Knowing the actual friction (live, on-board of a train), i.e. the amount of grip a train has, is important for such railway systems, since it determines significantly the braking distance. Currently, friction, or adhesion, is not known, hence one has to assume extremely low friction values, resulting in long braking distances to be maintained, to ensure safety (no collision of trains). The use of the adhesion sensor is not limited to knowing the braking distance only, but is crucial as well for applying friction modifiers such as Sandite on the right track and also updating travel times of trains to adjust the time tables (punctuality). Regarding maintenance, too low friction leads to wheel locking during braking, resulting in flat spots on the wheel tread and the involved downtime to restore it. Too high friction initiates rolling contact fatigue (RCF), which initiates and deteriorates cracks within the rail. Hence, the need for a live, on-board adhesion sensor is high.

For a rolling contact, such as the wheel-rail contact, traction curves are commonly used to describe the coefficient of friction based on the amount of slip. Preceding research by ProRail in collaboration with the University of Twente has led to a concept design of the adhesion sensor, the train tribometer (TTBM). The idea is to integrate such a sensor within the non-driven undercarriage or bogie (consisting of two wheelsets) of a train. When the train is driving, one wheelset (the braked-wheelset) will be briefly braked. By measuring the brake force and the wheel circumferential velocities of the braked and non-braked wheelset, one can determine the friction force and slip, respectively, which combined lead to the measured traction curve. This manoeuvre will be referred to as the TTBM brake.

Due to the complexity of the wheel-rail interface and the involved traction curves, a feasibility study has been carried out to proceed to the next design step (i.e. lab/field tests). Simulations of a train using the TTBM within multi-body dynamics software (VI-Rail) have been carried out under various track and operating conditions. This TTBM concept is promising, in many cases it is possible to use the TTBM brake to estimate traction curves.

The TTBM brake has a few design parameters. The measurement range of the traction curve, spanned by the maximum coefficient of friction and slip limit (μ_{\max} , S_{\lim}) one wants to measure. The second is the duration of the TTBM brake to carry out the measurement, T . The design parameters have certain trade-offs. The higher μ_{\max} is set, the higher the applied brake forces are. For T , decreasing it lower than one second will significantly increase the dynamic effects of the wheelset, while increasing the duration of the TTBM brake will lead to a larger track distance covered when a TTBM brake test is carried out.

For the simulations in this report, the TTBM brake design parameters are set to measure peak values of traction curves and beyond, up to a certain slip limit. Alongside this brake strategy (or measurement strategy), another brake strategy is proposed as well, which is to measure the creep coefficient of the traction curve instead and extrapolate it to estimate the peak value of the traction curve. Lower brake forces are needed, leading to lower induced jerk motion by the TTBM brake, which otherwise might lead to passenger discomfort.

Within the VI-Rail simulations for the given train model on straight tracks with track irregularities, an absolute slip error of roughly 0.6% has been found. It is caused by a combination of track irregularities and the hunting motion, leading to a change in rolling radii, which interfere with the slip measurement. Regarding the coefficient of friction, changes in normal forces occur as well by various causes that compound to the total relative change in normal force of roughly 15-20%. As for the friction force, the wheel-rail conditions are not constant, friction conditions within the left and right wheel-rail contact of a wheelset (which are often assumed as equal) may vary and flange contact may occur, which interfere with the interpretation of the TTBM data.

These traction curve measurement errors are insignificant if one measures traction curves beyond its peak value, but are significant when one only wants to measure the creep coefficient of the traction curve. However, the latter measurement strategy has certain advantages such as the lower required brake forces, further research is required to substantiate its feasibility.

For the friction force, normal force and slip measurement sub-systems, various design options are presented. Different use cases for the TTBM lead to varying system requirements, one may choose one TTBM design sub-system combination over the other.

Samenvatting

Wrijving, ook wel bekend als adhesie in het spoorwereld, in het wiel-rail contact is een complex fenomeen en een groot onbekende in de spoor industrie. De noodzaak om de efficiëntie (transport capaciteit, punctualiteit et cetera) van transport per trein te verhogen vraagt om het verbeteren van huidige spoor systemen als ERTMS en ATO.

Het weten van de actuele frictie (live, aan boord van een trein), dus hoeveel grip een trein heeft, is het meest belangrijke voor zulke spoor systemen, omdat het belangrijk is voor de lengte van de remweg. Momenteel is frictie, oftewel adhesie, onbekend en gaat men uit van lage wrijvingswaardes, wat resulteert in lange remwegen om de veiligheid te waarborgen (i.e. geen trein botsingen). Het gebruik van een dergelijke adhesie sensor is niet gelimiteerd tot het analyseren van de remweg, maar is ook cruciaal voor het toepassen van frictie modifiers, zoals Sandite, op het juiste spoor maar ook om reistijden van treinen te updaten om de tijdschema's aan te passen (punctualiteit). Met betrekking tot onderhoud, té lage wrijving leidt tot 'wheel lock' gedurende het remmen, wat resulteert in vlakke kanten op het loopvlak van het wiel en de benodigde uitvaltijd om het te repareren. Té hoge wrijving initieert rolling contact fatigue (RCF), wat leidt tot scheurvorming op het spoor. Om deze redenen is de behoefte groot voor live informatie van de wrijvingstoestand op het spoor en daarmee voor een trein adhesie sensor.

Voor een rollend contact, zoals het wiel-rail contact, tractie curves worden alom gebruikt om het gedrag tussen wrijving en slip te beschrijven. Voorgaand onderzoek door ProRail in samenwerking met de Universiteit Twente heeft geleid tot een concept ontwerp voor een dergelijke adhesie sensor, de trein tribometer (TTBM). Het idee is om de sensor in het onderstel of bogie (bestaande uit twee wielstellen) van een trein te integreren. Terwijl de trein rijdt wordt één wielstel kort geremd (het geremde wielstel). De wrijvingskracht en slip kunnen bepaald worden door het meten van de remkracht en de wiel omtreksnelheden van het geremde en ongeremde wielstel, respectievelijk, wat gecombineerd leidt tot een gemeten tractie curve. Deze manoeuvre wordt de TTBM-rem genoemd.

Vanwege de complexiteit van het wiel-rail contact en de tractie curves die erbij komen kijken is er een haalbaarheidsstudie uitgevoerd om vervolgens de volgende ontwerp fases te betreden (zoals lab en veld experimenten). Dynamica software (VI-Rail) is gebruikt om een trein met het TTBM system te simuleren onder verschillende spoor en operationele condities. Het TTBM concept is veelbelovend, in veel situaties is het mogelijk om met de TTBM rem tractie curves te bepalen.

De TTBM rem heeft een aantal ontwerp parameters, het meetgebied van de tractie curve wordt bepaald door de maximum wrijvingscoëfficiënt en tot een bepaalde slip limiet (μ_{\max} , S_{\lim}) men wilt meten en de tijdsduur van de TTBM rem om de meting uit te voeren, T . De ontwerp parameters hebben bepaalde compromissen. Des te hoger μ_{\max} is ingesteld, des te hoger de benodigde remkracht. Voor T , het verlagen tot onder een seconde leidt tot een significante toename in dynamische effecten van het wielstel, terwijl het verhogen van de tijdsduur leidt tot een grotere spoor afstand waarover gemeten wordt met de TTBM remtest.

Voor de simulaties in dit rapport zijn de TTBM rem ontwerp parameters zo ingesteld om over de piek waardes van tractie curves te meten, tot een bepaald slip limiet. Naast deze remstrategie (of meet strategie) is ook een ander rem strategie voorgesteld, welke zich richt op het meten van de creep coëfficiënt van de tractie curve, om dit vervolgens te extrapoleren en de piek waarde van de tractie curve af te schatten. Hiervoor zijn lagere remkrachten nodig, wat resulteert in een lagere schokbeweging wat anders eventueel tot passagier discomfort leidt.

Met de VI-Rail simulaties voor een gegeven trein model op recht spoor met spoor oneffenheden is een absolute slip error van grofweg 0.6% gevonden. Hetgeen is veroorzaakt door een combinatie van de spooroneffenheden en de klingelbeweging, wat leidt tot een verandering in rol radius dat de slip meting belemmerd. Met betrekking tot de wrijvingscoëfficiënt, verschillende oorzaken leiden tot veranderingen in normaalkracht, wat bij elkaar kan leiden tot 15-20% relatieve verandering van de normaalkracht. Wat betreft de wrijvingskracht, de wiel-rail condities zijn ook niet constant, frictie condities in het linker en rechter wiel-rail contact van een wielstel kunnen veranderen en flens contact kan ook voorkomen, wat de interpretatie van de TTBM meting belemmert.

Deze meetfouten zijn insignificant als over de piek waardes van tractie curves worden gemeten, maar worden significant wanneer alleen de creep coëfficiënt gemeten wordt van een tractie curve. De laatst benoemde meetstrategie heeft echter een aantal voordelen zoals een lager benodigde remkracht, verder onderzoek is nodig om de haalbaarheid aan te tonen.

Voor wrijvingskracht, normaalkracht en slip meet subsystemen, worden verschillende ontwerp opties voorgesteld. Voor verschillende gebruikerscases voor de TTBM komen andere systeem eisen naar voren, wat kan leiden tot een verschil in het TTBM ontwerp.

Acknowledgements

First and foremost, I would like to thank ProRail and the University of Twente for making such a large, engaging and challenging project possible, as well as the funding by ProRail. The learning experience, both in the research part regarding the tribology and dynamics of the the wheel-rail interface as well as the system engineering part by involving many stakeholders and setting goals and priorities, is invaluable.

Matthijn de Rooij, Rolf Dollevoet and Edwin Gelinck, I am grateful for the provided critical feedback, for supervising the project and the guidance needed to make the right decisions within the research.

Regarding the TTBM group, I would like to thank Ellard Groenewegen for managing the project and hosting the meetings. I am grateful to Jurjen Hendriks for the feedback throughout the multiple meetings and for arranging the ride-along on the CTO measurement train.

As for the people from the University of Twente, I would like to thank Aleks Vrčec and Mostafa Gargourimotlagh for helping with the twin disc machine experiments. Thank you, Peter Jansen, Debbie Vrieze-Zimmerman and Belinda Schaap-Bruinink, for providing kind support whenever needed.

Thank you, my brothers and sister, Jonathan, David, and Renata for always being there. I would like to especially thank my parents, Agnieszka and Dik, whom I have asked countless advice, and Frédérique for always being supportive throughout the project.

Contents

Summary	vii
Samenvatting.....	ix
Acknowledgements.....	xi
Nomenclature.....	xvii
Chapter 1 - Introduction.....	1
1.1 The need of a live, on-board of a train, adhesion sensor.....	1
1.2 Brief introduction to the TTBM concept and the TTBM brake.....	3
1.3 Aim of work	4
1.4 Thesis outline	5
Chapter 2 - TTBM project outline.....	7
2.1 Problem description: Railway systems in need of adhesion measurements..	7
2.1.1 ERTMS and ATO.....	7
2.1.2 Friction management	9
2.1.3 Maintenance downtime, punctuality and other related issues	11
2.2 TTBM TRL planning.....	11
2.3 Stakeholder analysis.....	14
2.4 Requirements	16
2.4.1 Adhesion sensor requirements	16
2.4.2 Operating condition requirements.....	18
2.5 Design goals.....	19
2.6 Conclusion	20
Chapter 3 – Tractive rolling contact	21
3.1 Slip within a rolling contact	21
3.1.1 Longitudinal slip	21
3.1.2 Lateral slip	24
3.3.3 Spin	25
3.2 Traction curves	27

3.2.1 Dry traction curve	28
3.2.2 Third body traction curve	30
3.2.3 Traction curve within the MBD simulation model	32
3.3 Two WRIs in one wheelset	32
3.3.1 Equal slip in left and right WRI	33
3.3.2 Slip difference between left and right WRI	34
3.4 Conclusion	36
Chapter 4 - Train tribometer	37
4.1 TTBM concept.....	37
4.2 Coefficient of Friction estimation	39
4.2.1 Friction force estimation – Brake system	39
4.2.2 Normal force estimation.....	42
4.3 Slip estimation braked wheelset	42
4.3.1 Translational velocity v_1	42
4.3.2 Rotational velocity v_2	43
4.3.3 Combining velocity values	43
4.4 Measurement Strategy - Design variables.....	44
4.5 Calibration and sensor resolution	47
4.5.1 Calibration of system parameters	49
4.5.2 Sensor resolution	50
4.6 Conclusion	51
Chapter 5 - Multi-Body Dynamics simulations	53
5.1 VI-Rail model.....	53
5.1.1 LOC-CTO model.....	53
5.1.2 Track	55
5.2 Perfect straight track	56
5.3 Track irregularities – Hunting	57
5.3.1 Track gauge.....	57

5.3.2 Straight track with periodically lateral shift	60
5.3.3 Cant on straight track	66
5.4 Normal force variations	68
5.5 Operating conditions	70
5.5.1 TTBM leading wheelset and drive direction	70
5.5.2 Comfort	72
5.5.3 TTBM brake during curve negotiation	73
5.6 Conclusion	75
Chapter 6 – Detailed design considerations	77
6.1 Design of the TTBM calibration system	77
6.1.1 Brake force measurement system concepts	77
6.1.2 Normal force measurement system concepts	79
6.1.3 Slip measurement system	81
6.2 TTBM brake strategy	83
6.2.1 ‘Peak and beyond’ traction curve measurement	83
6.2.2 ‘Creep coefficient’ traction curve measurement	83
6.3 TTBM design cycle	85
6.4 Conclusion	88
Chapter 7 – Conclusions and recommendations	89
7.1 Conclusions	89
7.2 Discussion	90
7.3 Recommendations	91
7.3.1 TTBM Design	91
7.3.2 Validation by lab experiments	92
7.3.3 Validation by field tests	92
7.4 Closure	93
Appendix A - Wheel/Rail/Bogie system	95
A.1 Wheelset and track properties	95

A.2 LOC-CTO system parameters.....	96
Appendix B – TTBM brake strategy	97
B.1 Deceleration	97
B.2 Brake force profile	99
B.3 Work wheelset within TTBM brake and normal braking.....	101
Appendix C – Sensor resolution.....	105
C.1 CoF	107
C.1.1 Friction force sensor	107
C.1.2 Normal force sensor	107
C.1.3 Braking distance	108
C.2 Slip	108
C.3 Parameter errors - Calibration	111
C.3.1 Slip error due to wheel radius error	111
C.3.2 Friction force error due to brake pad-center to wheel distance error	112
C.3.3 Normal force error due to expected static normal force error.....	112
Appendix D – VI-Rail simulations.....	115
D.1 change in rolling radii	115
D.2 VI-Rail simulations.....	117
D.2.1 F_N variations	117
D.2.2 Additional VI-Rail simulation results of chapter 5.....	120
D.2.3 Slip estimation by train speed and braked-wheelset only	123
Appendix E - Twin disc tests	125
Appendix F – Traction curves	127
F.1 Third body traction curves.....	127
F.2 Dry traction curves.....	128
F.3 Different traction curve output under same friction conditions.....	129

Nomenclature

Abbreviations

ABS	Anti-lock Brake System
AOA	Angle of Attack
ATO	Automatic Train Operations
CoF	Coefficient of Friction
ERTMS	European Rail Traffic Management System
FBD	Free Body Diagram
MBD	Multi-Body Dynamics
PS	Primary Suspension, between axle box (one side wheelset) and bogie frame
SS	Secondary Suspension, between bogie frame and wagon
TRL	Technology Readiness Level
TTBM	Train TriBo Meter
WRC	Wheel Rail Conditioning. Note, often in literature, WRC stands for wheel-rail contact. Throughout this report wheel-rail contact is fully written or WRI is used
WRI	Wheel Rail Interface
WSP	Wheel Slide Protection

Roman symbols

A	Amplitude for a certain periodical track irregularity [m]
a, b	WRI contact patch semi-axes, in longitudinal and lateral direction [m]
c	Distance between the center of the wheel and center brake shoe [m]
F_f	Average friction force of the left and right WRI [N]
F_z	Average expected static normal force of the left and right WRI [N]
F_N	Average normal force of the left and right WRI [N]

F_{pinch}	Pinch force between brake pad and brake disc [N]
F_R	Sliding brake force between brake pad and brake disc [N]
I	Inertia of the wheelset [Nm^2]
L	Wheelbase of the bogie, i.e. distance between the leading and trailing wheelset within the bogie [m]
R_0	Nominal radius of the wheel [m]
R	Actual radius of the wheel [m]
S	Slip within the WRI [-]
S_{lim}	Slip limit, the range one wants to measure with the TTBM [-]
T	Duration of the TTBM brake [s]
$V_{1,2}$	Velocity of bodies 1 and 2 in contact. Referred to TTBM rolling contact, v_1 is the translational velocity and v_2 is the circumferential velocity of the braked wheelset [m/s]
$V_{2,\text{lim}}$	The circumferential wheel velocity at the slip limit, S_{lim} [m/s]
V_{train}	Train speed, often referred to as v_1 , but strictly not the same [m/s]
V^+	Sum velocity of v_1 and v_2 [m/s]
V^-	Sliding velocity of v_1 and v_2 [m/s]
x_{brake}	Braking distance of the train [m]
x	Longitudinal direction of the track [m]
y	Lateral direction of the track [m]
z	Vertical direction of the track [m]

Greek symbols

α	Rotational acceleration [rad/s^2]
γ	Conicity of the wheel [-]
λ	Wavelength for a certain periodical track irregularity [m]

μ	CoF within the WRI, ratio of F_f over F_N [-]
μ_f	Friction limit, the maximum CoF in Carter theory or dry traction curves [-]
μ_{pad}	CoF between brake pad and brake disc, ratio of F_R over F_{pinch} [-]
ω	Rotational velocity [rad/s]

Chapter 1 - Introduction

1.1 The need of a live, on-board of a train, adhesion sensor

The railroad industry exists for quite a long time and is a conventional way of transportation for many people. Within the Netherlands (but also within other countries) the last couple of years, transportation by means of trains is increasing and most likely will continue to do so for the next years. By 2040, ProRail expects an increase of passenger transport by 30% and freight transport around 50% [1]. The focus on more train transportation is urged by the European government, by increased environmental awareness (which calls for the energy transition). NS is the largest Dutch railway operator and besides the higher transport capacity also wants to increase its punctuality, i.e., the on-time arrival of trains.

There are a few ways to increase the transport capacity. One could lay new tracks and use more trains to meet the higher demand, but this requires extra space and is expensive. The most direct way by improving transport capacity is by using the current railway system more efficiently.

There are promising railway systems in development that could resolve the extra demand by using the current infrastructure more efficiently. Currently, long braking distances are maintained between trains. European Rail Traffic Management System (ERTMS) is aimed to improve the communication between individual trains about their whereabouts, such that trains can drive closer together [2]. Automatic Train Operations (ATO) focuses on automation of the train, which gets more interesting lately due to the recent personnel shortage, including machinists, within the Dutch railway industry [3], [4].

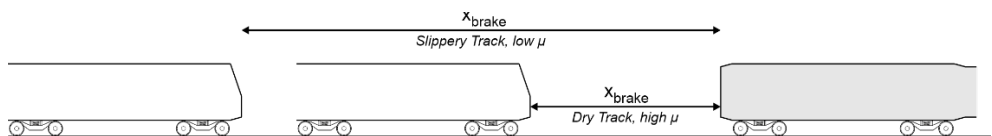


Figure 1-1: Braking distance.

Both ERTMS and ATO, among other railway systems, sound promising, but these systems depend heavily on the knowledge and measuring of friction (a.k.a. adhesion in the railway sector) within the wheel-rail interface. Friction within the wheel-rail contact determines the amount of grip a train has, which has huge influence on e.g. the braking distance, see figure 1-1, but also how fast a train can accelerate. Friction however remains one of the main unknowns within the railway industry since the very beginning.

The friction conditions change continuously and can be very unpredictable. E.g., during autumn when leaves fall onto the tracks is a well-known issue, see figure 1-2. The leaves problem just mentioned or ice on the tracks during winter leads to exceptionally low adhesion, which leads to delayed trains and is bad for the overall punctuality for the railway operators. Very low adhesion could also cause ‘wheel locking’ during braking, resulting in flat spots on the circumference of the wheel, see figure 1-3.



Figure 1-2: Leaves on track [5].



Figure 1-3: Flat spot due to wheel locking [6].

There are measures to counter the low adhesion problems. One way is by applying Sandite, to increase the friction, which is also known as a friction modifier to increase the friction in the contact. This substance however should only be applied where it is needed. Not knowing the actual, local adhesion levels makes it hard to anticipate to it. The other extreme, too high friction is not desired as well since this condition is prone to crack initiation and deterioration of the track surface by rolling contact fatigue (RCF) [7].

Excessive wheel slip during accelerating of the train or during braking can be registered and attenuated by e.g. Wheel Slide Protection (WSP) and Wheel Rotation Monitoring (WRM) systems, but it only detects the presence of ‘not high enough’ adhesion [8]. The experience of the machinist is used as well to ‘feel’ the grip within the wheel and rail contact [9]. However, this is qualitative instead of quantitative.

There are systems to analyse the adhesion on the rail. Conventional hand pushed tribometers or pushed by a car are often used to measure the friction on the rail [10]. Problem is that, carrying out these measurements using these devices requires that no train is passing by, which results in downtime of the track. If one wants to measure multiple tracks occasionally, then carrying out these measurements in this manner would be quite cumbersome.

Thus, an on-board adhesion sensor is needed that can measure the current levels of friction live and register the corresponding location on the track. One way to measure the adhesion is by using the driven wheelsets and the WSP systems to register excessive slip and the corresponding motor torque. This seems promising and might be looked at a later stage, however there are a few drawbacks with this system. Certain errors are introduced and hard to determine, such as the gearbox friction and reading out the motor torque, while the accuracy of slip measurement of the WSP system is not that accurate, since it is designed to detect excessive slip [9]. Furthermore, driven wheelsets are engaged when accelerating and partly during ED-braking. If one wants to measure adhesion on multiple track positions besides tracks close to the stations, the driven wheelsets need to be engaged more often as well.

By previous research conducted by ProRail in collaboration with the University of Twente, the train tribometer, TTBM, was proposed [11]. The design is still in the concept stage, hence a feasibility study of the TTBM design has been carried out in this work.

1.2 Brief introduction to the TTBM concept and the TTBM brake

The TTBM uses a non-driven bogie of the train, see figure 1-4, and is explained in detail in chapter 4. Within the bogie with two wheelsets, one is briefly braked. By looking at the response (the slip and friction force of the wheelset in contact with the rail), one could estimate the Coefficient of Friction (CoF) and corresponding slip (velocity difference between wheelset and train speed). The relation between the CoF and slip leads to the traction curve (explained in detail in chapter 3), illustrated in figure 1-5.

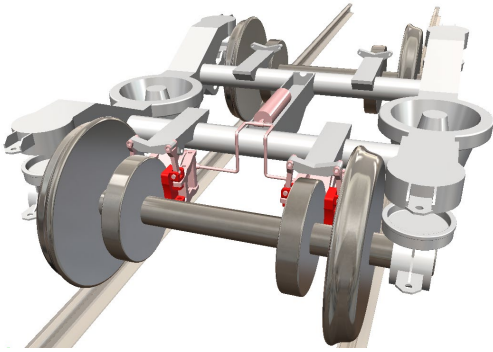


Figure 1-4. Non-driven bogie.

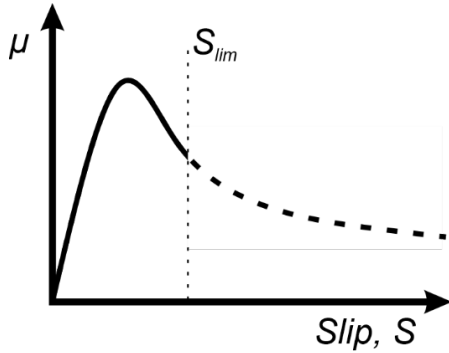


Figure 1-5. A traction curve, in which the TTBM measures up to a certain slip limit S_{lim} .

The TTBM brake is thus brief braking of a single wheelset, with a braking time only in the order of seconds. By braking the wheelset, slip is generated. Fully blocked wheels mean full slip or 200% slip, but that is not the purpose of the TTBM brake. Only up to a certain slip limit (S_{lim}), a few percent slip, around and beyond the peak value of the traction curve will be measured. Within this part of the traction curve all desired regular, operating braking (and accelerating) of the train wheels occur.

1.3 Aim of work

Different use cases (e.g., braking distance estimation or measure too low/high friction) lead to different requirements of the adhesion sensor, e.g., accuracy of the adhesion sensor. The purpose of the TTBM concept has yet to be determined, hence the feasibility will be investigated, such as its measurement accuracy and certain pitfalls of the concept.

How one is going to perform the TTBM brake (low or high brake intensity, short or long brake duration), referred to as the TTBM brake strategy, affects the design of the TTBM system as well. The important design parameters involving the brake strategy and their influence will be investigated.

The combination of use cases and the TTBM brake strategy leads to different concept designs of the TTBM.

1.4 Thesis outline

Chapter 1: Introduction

A small introduction into a few apparent railway system problems involving adhesion within the wheel-rail interface, and the lack of not knowing it. The need for an adhesion sensor is growing, a concept is introduced, the TTBM.

Chapter 2: TTBM project outline

The whole railway industry is quite large (many stakeholders and assets) and the projects are complex and take a long time to complete (multiple years), including the proposed adhesion sensor, the TTBM. In this chapter, the whole outline of the TTBM concept and the project will be shown.

First the problem description is given by showing various railway systems that demand for a live and on-board adhesion sensor, such as the TTBM. Different use cases (i.e. the aforementioned railway systems) also have different interests and requirements. Relevant to the TTBM and the EngD project, a stakeholder analysis is carried out. The Technology Readiness Level (TRL) of the current state of the TTBM is shown and the requirements regarding such an adhesion sensor, integrated within a train, are evaluated. From these analyses the goal of this EngD project will be formed.

Chapter 3: Tractive rolling contact

The required theoretical knowledge of the rolling contact, such as the wheel-rail interface (WRI), is explained. Within the WRI, the CoF depends heavily on the amount of slip, resulting in a traction curve. Two main conditions on the track, 'Dry' and 'Third body' (presence of dirt, lubricant, leaves etc. within the WRI) will be explained as well as their influence on the shape of traction curves.

The relevance of the theory to the TTBM will be shown as well as to the simulations carried out.

Chapter 4: Train tribometer concept

To measure traction curves, two forces and two velocities need to be determined. The conceptual TTBM uses multiple sensors to measure two wheel velocities and the brake force. The TTBM brake is explained as well.

Relevant topics to the TTBM such as the brake system (input) but also the role of the leading and trailing wheelsets will be shown.

Chapter 5: Multi-Body Dynamics simulations

The TTBM brake test is simulated using VI-Rail, which is a multi-body dynamics (MBD) program. The used train model including the Y32 bogie are explained as well as other relevant systems such as the used track and track profile.

Various simulations have been carried out, by looking at different track conditions (track irregularities, 'dry' and 'third body' traction curves, low and high friction) and operating conditions (constant train speed, de- and acceleration of the train, straight track and within a curve).

Chapter 6: Detailed design considerations

Based on the results of the simulations in chapter 5, the TTBM has a certain CoF and slip measurement accuracy. The TTBM consists of three main sub-systems: the brake force-, the normal force - and the slip measurement system. A few design options are presented for each sub-system as well as two TTBM brake strategies. Considering different use cases might lead to varying TTBM designs.

Chapter 7: Conclusions and recommendations

A discussion is given as well as the conclusions regarding the presented work. Finally, recommendations are made about the design of the TTBM and what needs to be researched to validate and improve the TTBM.

Chapter 2 - TTBM project outline

Within the whole idea to determine the adhesion within the wheel-rail interface and integrate such an adhesion sensor within the railroad system, the adhesion sensor itself (such as the TTBM concept) is one of the key elements. To place the TTBM within this whole project, a project outline (the need for such a system, a TRL scheme, stakeholder map, requirements and the goal of this report) is presented in this chapter.

2.1 Problem description: Railway systems in need of adhesion measurements

2.1.1 ERTMS and ATO

For railway systems such as ERTMS and ATO, the braking distance of a train is of main importance, as shown in figure 1-1. Currently, to maintain a safe distance between trains, the track is subdivided in many segments with a certain track length. Between two trains, always one segment needs to remain free with a certain distance (depending on the track velocity, at higher velocities, a larger braking distance is required).

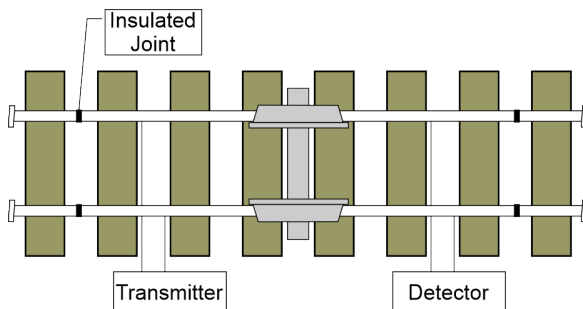


Figure 2-1. Track circuit for train detection, figure from [12].



Figure 2-2. Axle counter, figure from [13].

To detect if a section of a track is clear or occupied by a train, various signalling systems can be used. A track circuit as shown in figure 2-1 detects a train since the metal wheels will short the circuit. Axle counters as shown in figure 2-2 will be mostly used in the near future for the implementation of ERTMS, since it is more reliable [13]. It sends out a magnetic field, in the presence of a wheelset, the magnetic field changes and the number of wheelsets are counted. If the counted axles at the end of a track segment are of the same number as at the entry of the segment, the segment is proved to be clear. Equipping every train with a GPS seems to be the most accurate regarding the precise whereabouts of the train, but the

aforementioned systems are currently more reliable, hence a full GPS implementation is not within the near future.

The preceding systems are about reliable detection of the train and whether a track segment is occupied or not. But the increase in usage of the train network results in the need of increasing the train capacity (by implementing ERTMS and ATO), thus decreasing the distance between trains. Improved reliable detection of the train its location would help a bit, however, the required minimum distance between trains depends for a large part on the available adhesion between wheel and rail. For ATO, knowing the actual braking distance would help to stop the train at the right time when e.g., approaching a station.

The government of the Netherlands states that certain minimum braking distances need to be maintained [14], which are shown in Table 2-1.

v_{train} [km/h]	x_{brake} [m]	μ_{req} [-]
40	400	0.016
60	500	0.028
80	800	0.031
130	1000	0.066
160	1150	0.088

Table 2-1. Braking for various train speeds [14]. Note, the braking distances shown here are for a descending slope of 5 per mile or 0.5 degree. For simplicity, no slope considered.

The braking distance table is for extremely low adhesion, if these were to be used to estimate the braking distance, then the ERTMS will only have a minimal improvement on the train capacity on the track. If a train engages all its wheels to brake, the braking distance is then approximately:

$$a_{brake} = \mu g; \quad t_{brake} = \frac{v_{train}}{a_{brake}}; \quad x_{brake} = \frac{1}{2} \frac{v_{train}^2}{\mu g} \quad (2.1)$$

It is obvious that higher train speeds results in longer braking distances. One could also see the inverse dependency of the braking distance and CoF (a high CoF results in a low braking distance). But the sensitivity of the braking distance, especially when low friction is present, is less obvious.

Measuring the adhesion means a better approximation of the actual braking distance. Consider the 130 km/h case in Table 2-1, which requires a minimum of

1000 m braking distance to be maintained. By using equation 2.1, one could find the corresponding required friction coefficient, μ_{req} , to realise such a braking distance, as shown in the third column in Table 2-1. Now suppose the available friction coefficient is 0.15 and is measured, then the braking distance becomes 443 m, which is less than half of the safely required braking distance.

Note, this is a simplified example regarding braking and braking distances. Multiple levels of intensity regarding slowing down the train exist [9]. Different deceleration values at different speeds lead to a more tedious way of determining the braking distance, more can be found in [15].

Not knowing the actual adhesion, thus not measuring the adhesion on the track, would mean for ERTMS and ATO to use braking tables like Table 2-1 to maintain a safe braking distance. Because of this, only a slight improvement will be made compared to the current operations.

2.1.2 Friction management

Friction management, or Wheel Rail Conditioning (WRC), refers to adapting the current friction levels. Due to the various environmental conditions (rain, snow, leaves during autumn etc.), different substances are present within the wheel-rail interface. This could lead to (extremely) low adhesion and on its turn longer travel times and delays.

To counter low adhesion, friction modifiers are used that increase the friction levels significantly. Most often sand in combination with a gel and small metal particles (to maintain the wheel-rail contact for signalling purposes) are applied, Sandite is such a commercial product, see figure 2-3. However, sand consists of small but hard particles, which are either ejected or entrained within the surfaces. Due to this, a large increase in wear on both the wheel and rail follows [16]. Hence, one needs a status of the friction levels of the tracks, as shown in figure 2-4, to apply Sandite only on the slippery tracks.

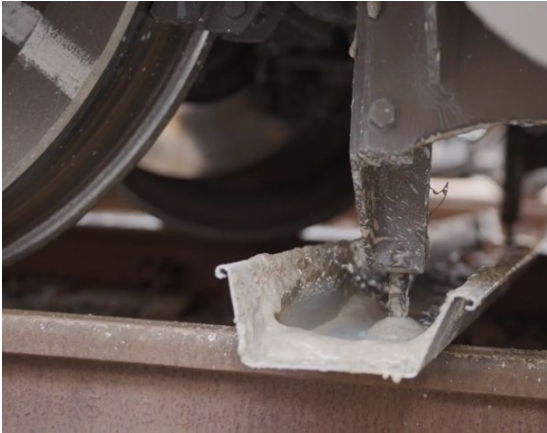


Figure 2-3. Sandite tested at a service point [17].

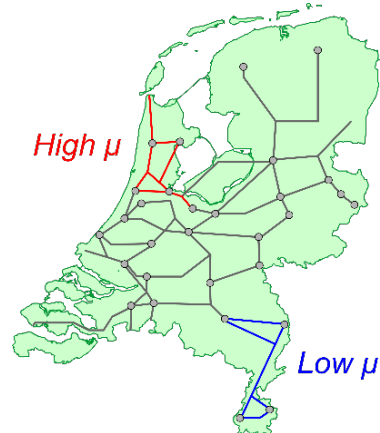


Figure 2-4. Varying adhesion conditions.

Too high friction, $\text{CoF} > 0.3$, is not desired as well since this leads to stress concentrations at the surface of the rail instead of sub-surface [18]. At the rail surface, the initiation and propagation of ratchetting also happens when a sufficient high CoF is present ($\mu > 0.25$), this causes crack initiation at the surface of the rail and leads to Rolling Contact Fatigue (RCF) damage at the surface [7], [19]. Rails are often grinded to remove the upper layer with small cracks, see figure 2-5.

Once cracks are initiated on the rail surface, the crack is deteriorated in several ways. A well-known issue is when liquid is present on the rail and the liquid enters the crack cavity. Upon passing of the wheel, the crack encloses and traps the liquid, pressurizing it and causing crack growth [20].

Thus, applying a friction modifier (lubricant to lower friction or Sandite to increase it) increases the amount of wear and deteriorates the RCF life of the rail. As mentioned earlier, one wants to apply a friction modifier only where it is needed. However, too low, and too high friction are hard to detect. The use of the live on-board adhesion sensor could indicate where a friction modifier is needed.

Another way to manage low friction is by the adaptation of the driving behaviour (braking and accelerating) of the machinists [9]. Experienced machinists can ‘feel’ low friction when driving and by informing each other, one brakes cautiously to prevent passing by a train station as well as flat spots. But this might only be needed on a few tracks instead of a common protocol when extreme low friction is expected.



Figure 2-5. Rail reprofiling, figure from [21].

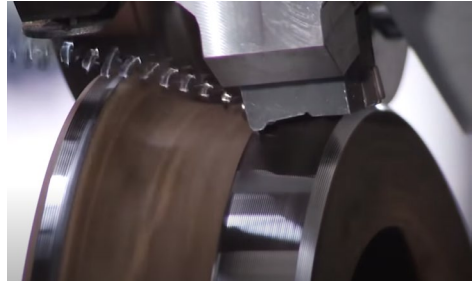


Figure 2-6. Wheel reprofiling, figure from [22].

2.1.3 Maintenance downtime, punctuality and other related issues

Wheel Slide Protection (WSP) is used to prevent excessive slip when applying a driven torque onto the driven wheelsets to accelerate the train. During braking, the anti-lock brake system (ABS) prevents excessive slip or ‘freezing’ of the wheels (i.e., no rotational velocity while the train still has a speed).

However, when extreme low friction is present, braking leads to a quick stop of rotation of the wheels, faster than the ABS can anticipate, causing the wheels to freeze for a moment. This can lead to ‘square wheels’, or flat spots on the circumference of the wheels, see figure 1-3. Because flat spots lead to discomfort and further damage of wheel and rail, wheels with flat spots need to be reprofiled, see figure 2-6. This leads to downtime of assets, which causes lower train occupancy and longer waiting times [23].

The time to get to cruise speed when accelerating and the braking distance mentioned in the previous section depend on the adhesion levels. When the adhesion is measured, one can determine the actual travel time of a train more accurately. A better prognosis can be made which can be used to update the timetables and improve overall punctuality.

2.2 TTBM TRL planning

The Technology Readiness Level (TRL) of a system indicates how far it is in its design process, which is introduced by NASA [24]. Such a TRL scheme is applied to the TTBM project, resulting in a global overview in Table 2-2. Given the complexity of the yet to be designed system and the friction problem, one would be better off by following the TRL scheme rather than directly jumping to building a full-scale prototype (TRL 6-7).

At TRL 1, already a lot of research carried out on the general rolling contact problem and specifically for the wheel-rail contact, as will be discussed in chapter 3. The work of Popovici can be regarded as the subsequent step, TRL 2, in which further knowledge about traction curves is acquired as well as a global TTBM concept is proposed [11]. The next step would be to investigate thoroughly the proposed TTBM concept, which will be carried out at TRL 3 and will be done within this design process.

TRL 4 would be the next step after this project, which is validating (parts of) the adhesion sensor using lab setups. TRL 5 to 7 are about integration of the adhesion sensor within an actual undercarriage of the train and carrying out field tests. The TU Delft has its own CTO measurement train which is often used for testing new technology and will be most likely used as well for testing of the TTBM. Discussion of the results and the recommendations shown in this report will be mainly focused on TRL 4 (lab tests) and what will be needed for TRL 5-7 (field tests).

A note on the TRL scheme: usually once the goals within a certain TRL are reached, one goes to the next TRL and set new goals based on the accompanying recommendations. In Table 2-2, green indicates the TRL has been passed whereas yellow shows the current TRL and is work in progress. However, this does not mean that one completely passed the previous TRL for good. New insights and results at higher TRLs could lead to re-evaluation of certain aspects at preceding TRLs.

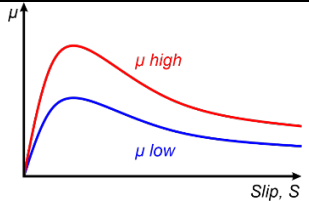
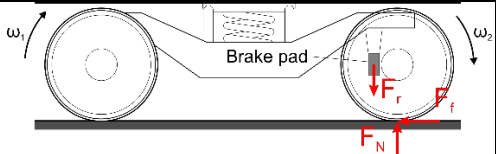
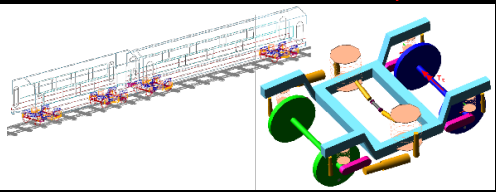

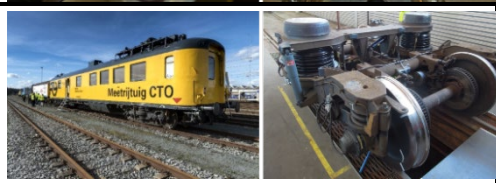
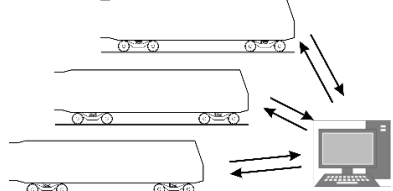
TRL	Description	
1	<i>Principles observed:</i> Rolling contact, traction curves, CoF and slip	
2	<i>Technology concept:</i> TTBM brake test of non-driven wheelset	
3	Feasibility of TTBM concept: MBD simulations within VI-Rail, simulating the TTBM brake test	
4	<i>Component validation in laboratory environment:</i> Testing and calibrating various aspects of the TTBM on a scaled/full-scale test rig	
5-6-7	<i>(sub) system prototype field test:</i> TTBM prototype within CTO, principle design TTBM calibration system	
8-9	<i>System test and integration:</i> Testing and integrating TTBM within train network and relevant railway systems (ERTMS, WRC, ...)	

Table 2-2. TRL scheme of the TTBM project.

2.3 Stakeholder analysis

The project is commissioned by ProRail and carried out by the University of Twente. Multiple projects within the TTBM project (in which the TU Delft is involved as well) are or will be worked on:

1. The feasibility and design strategy of the TTBM.
2. The integration of the TTBM within the train control and information system.
3. The analysis and processing of the TTBM data (from multiple TTBM's used within the country, how to monitor the TTBM, interpret the data and act accordingly).
4. Design of the calibration system of the TTBM.

The railroad industry comprises of large, various assets (tracks, trains, overhead cables, stations, etc.) and many different stakeholders (manufacturing and maintenance companies, government, service providers etc.). When the TTBM reaches the end of the design process, TRL 5-9, the number of stakeholders increases and becomes complex. At the current stage (TRL 3), it is less tedious, hence for simplicity three main stakeholders will be elaborated on and are shown in figure 2-7.

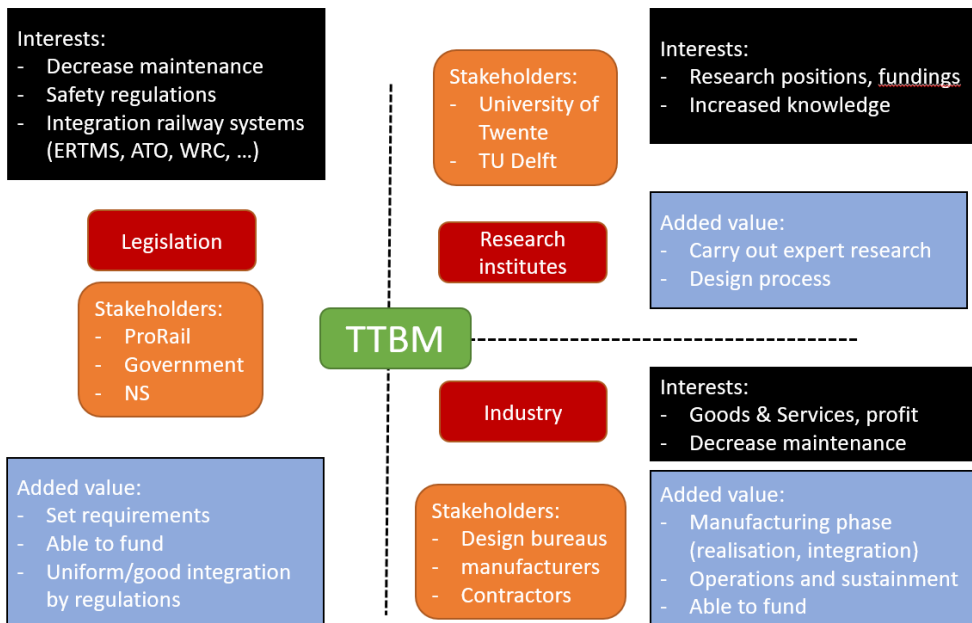


Figure 2-7. Stakeholder map, only the direct stakeholders regarding this project are shown.

Regulation and legislation: ProRail and NS own most of the assets regarding the railway industry in the Netherlands and maintain the railroads. Even though they operate independently as a government agency, they are still owned by the government. Both the government as well as ProRail and NS do the legislative work, i.e., how systems should operate and need to comply with certain rules. On a larger scale, the European Union describes the rules and guidelines for all countries in Europe, for a better transition and understanding between countries (Note that other service providers operating in the Netherlands such as Blauwnet and Arriva are again state owned by France and Germany).

Research institutes: For simplicity, only universities (University of Twente, TU Delft) involved in the project will be mentioned (most companies mentioned above or within the railroad industry have a R&D department or are innovating in a way).

Industry: Contractors (Asset rail, BAM, Strukton, etc.), manufacturers (Siemens, Bombardier, etc.) or design bureaus (Ricardo Rail, VolkerRail, etc.). They design and manufacture the assets or carry out the maintenance of the assets.

The biggest *incentive* for the development of the TTBM is that main, still in development, railway systems (ERTMS, ATO, WRC, etc.) and goals (higher punctuality, increased train capacity, less maintenance) depend heavily on the live, on-board, measurement of adhesion levels, as mentioned in section 2.1.

The main *conflicts of interests* are:

- *Responsibility:* NS and ProRail are service providers that want to have an adhesion sensor, but engineering and manufacturing is done by the industry/design bureaus. For NS and ProRail it would be desired that, instead of a mere stand-alone system, the industry would deliver the adhesion sensor as a whole service package, fully integrated within the trains (which are also manufactured by the industry). This would place the responsibility more to the industry. However, adhesion within the wheel-rail contact is a complex phenomenon, the industry is hesitant/not fully convinced in developing such an adhesion sensor and to take on the extra responsibilities. Extra research, in which Universities have the knowledge and the capabilities, is needed to tackle uncertainties, and show the business potential.
- *Time and (un)certainty:* It would take a multitude of years to get the TTBM from TRL 3 to TRL 9. If the industry were to take the step to invest, research and develop an adhesion sensor, it would then undergo significant

uncertainties and risks. One way to reduce this uncertainty is by widespread commitment among the many stakeholders into certain projects, such as ERTMS. Europe's Rail Joint Undertaking (EU-Rail) is one of those programmes to boost innovation in which multiple stakeholders from many countries are involved and investments are made for innovation, for more information see [25].

2.4 Requirements

Since the TTBM sensor is still in the concept stage, as shown in the TRL scheme in section 2.3, there are no precise requirements (e.g., accuracy and measurement range), only that the need of it is high (section 2.1). Section 2.4.1 describes the requirements on the adhesion sensor functionalities.

The TTBM project is still in the conceptual stage (TRL3, as shown in section 2.2). One must incorporate and see the importance of some of the other global requirements, which become more apparent in the later TRLs such as integration within a train, to design a proper TTBM system. This is kept in general terms in section 2.4.2 to keep it comprehensible.

2.4.1 Adhesion sensor requirements

Important railway systems need a proper, live, on-board adhesion sensor, these systems however have different requirements regarding the adhesion sensor. As stated in [26], the extreme low friction regime is when $\mu < 0.03$, the low friction regime is in the range $0.03 < \mu < 0.08$ and the dry friction regime (i.e. sufficient adhesion) is in the range $0.15 < \mu < 0.17$. The dry friction regime is sufficient for braking, in which all wheelsets are able to do so. However, only a few wheelsets are driven to accelerate the train to its cruise speed, hence higher friction is then desired ($\mu > 0.2$).

ERTMS and ATO programs are more concerned about the low to mid friction regimes since the braking distance changes the most within this region. Knowing how long a train takes to accelerate to reach its cruise speed as well as its brake manoeuvre will improve the accuracy of the timetables. Wheel Rail Conditioning, WRC, is focused on too low and too high friction ($\mu > 0.25$, see section 2.1.2).

For ATO and ERTMS, it is also desired to have a higher accuracy of the adhesion measurements (shown as $d\mu$ in figure 2-8), due to the sensitivity of the braking distance when low adhesion is present as mentioned in section 2.1.1, which is shown as well in Appendix C. This leads to the figure 2-8 to illustrate the difference in requirements of the adhesion sensor for various railway systems, on the x-axis

the measurement range and on the y-axis the accuracy of such an adhesion sensor (note, the lower the $d\mu$, the higher the accuracy).

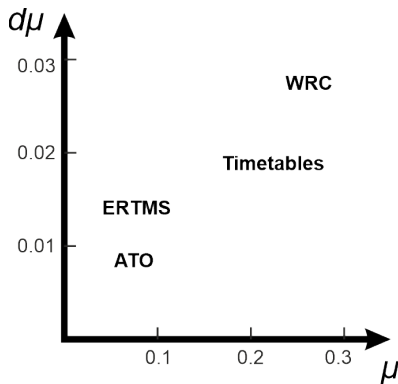


Figure 2-8. Illustrative map of various railway systems that demand different requirements of the TBM system.

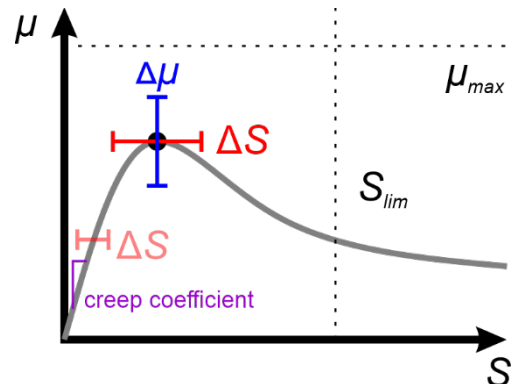


Figure 2-9. A traction curve illustrating the slip and CoF accuracies, ΔS and $\Delta\mu$, respectively. The measurement range is spanned by μ_{max} and S_{lim} .

Setting certain requirements for slip depends on what one wants to measure of the traction curve, i.e., the measurement range of the traction curve (μ_{max} and S_{lim}). If one focuses more on identifying the peak value and beyond, thus measure excessive slip, then the slip does not have to be that accurately measured ($dS=1\%$ might be sufficient). If one wants to measure the creep coefficient (chapter 3), a small error in slip estimation leads to a relatively large creep coefficient error, see figure 2-9, and thus a higher accuracy is required ($dS=0.1\%$). Also, the slip corresponding to the peak value of traction curves lies roughly within a range of 0.5% to 5% (also discussed in chapter 3).

The different use cases lead to different requirements. For now, the requirements are based on the low to mid friction regime in which the shape of the traction curve needs to be measured accurately and are shown in Table 2-3. Note that these requirements are not fixed.

Range CoF	Range Slip	Accuracy CoF	Accuracy Slip
$0 < \mu < 0.2$	$0\% < S < 5\%$	$d\mu = 0.01$	$dS = 0.1\%$

Table 2-3. Requirements of the TBM regarding the measurement range and accuracy of traction curves.

2.4.2 Operating condition requirements

Safety is one of the most important aspects within the railway industry. Every current and newly developed railway system must comply with the given safety regulations or needs to be adapted in such a way that the overall safety is safeguarded.

- Safety:
 - No risk of falling-off (parts of) the adhesion sensor, which could possibly lead to derailment.
 - Good integration of the TTBM system within the train itself and other railway systems. This means that the newly added system should not interfere with the train and its subsystems itself (e.g. the brake system should always work).
- Comfort: The deceleration and jerk of the TTBM brake test should not interfere with passenger comfort. Passenger comfort can be assessed in various ways, more information can be found in [27], [28].
- Maintenance:
 - The TTBM itself needs to fit within current maintenance operations. When the train or undercarriage is set up for maintenance then the TTBM needs to be checked as well.
 - The TTBM brake causes a certain amount of work to be done by the brake pads, this should not lead to significant decrease of lifetime.
 - Regarding WRC by using TTBM, to maintain the proper friction levels. Too high friction is not desired.

The measurement frequency of the adhesion sensor is different when one focuses on a different purpose of the adhesion sensor. For ATO and ERTMS, to safeguard the distance between the trains, the adhesion needs to be monitored with measurement data obtained with a high measurement frequency, e.g., measure every track a certain amount per day. Integration of the adhesion sensor within a passenger train would be needed.

For WRC it might be sufficient to measure less frequently, thus by measuring once in a few days and during critical times (e.g., during autumn) once per day on certain tracks or so. A service train rather than a passenger train could be equipped with the adhesion sensor, leading to less demanding requirements such as passenger comfort. ERTMS and ATO are main goals within the rail industry set by Europe in the upcoming years, hence the focus will be more on that.

2.5 Design goals

Based on the current TRL scheme, the TTBM design is still at the concept stage. Even though the need for an adhesion sensor is high, adhesion itself remains a large unknown, which makes it hard to set certain requirements regarding sensor accuracy or measurement range, as shown in section 2.4.1. Instead, the approach will be to investigate the capabilities of the TTBM.

How the TTBM sensor operates is explained in chapter 4. There are a few things to consider which could affect the TTBM measurements, such as hunting of the train, the dynamics of the wheelset itself and the interaction at the wheel-rail interface via traction curves.

Also, if the TTBM were to be fully integrated within a (passenger) train and used in daily operations, besides measuring accurately as stated in section 2.4.1, other requirements play a role as well, see section 2.4.2. Hence, the first and main goal of this project is:

Goal 1: Feasibility study of the TTBM concept.

- How accurate is the TTBM able to measure traction curves?
- Which factors or conditions could deteriorate the TTBM measurements?
- What are the potential pitfalls, or 'show-stoppers' of the TTBM?

The results of this part are used as input for the second goal.

Goal 2: Strategy design of the TTBM.

- How should one carry out the TTBM brake (the duration and propagation of the applied brake force)?

Since it is only TRL 3, various ideas will be presented. In the end, conclusions are presented in chapter 6 as well as recommendations focused on the next TRL, which is TRL 4.

2.6 Conclusion

Railway systems such as ERTMS, ATO and maintenance operations, such as WRC, require an adhesion sensor, otherwise the benefits would be severely limited. Measuring 'live and on-board of a train' the adhesion, thus quantifying it, by using the TTBM would enable:

- Braking distance estimation, improved distance monitoring between trains instead of extreme safe distances based on extreme low adhesion. Precautionary low friction values ($0.016 < \mu < 0.088$) lead to extreme long braking distances, whereas if e.g., the actual measured CoF is around 0.15, one would decrease the braking distance with more than 50%.
- Improved friction management, by knowing which track needs to be treated by e.g., a friction modifier. This leads to less maintenance, downtime of assets and improvement of the overall punctuality.

The TTBM project is currently at TRL 3, which is the focus of this report. The feasibility of the TTBM will be investigated as well as the strategy regarding the operations of the TTBM.

Chapter 3 – Tractive rolling contact

The goal of the report and research is to investigate the TTBM system and simulate the TTBM brake. The most important aspects of the rolling contact and traction curves (which are important to comprehend the simulation) and the conclusions are discussed here. First, the various types of slip (longitudinal slip, lateral slip and spin) present in the rolling contact of one wheel are shown in section 3.1. Subsequently, two main types of traction curves, the 'dry' and 'third body' traction curve, will be discussed in section 3.2. At last, the wheelset consists of two wheels which are rigidly fixed together and both wheels are in contact with the rail, leading to a wheel-rail interface (WRI) on the left and right side of a wheelset. How to interpret the measured TTBM data will be shown in section 3.3.

There is some overlap with chapter 4, which goes more into the specifics of the TTBM system and how it operates. This chapter focuses more on the theoretical concepts such as slip and friction within the rolling contact, traction curves and the two WRI within a wheelset and how to interpret the TTBM measurement.

3.1 Slip within a rolling contact

Within the rail industry, the x-direction is in the longitudinal direction and the y-direction in the lateral direction. Within a 3D rolling contact, one could define slip in the longitudinal and lateral direction, which are related to translational velocity differences between the two bodies. Spin is rotational velocity difference around the vertical z-axis, normal to the contact area, of the two bodies in contact.

3.1.1 Longitudinal slip

For two stationary but rotating bodies in contact, such as a twin disc machine schematically shown in figure 3-1, only the rotational circumferential velocities of the bodies determine the slip within the contact.

$$S = 2 \cdot \frac{v^-}{v^+} = 2 \cdot \frac{|v_1 - v_2|}{v_1 + v_2} \quad (3.1)$$

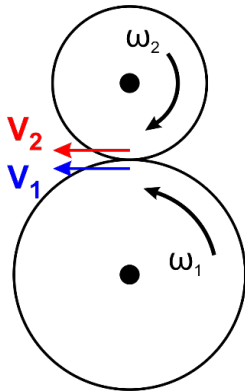


Figure 3-1. Two discs rotating in rolling contact.

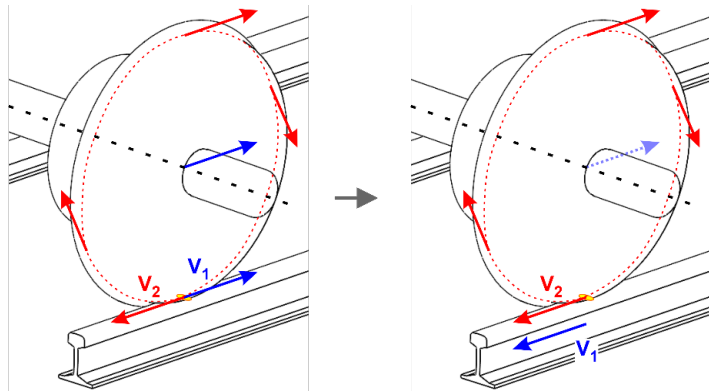


Figure 3-2. On the left, rolling contact of one body (i.e. the wheel) rotating and translating and the other body (i.e. the rail) being static. However, one could see it as on the right, the wheel only rotating (no translational velocity) while the track moves under the wheel in opposite direction with the translational velocity.

Now, for a rolling body on a flat surface, such as the train wheel on the rail as shown in figure 3-2, the rolling contact is also present, but the velocity interpretation is slightly different. The flat body is stationary and does not move (note, due to strain, there will be small, induced velocities, but these are insignificant when gross sliding occurs and are neglected for simplicity). The wheel consists of a sliding motion, v_1 , and a pure rotational motion, v_2 . When the wheel rolls freely, v_1 and v_2 are equal and cancel each other out in the contact point, resulting in no slip.

One could plot the velocity field, with the x-axis v_1 , the y-axis v_2 and the z-axis the corresponding slip value. Figure 3-3 shows the 2D top view of the velocity field and the lines corresponds to the 3D velocity field in figure 3-4.

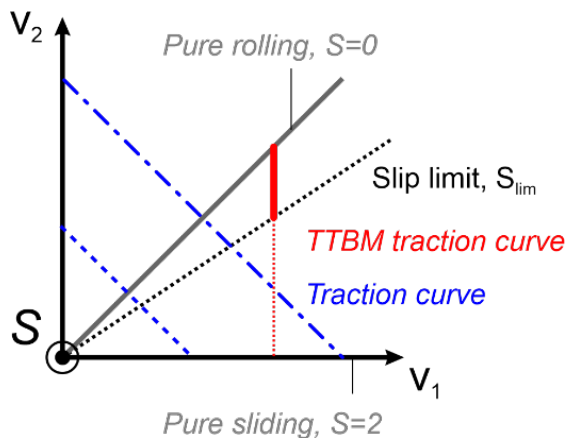


Figure 3-3. 2D velocity field. The coloured lines correspond to the lines shown in figure 3-4.

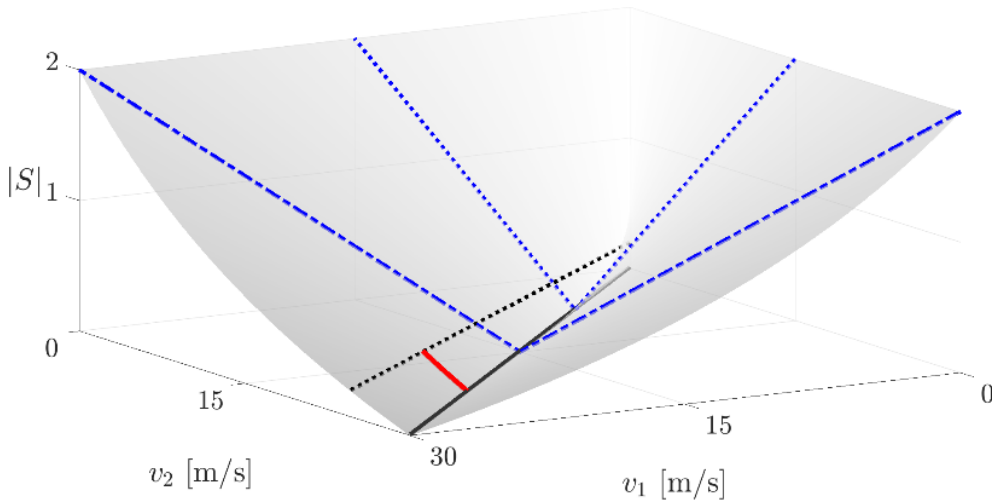


Figure 3-4. 3D velocity field. The black dotted line is the slip limit, which is shown here exaggerated as $S=0.2=20\%$.

Note the following about figures 3-3 and 3-4:

- At the 'pure rolling' line, $v_1 = v_2$ and thus $S = 0$.
- When 'pure sliding' occurs, v_1 or v_2 is zero. Note that by equation 3.1, if $v_1 = 0$ then $S = 2$ and if $v_2 = 0$ then $S = -2$. However, for simplicity only the absolute value is taken throughout the report. Also, knowing that v_1 is the train speed and v_2 is the circumferential wheel speed, two types of pure slip could occur. When the train has a certain speed and brakes too hard, wheel lock or freezing of the wheel could occur, meaning the wheel is not rotating ($S = 2$, $v_2 = 0$). Or when the train is standing still and accelerates, but there is too low grip and the wheels are spinning ($S = 2$, $v_1 = 0$).
- A traction curve relates the CoF to the slip, which will be discussed in section 3.2. Normally, traction curves are at a constant v^+ , orthogonal to the 'pure rolling line', and a varying v^- . Slip would then be: $S = 2/v^+ \cdot v^-$. Note that the slope is constant, but at a lower v^+ , the slope becomes larger, as can be seen by the two blue lines in figure 3-4.
- The TBM traction curve is the main topic throughout the report. During a TBM brake, for a brief period the wheel velocity v_2 is lowered by braking the wheelset. During this period, the train speed v_1 stays roughly constant, while v_2 decreases. This causes a different orientation of the traction curve, as shown in red, in figures 3-3 and 3-4. Note that only up to a certain slip limit will be measured, i.e., braking the wheel to a certain wheel velocity, say 0.1 or 10% slip, since this is the most interesting part of the traction

curve (all braking and accelerating is done within this region, excessive slip, roughly $S > 0.2$, is undesired).

3.1.2 Lateral slip

The wheel is also able to have an angle of attack (AoA) compared to the rail, as shown in figure 3-5.

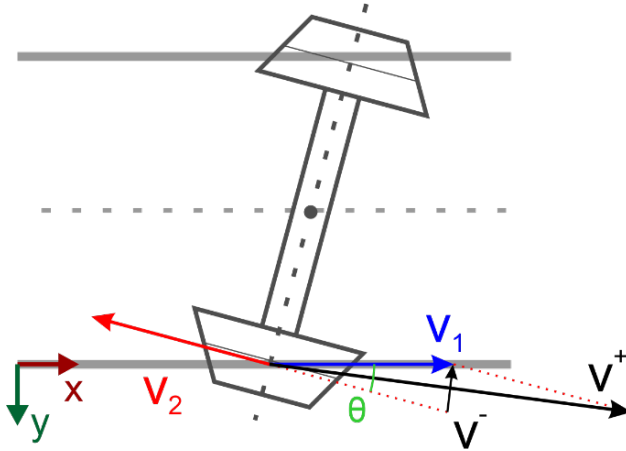


Figure 3-5. The v_1 and v_2 arrows correspond to the left case in figure 3-2. Induced lateral slip by an AoA (shown as theta, θ), changing the direction of v_2 .

To keep the formulas comprehensible and relatable to the TTBM system, a few assumptions were made:

- Only small AoA, up to 8 degrees max.
- V_2 is directed in the direction of the wheel, which is on its turn directed by the AoA.
- V_1 is directed in x-direction.
- During a TTBM brake test, v_2 decreases only a small amount (up to 10% decrease).

The longitudinal slip becomes:

$$S_x = \frac{2 \cdot v_x^-}{v^+} = 2 \cdot \frac{v_1 - \cos(\theta) v_2}{v_1 + v_2} \approx 2 \cdot \frac{v_1 - v_2}{v_1 + v_2} \quad (3.2)$$

Which is roughly the same as equation 3.1. Assuming $v_2=v_1$, the lateral slip reduces to:

$$S_y = \frac{2 \cdot v_y^-}{v^+} = \frac{2 \cdot (0 - \sin(\theta) v_2)}{v_1 + v_2} \approx -\theta \quad (3.3)$$

The lateral slip is mainly induced due to the AoA. Note, within this report if slip is mentioned, then the longitudinal slip (S_x) is referred to. Lateral slip is important when low longitudinal slip is present, however if longitudinal slip is dominant (large compared to lateral slip), which is the case during a TTBM brake, the lateral slip attenuates [11].

3.3.3 Spin

There is also a third type of slip: spin, which is about the rotational velocity discrepancy between the two bodies. For two stationary bodies in contact, see figure 3-6, which only have a rotational velocity among the normal of the contact, the spin velocity is $\omega_{1,z} - \omega_{2,z}$.

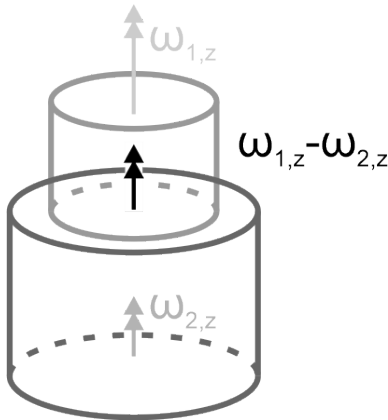


Figure 3-6. Two bodies in contact, only rotating about the vertical z-axis, inducing spin.

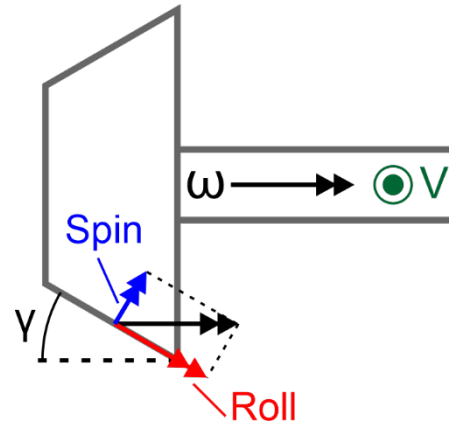


Figure 3-7. The conicity (shown as gamma, γ) causes the rotation motion of the wheel ω to be decomposed in a spin and roll motion in the WRI.

Within a rolling contact, spin could also be present. For the wheel-rail case, spin is introduced by the conicity of the wheel, γ , see figure 3-7. By neglecting the yaw velocity of the wheelset, one could decompose the rotational velocity ω in a pure roll and spin motion. For simplicity, assume $v_1=v_2=v=\omega R$, $\omega_{1,z}=\omega \sin(\gamma)$ and $\omega_{2,z}=0$.

Analogous to the longitudinal and lateral slip, divide the spin velocity by the sum velocity, then the spin (ϕ) could be calculated in the following way:

$$\phi = 2 \cdot \frac{\omega_{1,z} - \omega_{2,z}}{v_1 + v_2} \approx 2 \cdot \frac{\omega \sin(\gamma)}{2\omega R} = \frac{\sin(\gamma)}{R} \quad (3.4)$$

Note, the dimension of spin is [1/m]. A similar equation can be found in [29], however slip has been made dimensionless by multiplying equation 3.4 with $(ab)^{1/2}$, with a and b being the semi-axes of the contact patch. Equation 3.4 has been used instead since this form has been used within VI-Rail [30].

If there is no conicity, then there would be no spin. By increasing the conicity, the spin increases as well. Conicity is not constant among the profile of the wheel, due to the nonlinear profile (the flange has a large conicity, see Appendix A). Also, due to wear of the wheel profile, the conicity changes.

There is a difference in the effects of spin between the stationary spinning contact case (figure 3-6) and the rolling contact case (figure 3-7). Within the stationary spinning contact, only a net torque is present within the contact. For the rolling contact, an additional but small net lateral creep force is present. This effect is known as camber thrust, which is caused by the spin pole being not located at the center of the contact, for more information see [29].

When slip increases, which happens during a TTBM brake test, the effect of spin attenuates and become insignificant. Throughout the report, spin and its effects will not be considered. However, one should know about the presence of slip. Also, spin will become of importance regarding the estimation of the creep coefficient in one of the recommendations in chapter 7.

3.2 Traction curves

Slip was discussed in the previous section. For a rolling contact, free rolling is when there is no slip, i.e., no difference in velocity between the two bodies in contact. When there is a difference in velocity, then the rolling contact can be described by a combination of pure rolling and pure sliding. Within a contact, the CoF is the ratio of the apparent friction force, or tangent force and the normal force:

$$\mu = \frac{F_f}{F_N} \quad (3.5)$$

Within a rolling contact, traction curves relate the coefficient of friction to slip. There are numerous traction curve models that describe the traction curve for a given wheel-rail contact. To keep it comprehensible and relevant for the TTBM project, two types of traction curves will be discussed: the 'dry' and the 'third body' traction curve. The dry traction curve is more related to perfectly described bodies in contact, without the presence of a third body, such as oil, grease, or lubricant, within the contact. The third body traction curve takes the presence of a lubrication film or any kind of third body within the rolling contact into account (lubrication, moist, dirt, leaves etc.), as shown in figure 3.8.

First, three main characteristics of the traction curve will be explained, which are also shown in figure 3.8.

- The creep coefficient is the initial slope of the traction curve. The first part of the traction curve is often referred to as the stable part (positive slope) in literature.
- The peak of the traction curve, the maximum CoF value and its corresponding slip value. Note that for the dry friction curve, the peak value is when the friction limit is reached.
- Behaviour of traction curve at excessive slip, which is after reaching the peak value. For dry friction models the CoF is often constant over slip, but for third body models it depends on the lubrication type, heat development, etc. The region of the traction curve beyond the peak value is in literature often referred to as the unstable part (negative slope).

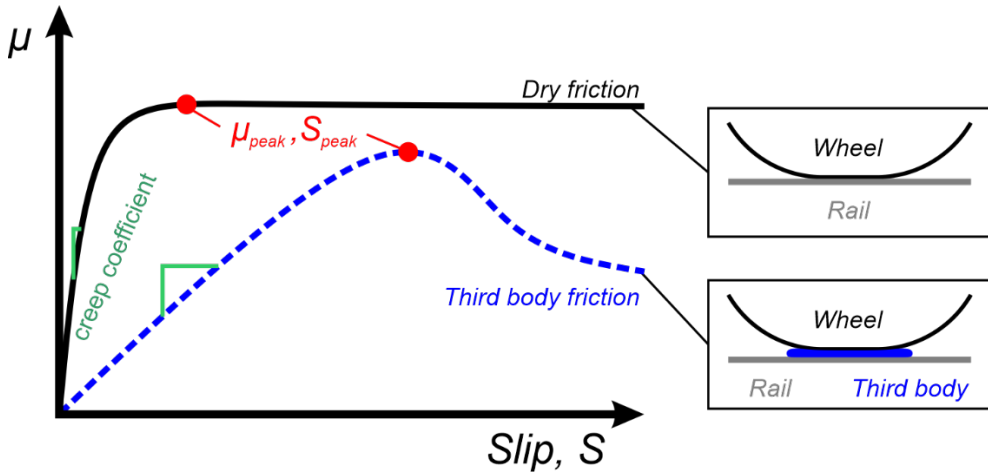


Figure 3-8. Illustrative 'dry' and 'third body' traction curves. The creep coefficient is the slope of the traction curve near $S=0$. The peak value (μ_{peak} , S_{peak}) is when full adhesion is reached (i.e. maximum CoF value) and beyond the peak value is excessive slip or the unstable region.

Note that a huge amount of research is involved regarding traction curves, only the relevance regarding the TTBM system is mentioned here. For both the 'dry' and 'third body' traction curves, a significant number of models exists and have been measured or validated by lab setups. In Appendix F, both the 'dry' and 'third body' traction curves are explained in detail. In figure 3-12 they are compared as well.

3.2.1 Dry traction curve

Hertz gave an analytical solution for the normal contact problem for non-conformal, elastic bodies in contact [31]. The half-ellipsoidal normal pressure distribution could be found as well as the size of the contact patch, given a certain input (material properties, reduced radii, applied normal force). This concerns mainly the normal pressure/force distribution in the contact area, the next step would be the tangential pressure distribution, i.e., friction.

There are lots of theories and models trying to describe the tangential contact problem, various models are well explained in the book of Johnson [29] and the work of Shahzamanian Sichani [32].

The 3D numerical Kalker model is widely used in MBD simulations (also VI-Rail) [33]. Here, the 2D theoretical Carter model will be briefly presented, since the shape and theory behind it is like that of Kalker [34] (Appendix F shows the similarities between Kalker and Carter theory):

$$S = -\frac{\mu_f a}{R} \left\{ 1 - \left(1 - \frac{F_f}{\mu_f F_N} \right)^{\frac{1}{2}} \right\} \quad (3.6)$$

In which μ_f is the friction limit (note, the maximum friction force is bounded by $\mu_f F_N$), a the semi-axis width and R the reduced radii. The shape of the curve remains the same for different friction limits μ_f , as can be seen in figure 3-9. The larger the friction force becomes (and thus the actual CoF), the larger the slip zone is, as shown in figure 3-9. In figure 3-11, the same curves are shown but now with the x- and y-axis as slip and CoF, respectively. One thing to note in figure 3-11 is that, for the same contact problem, the creep coefficient remains the same even when the friction limit changes.

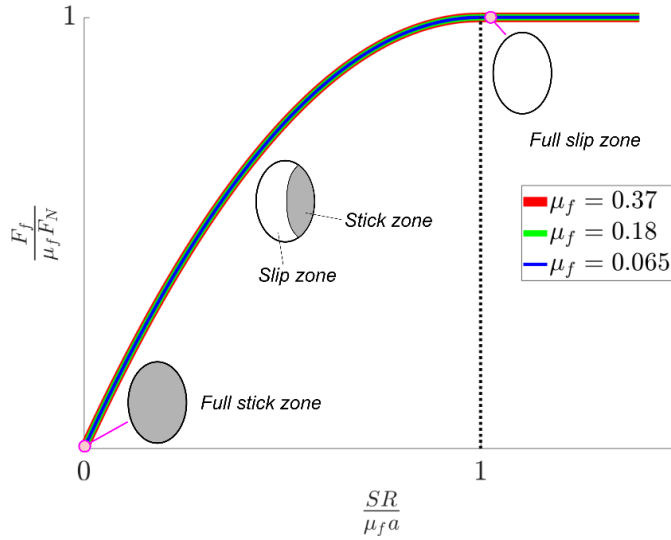


Figure 3-9. The non-dimensional traction curve by Carter theory, equation 3.6. Carter curves shown for different friction limits. The Kalker curve resembles in a similar way, as shown in Appendix F, as well as the contact zone divided in stick-slip zones, hence the elliptical contact patches.

$R_1 = \text{inf.}$, $R_2 = 0.46 \text{ m}$, $F_N = 50 \text{ kN}$, $a = 5.5 \text{ mm}$.

The theoretical/numerical traction curves, by Carter and Kalker, have a proper foundation and have been validated as well with lab tests [29]. However, within these lab tests, the discs used for these experiments were extremely clean and perfect, which is generally not found in real life. Even though that these models have been experimentally validated, other studies carried out experiments under railroad conditions and one main finding was the difference in creep coefficients,

see figure 3-10 [35] and 3-11 [36]. This is also observed in the work of Popovici [11], which would also result in a difference of peak location (figure 3-11) of the traction curve.

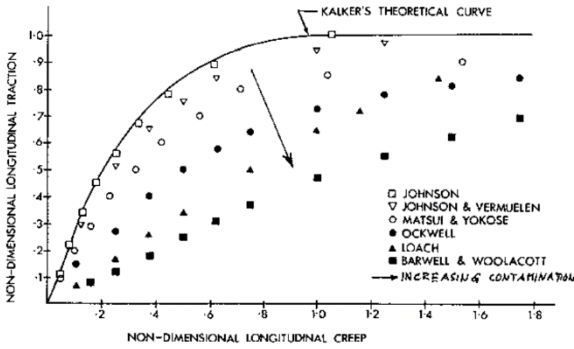


Figure 3-10. Reproduced from [37], data from [35]. Kalker's theoretical curve compared with measured data.

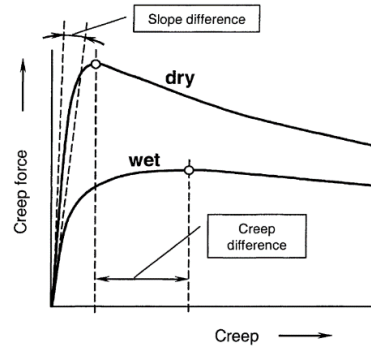


Figure 3-11. Traction curves in presence of a dry and wet contact, figure from [36].

3.2.2 Third body traction curve

In the work of Popovici [11], a friction model is proposed as well, the focus was more on a contact in the presence of a lubrication. In order to describe the Mixed Lubrication (ML) contact, the model incorporates both the boundary layer (BL) contact (which follows the work of Gelinck [38]) and the Elasto-Hydrodynamic (EHL) contact:

$$f_{ML} = \frac{F_{f,BL} + F_{f,EHL}}{F_N} \quad (3.7)$$

In 2010, traction curve measurements have been carried out on the Dutch Railway system by using a roller system. Most of the measured curves could be described by equation 3.7. In [11], the model in equation 3.7 is explained in detail and shows that it depends on rheological and fit parameters, which makes the model rather complex. Rheological parameters of various types of lubricant or grease, typical for the railway environment, have been investigated as well and vary a lot [39]. The model could be used to identify the type of contact (BL, ML or EHL) and to possibly find the rheology parameters of the third body.

In [11], the measured traction curves were sorted based on their peak CoF values into five categories, from high to low and each category is represented by a single

traction curve, which are shown in appendix F. In figure 3-11, three of them are shown and compared with the Carter curves of figure 3-9.

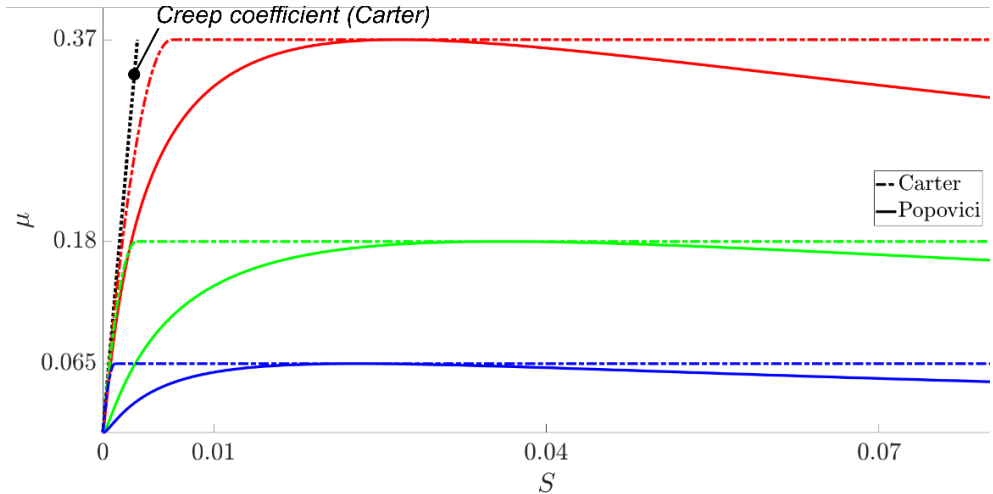


Figure 3-12. Three traction curves by Popovici, as shown in appendix F, compared to the Carter curves shown in figure 3-9.

A few notes on the 'third body' traction curve, compared to the 'dry' traction curve:

- Although a part of the measured traction curves carried out in [11] showed a steep creep coefficient (BL regime or presence of a dry traction curve), the majority showed a much lower creep coefficient. Also note that the creep coefficient varies a lot within 'third body' traction curves, as can be seen in figure 3-11.
- The location of the peak, i.e., at which slip value S_{peak} is the peak CoF or friction limit reached, is different. For the third body traction curve, there might be a relation between the creep coefficient and the peak value. Note that for the dry traction curve, S_{peak} is in the order of 0.1% to 0.5% and for the third body traction curve in the order of 1% to 5%.
- For dry traction curves, once the friction limit is reached, the CoF remains constant and equal to the friction limit, even at higher slip. The third body traction curve behaves differently at higher slip values and show most often a drop in CoF, mainly due to a combination of the presence of a lubricant and heat generation within the contact (which alters the rheological parameters). During normal train operations, one wants to prevent excessive slip within the wheels and thus it is desired to remain within the first part of the traction curve. But it is not uncommon that the wheels will

often operate within this high slip regime, due to presence of low friction and a slow response of the brake system to relieve the brakes.

3.2.3 Traction curve within the MBD simulation model

Both types of traction curve models are validated or measured, as stated in sections 3.2.1 and 3.2.2. Regarding to using it as a numerical model for MBD simulations, both the 'dry' and 'third body' traction curves have their pros and cons.

Kalker creep curves are widely used and accepted, especially in MBD simulations, and Kalkers FastSim is implemented within VI-Rail as well [40]. Because of this, the Kalker, or dry traction curve, will be mainly used.

It is possible to implement custom traction curves, by inserting the CoF and corresponding (longitudinal) slip values. This way, the third body traction curves as mentioned in Appendix F can be used within the VI-Rail simulations, which are discussed in chapter 5.

3.3 Two WRIs in one wheelset

Within one wheelset, two wheels are rigidly connected and are both in contact with the rail. This leads to two wheel-rail interfaces (WRI) within one wheelset, see figure 3-12.

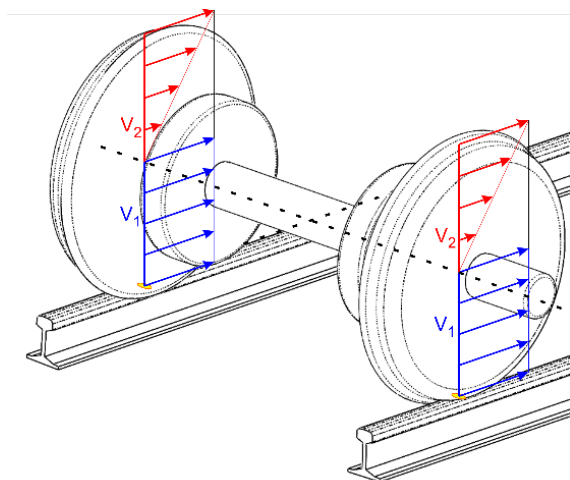


Figure 3-13. The left and right wheel in contact with the rail, resulting in two WRIs. V_1 is the translational velocity of the wheel and v_2 the circumferential velocity of the wheel.

The left and right wheel have the same rotational velocity since they are rigidly connected.

3.3.1 Equal slip in left and right WRI

For simplicity, assume the v_1 profiles and v_2 profiles of the left and right wheel to be the same (note, v_1 and v_2 not necessarily equal). There are a few scenarios mentioned below, leading to slip (equal slip in the left and right WRI):

- Decelerating of a non-driven driven wheelset (by mechanical braking of the wheelset), which leads to the decrease of v_2 , the v_1 reacts but lags (i.e., there is a time difference between the decrease of v_2 and v_1). This is shown in figure 3-14. Note, the TTBM brake is within this category.
- Accelerating of a driven wheelset (by the motor, torque applied in same direction as rolling direction). This leads to the increase of v_2 . As shown in figure 3-15, the v_1 profile reacts but lags, which is roughly equal to the train speed. Decelerating of the driven wheelset (by e.g., electric braking) leads to a decrease of v_2 while v_1 reacts, which is eventually the same scenario as in figure 3-14.
- Accelerating of a non-driven wheelset means it is pushed by the train itself. E.g., when the train stands still and the driven wheels are engaged to accelerate, the train then pushes the non-driven wheelsets at the axles. This increases the v_1 profile, the v_2 profile reacts but lags. Decelerating of the train itself pulls the non-driven wheelsets in the same manner, causing a decrease in the v_1 profile, the v_2 profile reacts but lags.

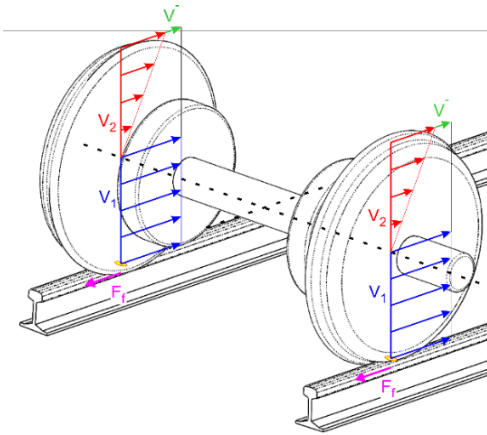


Figure 3-14. Decelerating the wheelset decreases the v_2 , while the v_1 reacts slowly. Slip is induced, causing a friction force F_f that will eventually reduce v_1 .

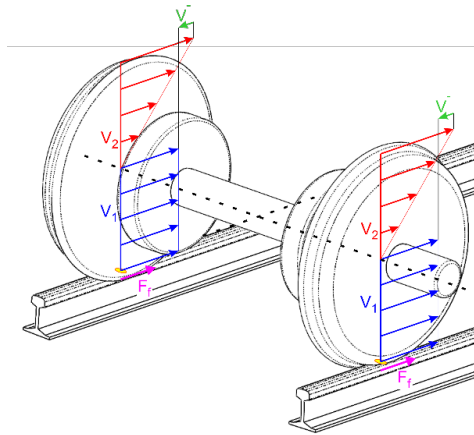


Figure 3-15. Accelerating the wheelset increases the v_2 , while the v_1 reacts slowly. Slip is induced, causing a friction force F_f that will eventually increase v_1 .

3.3.2 Slip difference between left and right WRI

The slip in the left and right wheel in figures 3-14 and 3-15 are roughly the same. However, due to various circumstances, the slip in the left and right contact may differ at certain moments. Due to a yaw velocity or a change in different rolling radii between the left and right wheel, the slip differs between the left and right WRI, as can be seen in the figures 3-15 and 3-16, respectively.

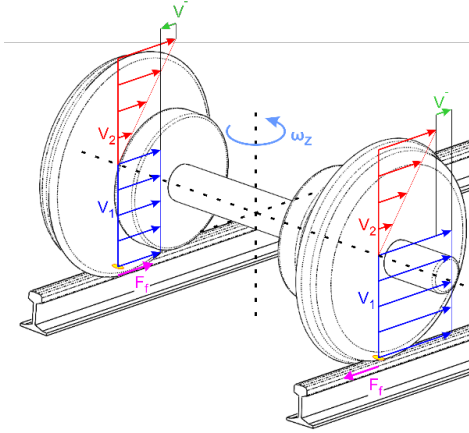


Figure 3-16. Yawing of the wheelset (ω_z). The V_2 profile left and right wheel are the same, due to yawing a different v_1 profile between the left and right wheel.

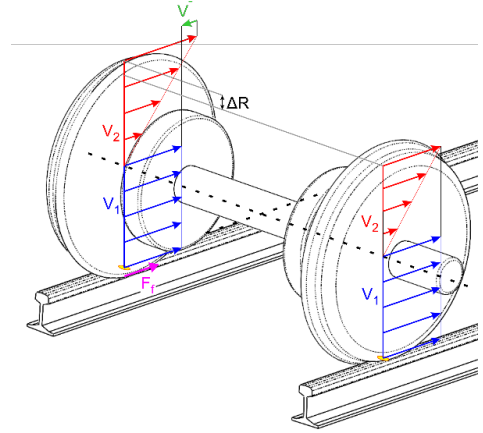


Figure 3-17. A difference in rolling radii (ΔR). The V_1 profile left and right wheel are the same, due to ΔR , a different v_2 profile between the left and right wheel.

Besides a difference in slip, the normal forces could differ as well among the two WRIs, e.g., when the train is passing a curved track (larger normal force on the outer wheels). Under the same friction conditions, this would still lead to different friction forces within the left and right WRI of a wheelset.

Slip and friction force in the longitudinal direction are of interest since these will be measured by the TTBM. The TTBM measures the average slip and friction force of the left and right wheel of the wheelset. Because of this, the average of the left and right WRI will be taken in the following manner:

$$F_{N,LR} = \frac{F_{N,L} + F_{N,R}}{2}; \quad F_{f,LR} = \frac{F_{f,L} + F_{f,R}}{2}; \quad S_{LR} = \frac{S_{x,L} + S_{x,R}}{2} \quad (3.8)$$

The lateral forces, caused by either lateral creepage and/or spin, are not significant at gross slip. Also, these forces will not be measured by the TTBM, since these forces are parallel to the axis of rotation. Only friction force in longitudinal direction will be measured, since it is the only direction where the sensor is sensitive for as it is mounted on the brake, see chapter 4. Hence, these will remain more on the background and only specifically mentioned where needed throughout the report. A visual representation of it is shown in figure 3-18.

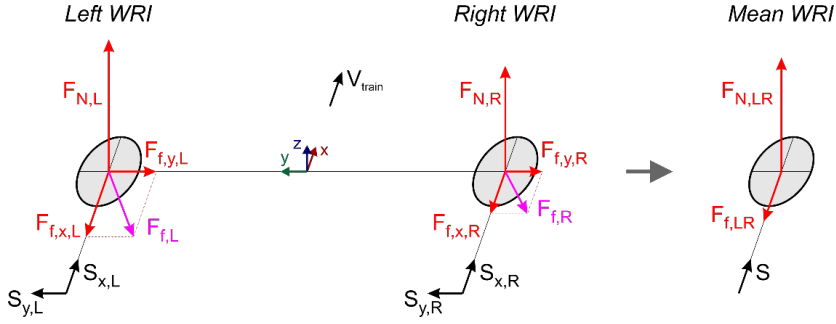


Figure 3-18. The left and right WRI, indicated with the subscripts L and R respectively, are combined to one average WRI using equation 3.8. The subscripts x and y mean longitudinal and lateral direction, respectively.

3.4 Conclusion

Within a rolling contact, such as the WRI, relating the occurring friction coefficient to the induced slip results in a traction curve. Two types of traction curves are presented in this chapter, the ‘dry’ and ‘third body’ traction curves. The dry traction curve has a high, relatively constant, creep coefficient and a constant CoF at excessive slip whereas the third body traction curve has a relatively low, and a variety of creep coefficients (depending on the contaminant within the WRI) and shows most often a drop in CoF at excessive slip. The ‘dry’ traction curves are mostly present under lab conditions (clean and smooth) whereas the ‘third body’ traction curves occur more often within the wheel-rail interface. Both traction curve types will be included within the simulations.

The two contact points of the wheelset, i.e., the two WRIs, are coupled and will influence each other, which will be a cause for errors. Regarding the TTBM system and throughout this report, the longitudinal slip and friction force will be of main interest. Lateral slip and spin are present as well and will be a source of measurement errors, as they are expected to be less relevant, they will not be considered in this thesis.

Also, the average of the left and right contact will be measured by the TTBM. Slip, friction force and normal force within the wheelset will be referred to as equation 3.8. The slip and CoF will be determined in the following way:

$$S = 2 \cdot \frac{|v_1 - v_2|}{v_1 + v_2}; \quad \mu = \frac{F_f}{F_N} \quad (3.9)$$

Chapter 4 - Train tribometer

4.1 TTBM concept

A train consists out of a certain number of wagons. The wagons are connected by means of buffers. A wagon typically has two bogies underneath it. Throughout the report, the Y32 bogie will be referred to, which is shown in figure 4-1. The bogie consists of the bogie frame, two wheelsets or axles and four axle boxes. One wheelset contains two wheels and two brake discs. The primary suspension (PS) is the suspension between the wheelset and bogie, on both sides of the wheelset. The secondary suspension (SS) is between bogie and wagon.

Within a non-driven bogie, for a brief period (in the order of seconds) one wheelset will be braked. The applied brake force by the brake pads results in a brake torque T_R , as shown in figure 4-2, which reduces the rotational velocity of the braked wheelset ω_2 . This results in slip and the accompanying friction force within the WRIs of the braked wheelset. By measuring the rotational velocity of the non-braked wheelset (ω_1) and braked wheelset (ω_2), one can determine the slip.

The traction curve is the relation between the CoF and the slip, in this case within the WRI. The CoF part will be discussed in section 4.2, which involves the brake system to determine the friction force and the normal force. In section 4.3, the slip, and its longitudinal and circumferential velocity, v_1 and v_2 respectively, will be discussed how it is measured. Section 4.4 shows the design parameters for the TTBM brake, which involves the measurement range of the traction curves and how fast one wants to carry out the TTBM brake. Section 4.5 is about the right calibration and the effect of train parameters errors on the CoF and slip estimation as well as the required resolution of sensors given a certain CoF and slip resolution.

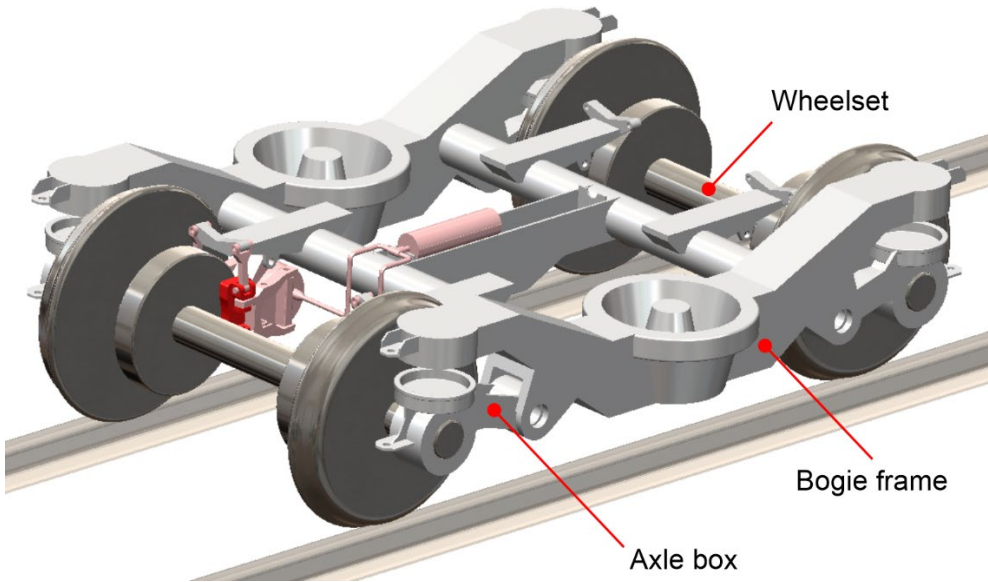


Figure 4-1. A non-driven Y32 bogie, in which the TTBM system will be integrated.

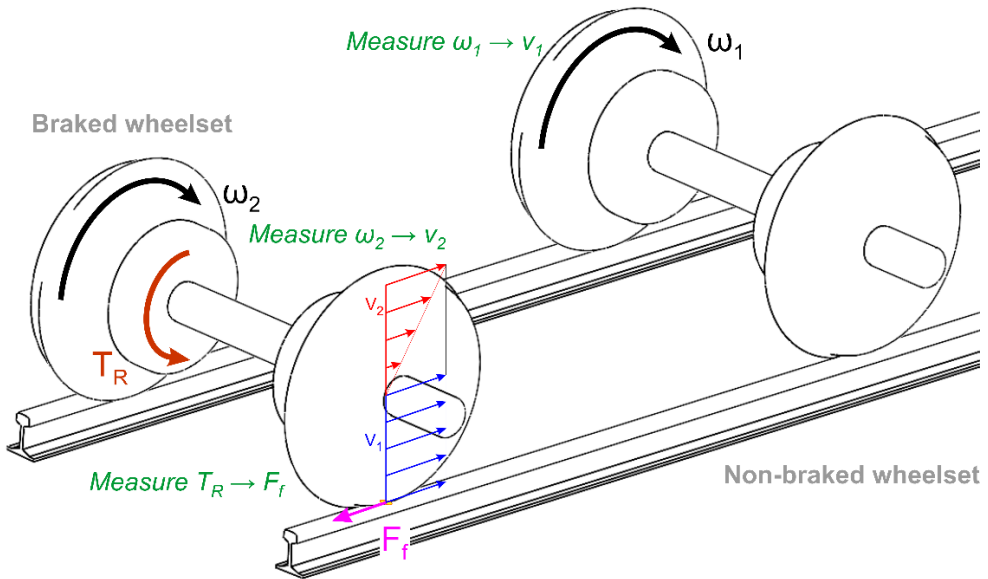


Figure 4-2. The velocities and forces of the TTBM. V_1 and V_2 are estimated by measuring ω_1 and ω_2 , respectively. The friction force will be estimated by measuring the applied brake torque, T_R .

4.2 Coefficient of Friction estimation

Within the TTBM, the longitudinal friction force will be determined:

$$\mu = \frac{F_f}{F_N} \quad (4.1)$$

4.2.1 Friction force estimation – Brake system

In figure 4-1, the brake system of a single wheelset is highlighted in red. In figure 4-3, the forces during braking are shown. The cylinder is being pressurized, F_{cyl} , and extends. The horizontal hinges pivot about the fixed plate and pinch the brake pads, F_{pinch} , onto the brake disc.

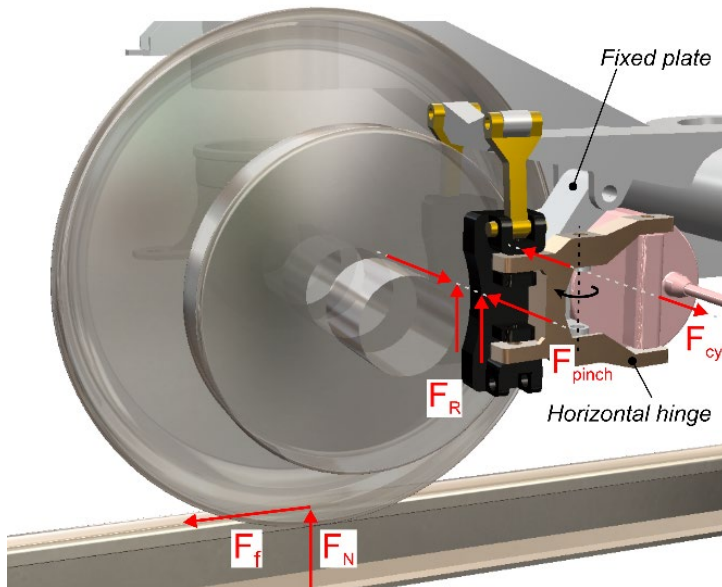


Figure 4-3. The forces involved within the brake system.

A sliding contact is present between the brake pad and brake disc, in which the brake force is generated:

$$F_R = \mu_{pad} F_{pinch} \quad (4.2)$$

Note that μ_{pad} is the CoF between brake pad and brake disc. F_R is the actual brake force that decelerates the rotational velocity of the wheelset. The μ_{pad} is a varying

parameter, which is hard to determine. Hence for the simulations in chapter 5, the model is simplified by directly applying the brake torque T_R .

The brake force is applied to rotationally slow down the wheelset to induce slip, which on its turn generates the friction force within the WRI. The distance between brake pad and center wheel, c , is the arm of the brake force resulting in the brake torque, T_R . The friction force in combination with the wheel radius also leads to a torque, T_f :

$$T_R = c \cdot F_R; \quad T_f = R \cdot F_f \quad (4.3)$$

By looking at the forces and moments acting on the wheel in figure 4-4 and by solving the momentum equation about the wheel axis, one finds:

$$I\alpha = T_f - T_R \quad (4.4)$$

In which I is the inertia of the wheelset and α the rotational acceleration.

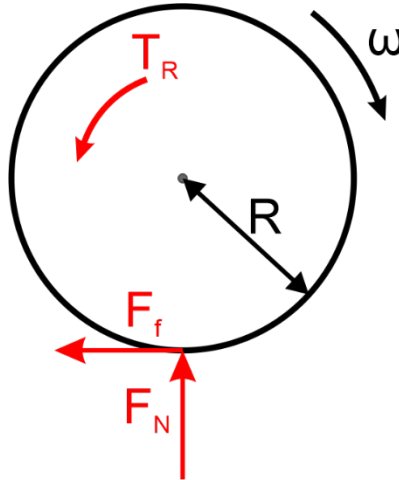


Figure 4-4. Simplified 2D of figure 4-3. Note, $T_f = R \cdot F_f$.

The friction force can be determined by substituting equation 4.3 into 4.4 and to solve for F_f :

$$F_f = \frac{c}{R} F_R + \frac{I}{R} \alpha \quad (4.5)$$

In which R is the radius of the braked-wheelset. The first term on the RHS in equation 4.5 is determined by measuring the applied brake force F_R .

The second term on the RHS in equation 4.4 involves the dynamic part. This term is especially important during a TTBM brake test in presence of low adhesion. By measuring ω_z (section 4.3), one could estimate α by taking the time derivative. However, the deceleration is hard to determine, due to the certain resolution a tachometer has.

The applied brake force is the input of the system. The influence of the shape of the brake force (ramp or step function) and how the system reacts is discussed in Appendix B. To lower the rotational deceleration of the wheel and the jerk motion, the ramp function has been mainly used within the simulations, as shown in figure 4-5. The duration of the TTBM brake (T) and the height of the applied brake force ($F_{R,max}$) will be discussed in section 4.4, which are related to the TTBM brake strategy.

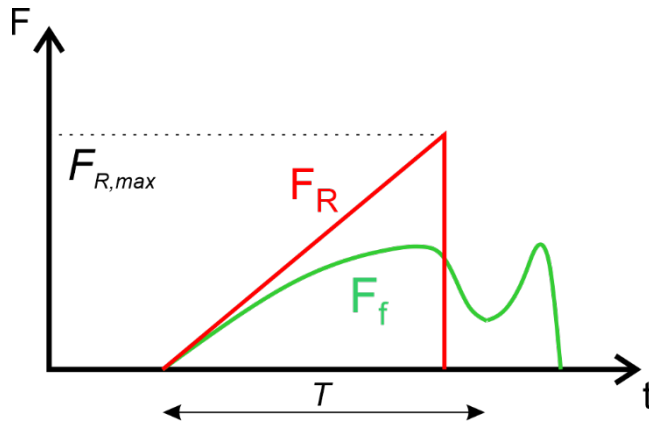


Figure 4-5. Brake force input profile, with T the duration of the TTBM brake and height F_R linked to the μ_{max} one wants to measure, as indicated in equation 4.9. F_f , the friction force, is the response.

4.2.2 Normal force estimation

There are a few ways to determine the normal force in the wheel-rail contact. The simplest one is by determining the expected static normal force on the wheelset, F_z , by just simply weighing the train to determine the static normal force felt on the braked wheelset. This expected static normal force on the wheelset can also be estimated by looking at the mass distribution among the wheelsets:

$$F_z = g \cdot \frac{1}{4} M_{CTO} = g \cdot \left(\frac{1}{4} M_{wagon} + \frac{1}{2} M_{bogie} + M_{wheelset} \right) \quad (4.6)$$

In which g is the gravitational acceleration and M the mass (the subscript refers to a certain body, the weight values are shown in Table 5-1 in chapter 5). The normal forces among all wheelsets and among the left and right wheel of one wheelset during normal train operation and during a TTBM brake test will vary, which will be further elaborated within section 5.4. To account for these dynamic normal force variations, one could use a mathematical model to estimate these variations during a TTBM brake test, or integrate normal force transducers within the bogie, as is presented in section 6.2. To keep the simulation results in chapter 5 comprehensible, only equation 4.6 is used.

4.3 Slip estimation braked wheelset

4.3.1 Translational velocity v_1

Note that both the v_1 and v_2 components are within the braked wheelset, but often the v_1 component is assumed to be the train speed, which is not necessarily the same. The longitudinal velocity of the braked wheelset will be determined in the following way:

$$v_1 = \omega_{non-braked} \cdot R_{non-braked} = \omega_1 \cdot R_1 \quad (4.7)$$

In which ω_1 is the rotational velocity and R_1 the radius of the non-braked wheelset in figure 4-2.

4.3.2 Rotational velocity v_2

The circumferential velocity of the braked wheelset will be determined in the following way:

$$v_2 = \omega_{braked} \cdot R_{braked} = \omega_2 \cdot R_2 \quad (4.8)$$

In which ω_2 is the rotational velocity and R_2 the radius of the braked wheelset in figure 4-2. Note that throughout this report R_2 will be often simply written as R .

4.3.3 Combining velocity values

As discussed in chapter 3, within the TTBM, the velocity components v_1 and v_2 within the rolling contact were explained. The longitudinal slip is:

$$S = 2 \cdot \frac{v_1 - v_2}{v_1 + v_2} \quad (4.9)$$

By substituting equations 4.7 and 4.8 into 4.9, one finds:

$$S = 2 \cdot \frac{\omega_1 R_1 - \omega_2 R_2}{\omega_1 R_1 + \omega_2 R_2} \quad (4.10)$$

The nominal radii (R_0) of the braked and non-braked wheelsets need to be determined. Note that the wheel profile is conical and non-linear (it has a flange) as shown in Appendix A. The train and its wheelsets do not roll on one fixed radius, the train hunts and as a result the actual rolling radii changes slightly.

4.4 Measurement Strategy - Design variables

In chapter 2, the measurement range of the traction curve was mentioned and is shown in figure 4-6. Here, the effects on the TTBM system by changing the measurement range, which is spanned by the maximum CoF one wants to measure (μ_{max}) and up to a certain slip limit (S_{lim}), will be discussed further.

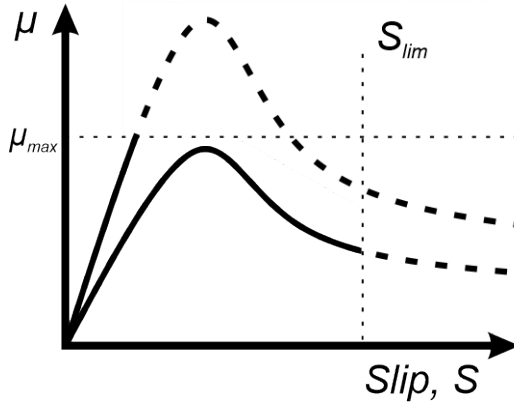


Figure 4-6. Traction curve measurement range.

By rewriting equation 4-1, substituting into equation 4-5 and solve for F_R , gives:

$$F_{R,max} = \frac{R}{c} \mu_{max} F_N - \frac{I}{c} \alpha \quad (4.11)$$

Note, if one wants to measure up to a higher CoF, one needs to apply a larger brake force. Looking at the requirements in section 2.4.1, μ_{max} will be set on 0.2 (note, the requirements in Table 2-3 are not fixed, a different use case leads to different requirements and thus may change). Measuring above a CoF value of 0.25 would not make sense since the available friction is already high enough and above that value one would measure too high friction.

The dynamic part in equation 4.11 is less obvious, but if one wants to brake fast, i.e., in a short time window to reach the desired slip limit, then the dynamic terms can become significant.

Suppose a TTBM brake is carried out up to a certain slip limit and at a constant train speed (assume v_1 is roughly constant and equal to the train speed). One could rewrite equation 4.9 to find the value of the circumferential velocity of the braked wheelset at the slip limit:

$$v_{2,lim} = \frac{2 - S_{lim}}{2 + S_{lim}} \cdot v_1 \approx (1 - S_{lim}) \cdot v_1 \quad (4.12)$$

In which the approximation step is valid for small slip, one could use a simplified slip equation: $S = \frac{v_1 - v_2}{v_1}$ (at $S_{lim} = 0.1$, or 10% slip, the slip error is less than 1% using the simplified form) [41]. The rotational velocity of the braked wheelset was at the initial state at v_1/R and when reaching the slip limit at $v_{2,lim}/R$. If the TTBM brake is carried out within the time window T , the average rotational deceleration is then:

$$\alpha = \frac{(v_{2,lim} - v_1)}{R \cdot T} = -\frac{v_1 S_{lim}}{R \cdot T} \quad (4.13)$$

In which T is the duration of the TTBM brake (going from v_1 to $v_{2,lim}$). Note, this is an average deceleration. Due to the non-linear behaviour of the traction curve, equation 4.13 should be treated carefully. When the applied brake force is high enough to reach the peak value of the traction curve, a sudden increase in deceleration of the wheel will follow due to the drop in available friction.

One way to attenuate the dynamic term is thus by increasing slowly the brake force. However, at a train speed of 108 km/h, a four second duration of the TTBM brake would already lead to 120 m distance covered on the track, which is not desired. Also, the longer the TTBM brake, the longer the actual brake force and thus friction force within the WRI are present. This will slightly slow down the train and leads to increased wear as well.

Decreasing the time to brake would lead to a measurement over a short track distance, but a higher brake force is needed in order to reach the slip limit within the shorter interval. This will result in higher deceleration values. In Appendix B, an example is given and shows that for roughly a brake duration of 1 second, the inertia term in equation 4.11 is about 5% of the total brake force. Decreasing the

time to brake further will significantly increase the inertia term in equation 4.11, leading to a larger required brake force. Hence the TTBM brake will be set onto 1 second.

The higher the slip limit, the higher the circumferential velocity drop is, as can be seen in equation 4.12. One wants to keep this low to reduce wear, however a certain part of the traction curve needs to be measured. For now, this value should be beyond the peak value to measure the actual peak value of the traction curve, see figure 4-6, and to attenuate lateral slip effects (section 3.1.2). Hence the slip limit will be set at least at 5%, due to the location of the peak value of the ‘third body’ traction curves mentioned in section 3.2.

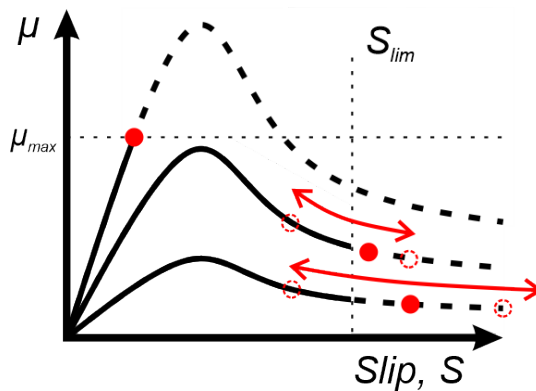


Figure 4-7. In presence of extreme low friction, overshoot may occur. In presence of extreme high friction, the slip limit may not be reached.

There are a few points to consider regarding the ‘fixed’ brake force profile, which are explained in detail in Appendix B as well:

- In presence of extreme low friction, the applied brake force will decelerate the wheelset fast, which leads to a fast-reaching slip limit of the braked wheelset. When the slip limit is reached, the brake force needs to be relieved. If this response (the relieve of the applied brake force) is not fast enough, the wheelset will continue to decelerate and the slip increases, see figure 4-7, which leads to wheel locking (i.e. high or even full slip) and flat spots. A fast-responding brake system is needed.
- When the actual available friction is higher than the friction one wants to measure (μ_{max}), one does not reach the slip limit but stays in the stable part of the traction curve, as can be seen in figure 4-7 as well.

How the actual brake force profile is going to look like is not definitive. Many parameters are involved, and one can design various brake strategies. This brake force profile should be designed to decrease the TTBM brake time (T) while keeping the deceleration values insignificant. Also, if one wants to increase the frequency of measurements, the amount of work done within the brake pads and WRI increases as well, as shown in Appendix B. The TTBM brake design parameters are shown in Table 4-1.

μ_{\max}	S_{\lim}	T
0.2	5%	1 s

Table 4-1. TTBM brake design parameters

4.5 Calibration and sensor resolution

For convenience, the slip and friction coefficient formulas are shown here. In equations 4.14 and 4.15, the red symbols are system parameters, and the blue symbols are the parameters measured by the sensors.

$$S = 2 \cdot \frac{v_1 - v_2}{v_1 + v_2} \rightarrow v_1 = \omega_1 \cdot R_1; \quad v_2 = \omega_2 \cdot R_2 \quad (4.14)$$

$$\mu = \frac{F_f}{F_N} \rightarrow F_f = \frac{c}{R} F_R + \frac{I}{R} \alpha; \quad F_N = F_Z \quad (4.15)$$

Three types of errors will be discussed within this report:

- The first type of error, the system parameter calibration error, discussed in section 4.5.1, will be referred to as the Δ_c error and is about the systematic error or bias in the measured data, see figure 4-8.
- The second type of error, the sensor resolution, discussed in section 4.5.2, is about the minimal change needed at the input to be detected by the sensors. This will be indicated with the letter 'd', an example of a schematic slip measurement is shown in figure 4-9, in which the slip resolution is indicated with dS.
- The third type of error, the estimation error, is introduced by the TTBM itself and how it measures, this will be referred to as the Δ error and will be discussed in chapter 5. This error has to do with deviation or spread, see figure 4-8.

An example is shown in figure 4-9 regarding a schematic slip measurement, in which the slip is increased linearly over time. Figure 4-9 shows the first error (the slip calibration error $\Delta_c S$) and the second error (the sensor resolution dS). In chapter 5, these two errors will not be regarded, perfect train system calibration, sensor calibration and sensor resolution will be assumed. A third type of error still exists, also shown in figure 4-9 as the slip estimation error ΔS , which will be investigated in chapter 5.

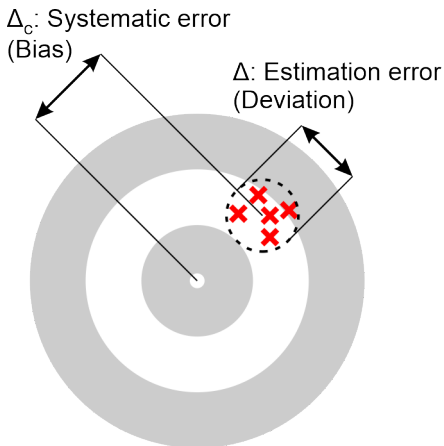


Figure 4-8. Schematic representation of the bias error (calibration error Δ_c) and the deviation error (estimation error Δ).

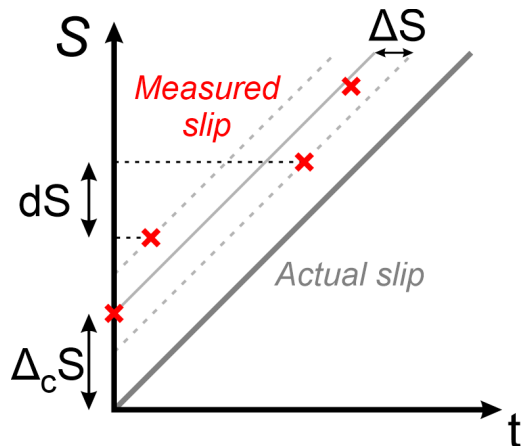


Figure 4-9. Schematic slip measurement, showing the slip system parameter calibration error Δ_c , the slip resolution step dS and the slip estimation error ΔS .

Note, when talking about measuring traction curves, 'resolution' is about how refined the traction curves are measured. E.g., a high resolution traction curve means that both the CoF and slip needs to be measured with small resolution steps, i.e. $d\mu$ and dS , respectively.

Also, one may encounter words as 'accuracy' and 'precision' when dealing with sensors, however they may mean different things or remain unclear when considering for example the different types of errors. For simplicity, in this report, these words correspond to the degree of overall error. If the measured traction curve is of high resolution, it may still be congested with certain errors. However, if the measured values are close to the actual values, the error is small, then the measured data is of high accuracy.

4.5.1 Calibration of system parameters

Upon determining the CoF and slip, as discussed in sections 4.2 and 4.3, a few system parameters showed up which need to be determined: The distance between brake force and center wheel, the wheel radii, wheelset inertia and the mass of the train. Those parameters are treated as fixed in equations 4.14 and 4.15, but still need to be determined correctly by calibration.

No or wrong calibration could lead to significant errors of these parameters which on their turn lead to errors in determining slip and CoF. Derivations of the formulas regarding CoF and slip errors due to errors in system parameters as well as numerical examples and explanations are presented in Appendix C, Table 4-2 is the short version of Appendix C.

CoF error, $\Delta_c\mu$	
Error in distance estimation between brake force and center wheel, 'c'	$\Delta_c\mu = \frac{\frac{\Delta_c c}{R} F_R}{F_Z}; \quad \frac{\Delta_c\mu}{\mu} = \frac{\Delta_c c}{c}$
Error in expected static normal force F_Z	$\frac{\Delta_c\mu}{\mu} = -\frac{\Delta_c F_Z}{F_Z + \Delta_c F_Z}$
Slip error, $\Delta_c S$	
Slip error (for $S < 10\%$), due to change in rolling radius R_2 (same formula if only R_1 has an error $\Delta_c R$ in wheel radius)	$\Delta_c S = \frac{\Delta_c R}{R_2}$

Table 4-2. Errors in parameters leading to certain CoF and slip errors.

Note that certain parameters may not be constant over time. Due to wear, the radii of the wheel decreases and will reduce the inertia of the wheelset as well. Wear of the brake pads might lead to slight changes in distance between applied brake force and center wheel. How these parameters need to be calibrated and which strategies to use for e.g., a changing wheel radius during its lifetime, will not be discussed in this report and such parameters are assumed to be known.

An important note regarding wheel radii. In Appendix A, the wheel profile is shown, which is conically shaped in the linear part and has a flange, the non-linear part. Within such a profile, a nominal wheel radius, R_0 , is often denoted. One could calibrate/determine this nominal radius perfectly. But due to hunting and track irregularities, the actual rolling radius changes continuously. This will be discussed in chapter 5.

4.5.2 Sensor resolution

When measuring the CoF and slip, a certain measurement resolution ($d\mu$ and dS) is desired. In Appendix C, the required friction and normal force resolution as well as the required v_1 and v_2 resolution for a certain desired slip and CoF resolution are derived. Table 4-3 summarizes the resolution formulas (note, as stated in section 2.4.1, the values for $d\mu$ and dS are not fixed). By using the values stated in Table B-1 in Appendix B, one would get the values in the last column in Table 4-3.

CoF ($d\mu = 0.01$)		TTBM train considered
Friction force resolution	$dF_f = F_N d\mu$	$dF_f = 1.09 \text{ kN}$
Brake force resolution	$dF_R = \frac{R}{c} F_N d\mu$	$dF_R = 2.28 \text{ kN}$
Normal force resolution (at $\mu = 0.2$)	$dF_N = -F_N \frac{d\mu}{\mu}$	$dF_N = 5.45 \text{ kN}$
Slip ($dS = 0.001$)		
Braked wheelset tachometer resolution (at $v_1 = 40 \text{ m/s} = 144 \text{ km/h}$)	$dv_2 = -v_1 dS$	$dv_2 = 0.04 \text{ m/s}$
Braked wheelset tachometer resolution (at $v_1 = 10 \text{ m/s} = 36 \text{ km/h}$)	$dv_2 = -v_1 dS$	$dv_2 = 0.01 \text{ m/s}$

Table 4-3. The required resolutions of sensors for a certain slip and CoF resolution.

The friction force is determined by measuring the brake forces. However, if force transducers within the brake pads are used, one needs to be careful of heat generation, which could influence the readout of the sensors. Again, calibration of these sensors will not be discussed in this report but will be done at a later stage.

Most tachometers are equipped with an encoder, the number of pulses determine the rotational velocity. One should be aware of the operating conditions of these tachometers. At low train speeds (lower than 40 km/h) the tachometers might have a different resolution than at high speeds (140 km/h). The same slip resolution step is desired, however at lower train speeds, it might be harder to achieve the desired

slip resolution, see Appendix B. One might consider altering the brake force profile (e.g., increase the duration of the TTBM brake) at lower train speeds.

4.6 Conclusion

How the TTBM operates and how the CoF and slip are measured were presented in this chapter. The brake force is the input of the system, which generates slip within the WRI and leads to the friction force within the WRI. The brake force will be measured to estimate the friction force and the static normal force will be used to estimate the normal force, which combined lead to the estimation of the CoF. Both the rotational velocities of the braked wheelset (to estimate the circumferential velocity v_2) and non-braked wheelset (which will be used to estimate the translational velocity v_1 of the braked wheelset) will be measured to determine the slip in the braked wheelset.

The brake force profile has multiple design parameters, in which the measurement range (μ_{\max} , S_{\lim}) and the duration of the TTBM brake (T) can be tuned for different purposes. To meet the requirement set in section 2.4.1, these will be roughly set to:

- μ_{\max} will be set to 0.2, to measure the low friction regime and if sufficient friction is present for accelerating the train.
- S_{\lim} should be at least 5% to measure the peak values of traction curves.
- The duration of the TTBM brake (T) will be set roughly to 1 second. Lowering this value would lead to increased rotational acceleration of the wheelset, which requires a significantly higher brake force. Increasing the duration would lead to larger track distance covered when carrying out the TTBM brake test.

Several compound of errors occur when determining CoF (by the estimation of the friction and normal force) and slip (by the estimation of the translational velocity v_1 and circumferential velocity v_2). Two types of errors are presented in this chapter. The first one originates from faulty or imperfect system parameter calibration (bias error) and the second one is about the sensor resolution (step increment in measuring data). Calibration of the system parameters (radii wheels, train weight etc.) and calibration of the sensors are important, but how the calibration method is going to be will be done at a later stage (TRL 4 to 7).

A summary of the calibration errors and required sensor resolution are shown in Tables 4-2 and 4-3, but will not be considered within the simulations in the next chapter, perfect calibration and sensor resolution will be assumed. Instead, a third

type of error will be investigated, which is about how the TTBM operates. The measured non-braked wheelset rotational velocity is an *estimation* of the translational velocity of the braked wheelset, *variation* in normal forces do occur during train operations and one may encounter flange contact due to track irregularities. This will introduce certain errors in estimating the traction curves, which will be discussed in chapter 5.

Chapter 5 - Multi-Body Dynamics simulations

Within the VI-Rail multibody dynamic simulation software, the train tribometer is simulated. Recalling the goals set in section 2.5, the focus of the simulations is to do a feasibility analysis of the TTBM. Errors made within the TTBM as well as potential pitfalls of the TTBM system will be analysed.

5.1 VI-Rail model

5.1.1 LOC-CTO model

A locomotive and CTO measurement train (LOC-CTO) combination has first been modelled, in which the trailing bogie of the CTO is the TTBM bogie, see figure 5-1.

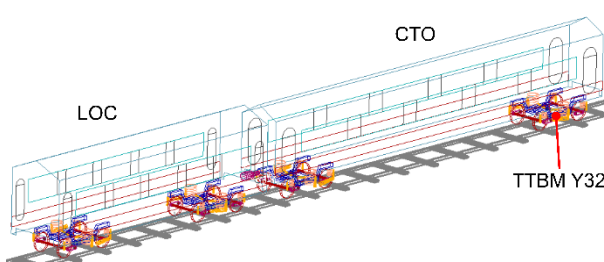


Figure 5-1. LOC-CTO model in VI-Rail.

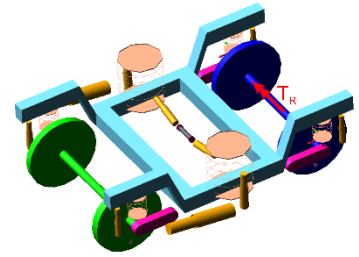


Figure 5-2. TTBM Y32 bogie.

The Y32 bogie is shown in figure 5-2, in which the trailing wheelset is the TTBM wheelset, on which the brake torque T_R is applied for a brief moment. The relevant data of the LOC-CTO and the Y32 are shown in Table 5-1. The S1002 wheel profile has been used for the wheelsets with a nominal rolling radius of 0.46 m, which is shown in Appendix A.

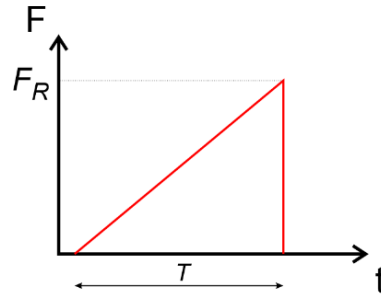
Parameter	Value
M_{LOC}	72.5 ton
M_{CTO}	43.5 ton
$I_{wheelset}$	122 kg m ²
R_0	0.46 m
c	0.22 m
V_{train}	80 km/h

Table 5-1. CTO-LOC parameters used for the simulations.

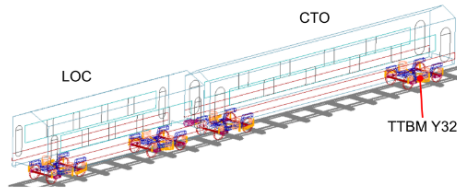
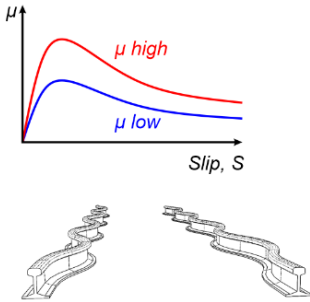
By linking Matlab-Simulink to VI-Rail, one is able to implement the input brake force profile. The input, system itself and output of the model are shown in figure 5-3.

Input

Set: track and irregularities,
train speed, traction curve,
train de-/acceleration



System



Output

'Unknown' parameters:
Slip, friction force,
normal force

'Measured' parameters:
Brake force,
rotational velocities ω_1 , ω_2

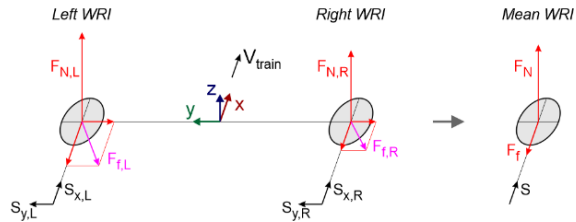


Figure 5-3. The input-system-output within the Simulink and VI-Rail simulations.

The train (wheelsets, bogie frames, wagons etc.) interacting with the rail is the system. The brake force profile F_R is the input of the system (as well as the initial conditions, e.g., train speed and used traction curve). The normal forces $F_{N,L}$ and $F_{N,R}$, friction forces $F_{f,L}$ and $F_{f,R}$, and slip values S_L and S_R , are calculated by VI-Rail. These parameters are the output of the system and are treated as 'unknown'. The rotational velocities ω_1 and ω_2 are also output parameters, which are measured. The brake force F_R is also measured and regarded as known as well.

5.1.2 Track

Straight tracks will be mainly investigated. Curved tracks are considered as well but limited to a few scenarios since curved tracks introduce a huge number of extra parameters. Perfect straight tracks would have the same rail profile in longitudinal direction (no small errors in the track occur), as can be seen in figure 5-4, subfigure a.

The UIC54 profile is mainly used for the tracks in the Netherlands and thus has been used in the simulations and is shown in Appendix A. The track width is 1.435 m and the rails are 1/40 inclined.

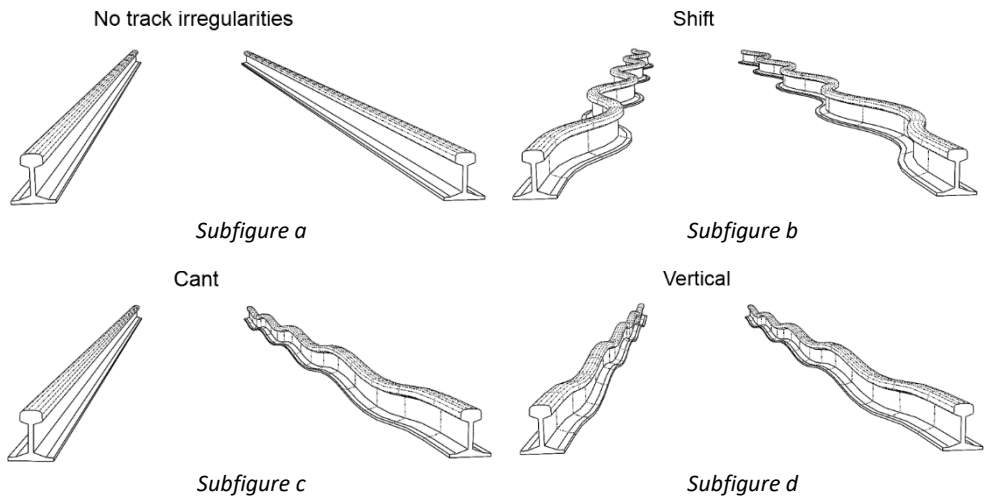


Figure 5-4. Perfect straight track and straight track with various irregularities.

But perfect tracks do not exist, there are all kinds of track irregularities, as shown in figure 5-4. Shift in lateral direction (subfigure b), cant (height difference between the two rails, subfigure c), vertical displacement (subfigure d) of both rails and variation in track gauge exists (not shown in figure 5-4), which causes a different behaviour of the train movement. These are all irregularities regarding the change in location of the rail profile compared to the perfect track. In most simulations, a sinus function has been used to change the position of the UIC54 profile on one or both sides. The used amplitude and wavelength for the different track irregularities are shown in Table 5-2 and are based on track requirements set by ProRail [42]. For the track gauge, it may vary between 1.431 m to 1.455 m.

Track irregularity	Wavelength, λ	Amplitude, A
Lateral shift	18 m	7 mm
Vertical shift	30 m	20 mm
Cant	48 m	20 mm

Table 5-2. Periodical track irregularities with a certain amplitude and wavelength, obtained from [42].

5.2 Perfect straight track

This scenario is used to explain how the simulations are carried out and how the results are analysed. In figure 5-5, a TTBM brake test is carried out within the time frame 1 to 2 seconds, in which the brake, normal and friction forces are shown. A 'dry' traction curve with $\mu_{\text{lim}}=0.2$ is present. The dip in normal force during the TTBM brake will be discussed in section 5.4. Note that the brake force F_R applies to the wheelset, but one looks at the average of the left and right wheel, hence it is divided by 2. The same reasoning holds for the expected static normal force F_Z and the dynamic part for determining the friction force ($\frac{I\alpha_2}{R}$).

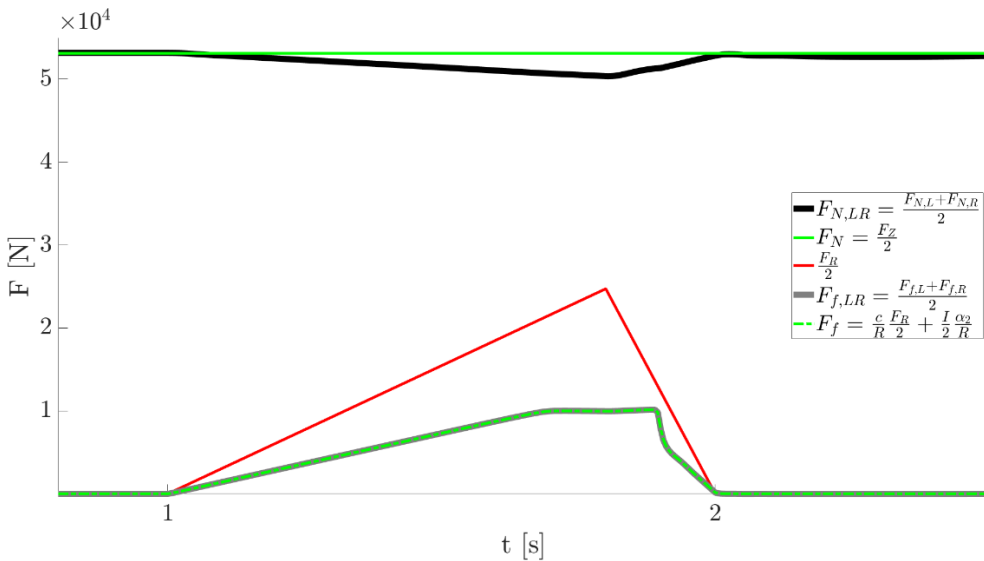


Figure 5-5. The normal, brake and friction force over time.

The applied brake force leads to rotational deceleration of the braked wheelset. The generated friction force leads to a small deceleration of the whole train, as can be seen in figure 5-6.

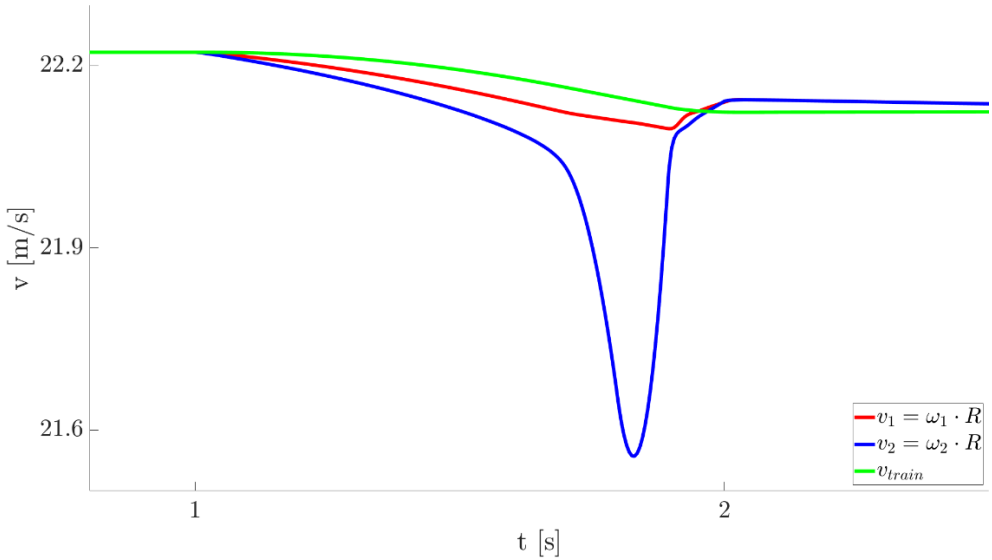


Figure 5-6. The estimated rotational velocities of the non-braked wheelset v_1 and braked wheelset v_2 , and the train speed v_{train} corresponding to the TTBM brake simulation in figure 5-5.

5.3 Track irregularities – Hunting

In reality, a perfect straight track does not exist, thus without track irregularities as shown in figure 5-4, subfigure a. Multiple types of track irregularities could be present at the same time but have a different effect on the behaviour of the dynamics of the wheelset and the whole train, hence these track irregularities will be investigated individually.

5.3.1 Track gauge

First the change in track gauge, by symmetrically shifting the rail on both sides outward as shown in figure 5-7, will be investigated. The track has first a track gauge of 1.431 m and ends with a track gauge of 1.455 m. In between is the transition zone (50 meter long).

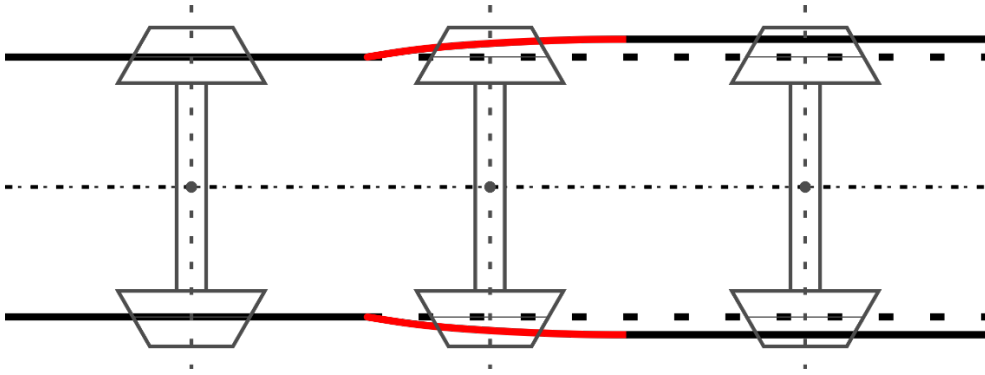


Figure 5-7. Changing track gauge, track shown in red is the transition zone.

The rolling radii before and after the transition zone changes from 0.4607 m (when the track gauge is 1.431 m) to roughly 0.4597 m (when the track gauge is 1.455 m), a change of 1 mm, as shown in figure 5-8. Note that most VI-Rail simulations have been carried out with a track gauge of 1.435 m, which led to a rolling radius of 0.4602 m, hence this value will be used for the nominal rolling radius (R_0).

One might expect that this static rolling radius change would lead to a certain slip error in the slip estimation. But at the end of the track, compared to the beginning of the track, the rolling radii of both the leading and trailing wheelset drops an equal amount. This leads to an error in both wheelsets to be approximately equal which cancels each other out and the slip estimation error is close to zero.

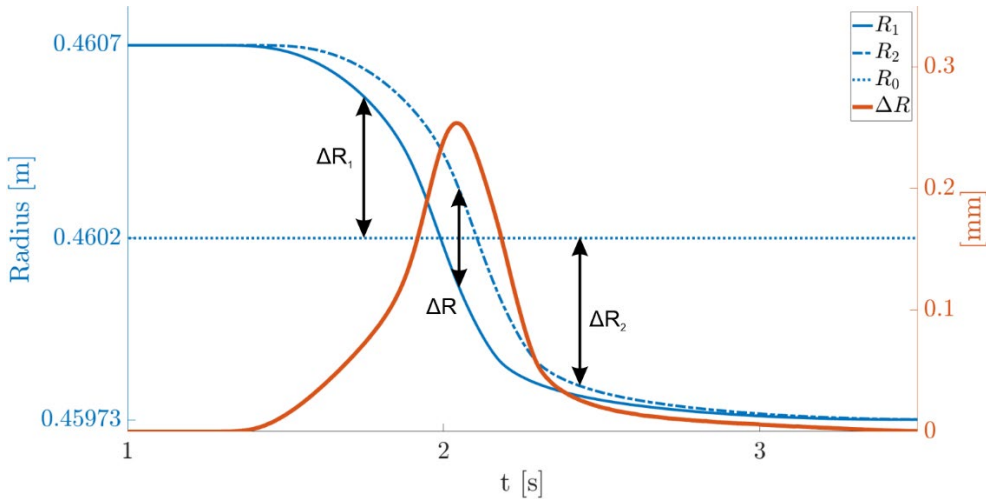


Figure 5-8. Change in rolling radii of the leading and trailing wheelset. The Difference between these rolling radii is denoted as ΔR .

However, within the transition zone, a difference exists between the leading and trailing wheelset, stated as ΔR and shown in figure 5-8 as well. In Appendix D, a derivation is given for the slip estimation error (ΔS) by changing the rolling radii with ΔR_1 and ΔR_2 of the leading and trailing wheelset, respectively. Looking independently at ΔR_1 or ΔR_2 , both change in rolling radii and introduce a slip error. One assumes the calibrated rolling radius of R_0 , but the actual rolling radius is slightly different. Suppose that the train speed is constant and at a certain moment the actual rolling radius of the trailing wheelset increases with 1 mm, then the rotational velocity of the wheelset decreases. However, if these change in rolling radii in the leading and trailing wheelset is the same (e.g., the actual rolling radii is increased by 1 mm for both wheelsets, i.e. $\Delta R_1 = \Delta R_2 = 1$ mm), both slip errors will cancel each other out. The slip estimation error depends on the radii difference between the leading and trailing wheelset ($\Delta R = \Delta R_2 - \Delta R_1$):

$$\Delta S = \frac{\Delta R}{R_0} \quad (5.1)$$

Note, this is a different error than stated in the end of chapter 4 ($\Delta_c S = \frac{\Delta_c R_2}{R_0}$, which is about calibration of the rolling radius of a single wheelset). It turns out that the slip estimation error ($\Delta S = S_{LR,x} - S$) is largely due to ΔR , which is the difference in ΔR_1 and ΔR_2 , as shown in figure 5-9. The actual slip is close to zero, but the slip estimation gives an error of $\Delta S = 0.25/460 = 0.05\%$. This is a low slip error, however, if the length of the transition zone were to be decreased, one would have a larger difference in rolling radii between leading and trailing wheelset (but shorter in duration), leading to a larger slip estimation error.

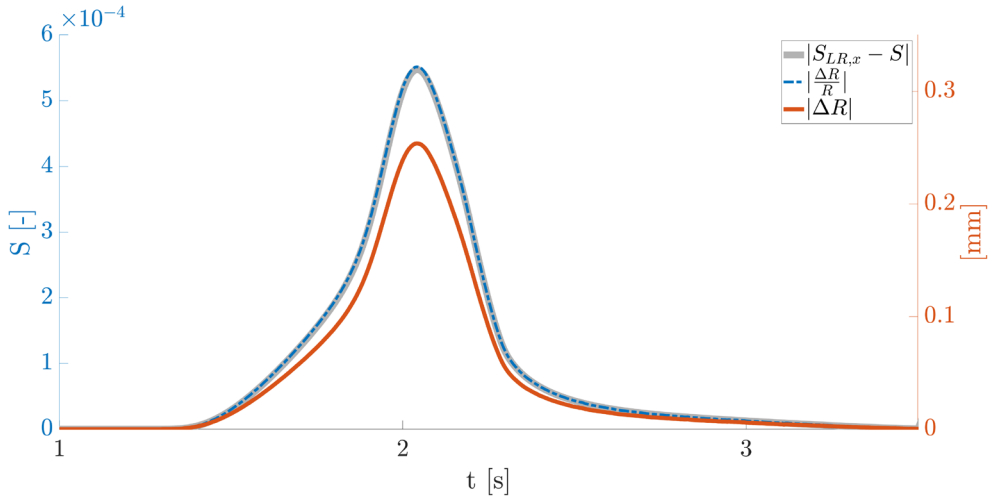


Figure 5-9. The actual slip $S_{LR,x}$ and the change in rolling radii ΔR_1 and ΔR_2 , leading to ΔR . The determined slip shows an error compared to the actual slip (i.e. $S_{LR,x} - S$).

5.3.2 Straight track with periodically lateral shift

A straight track with a periodically lateral track irregularity (shift) will be investigated, see figure 5-4 (wavelength 18 m, Amplitude 7 mm). Upon entering the track irregularity by the wheelsets, the sudden change in lateral track position leads to a different contact point between wheel and rail, on both sides, as can be seen in figure 5-10. The left and right wheel can have different rolling radii, the mean value will be referred to as the rolling radii of the wheelset.

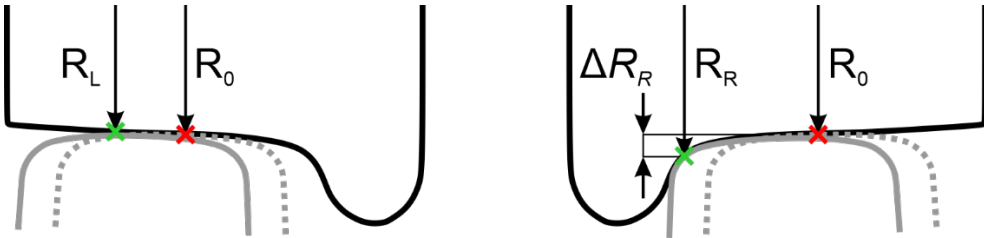


Figure 5-10. Nominal rolling radius R_0 and the actual rolling radii of the left and right wheel R_L and R_R , respectively, changed due to shift (lateral displacement) of the track. ΔR_L not shown here (small compared to ΔR_R).

Both in the leading and trailing wheelsets, a change in rolling radii occur. First the dry traction curve will be investigated, the development of the rolling radii of the leading and trailing wheelset is shown in figure 5-11. Note, the wavelength is 18 m, the train speed is 80 km/h, hence the time to pass one wave is about 0.81 s.

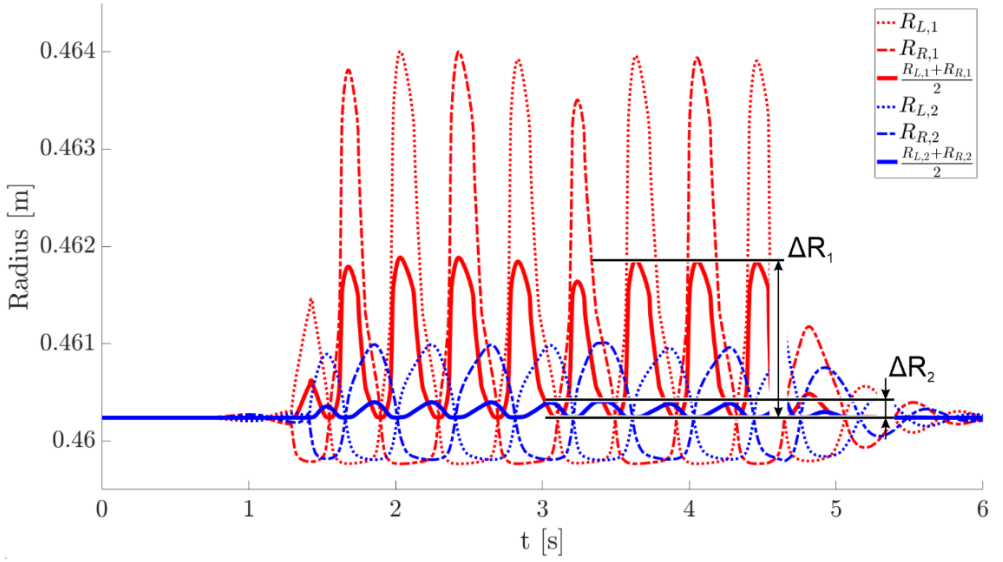


Figure 5-11. Dry traction curve. Change in rolling radii of the leading and trailing wheelset, $\Delta R_1=1.6$ mm and $\Delta R_2=0.16$ mm.

The same reasoning applies here as well, when the ΔR increases, so does the slip estimation error ΔS as shown in figure 5-12. Note that the slip estimation error in equation 5.1 is not a perfect estimation, at the peak values there is a slight offset, which probably has to do with dynamic effects of the wheelset itself (e.g., sudden accelerations of bodies) and flange contact may intervene as well.

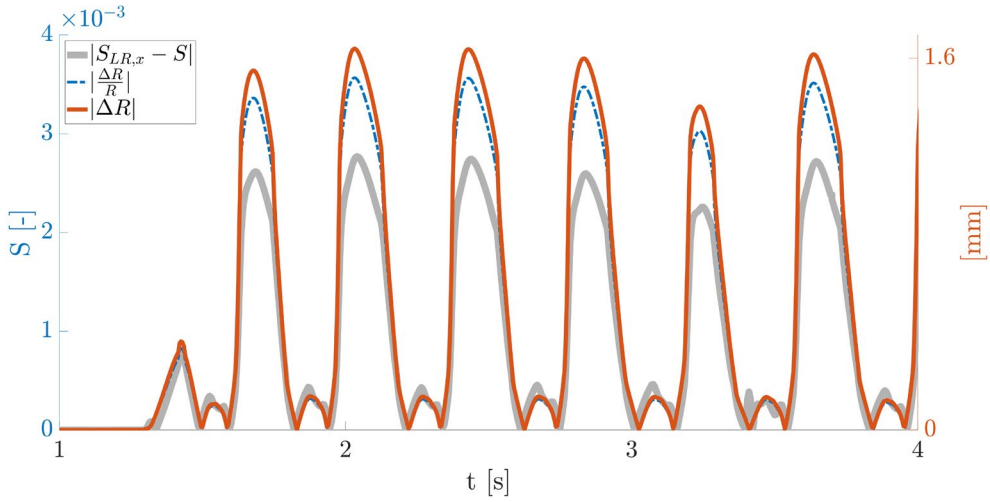


Figure 5-12. The actual slip ($S_{LR,x}$) and the change in rolling radii difference (ΔR) are the output by VI-Rail (and unknown). The determined slip shows an error compared to the actual slip (i.e. $S_{LR,x} - S$).

The slip estimation error by the TTBM can be seen as follows. The slip estimation equation 4.20 uses ‘fixed’ radii, however due to the apparent changing rolling radii, the rotational velocities change as well, which is measured by the TTBM, as can be seen in figure 5-13. The mean change in actual rolling radius within the leading wheelset (ΔR_1) is higher than the trailing wheelset (ΔR_2), leading to a larger fluctuation in velocity estimation (v_1).

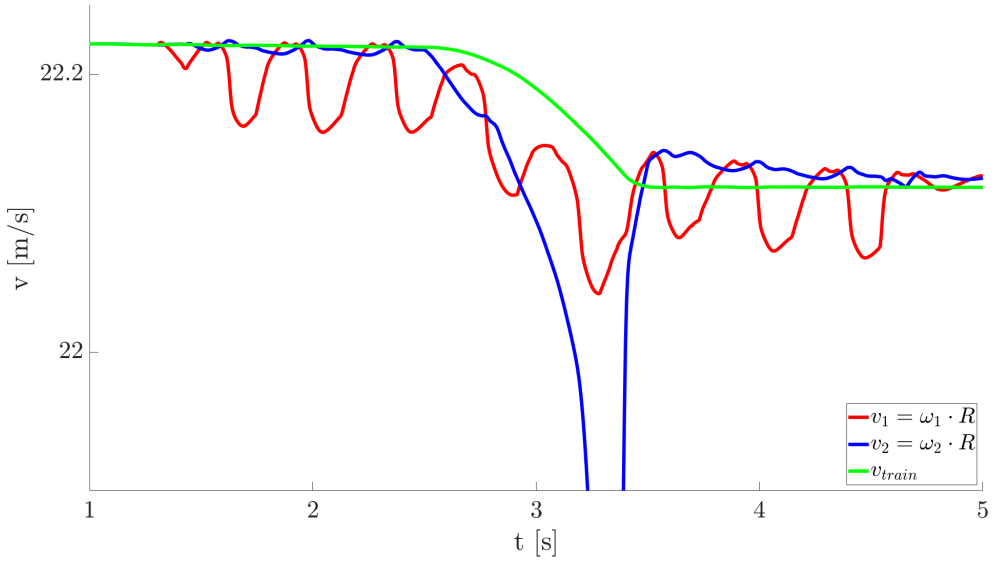


Figure 5-13. The estimated rotational velocities of the non-braked wheelset v_1 and braked wheelset v_2 , and the train speed v_{train} , corresponding to figure 5-12.

The same simulation has been carried out, but now in the presence of a ‘third body’ traction curve ($\mu_{peak}=0.18$). The change in rolling radii between the leading and trailing wheelset is less significant, hence the apparent slip estimation error is lower as well, as shown in figure 5-14.

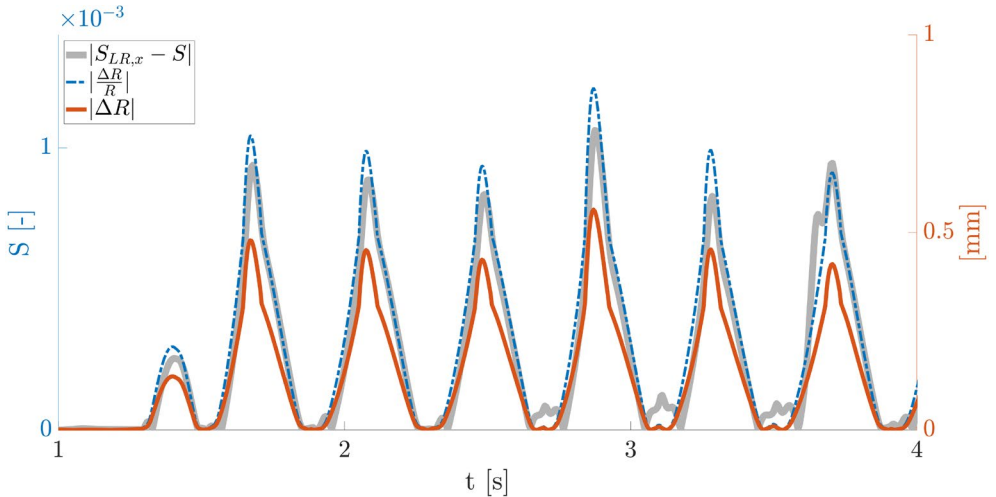


Figure 5-14. The actual slip ($S_{LR,x}$) and the change in rolling radii difference (ΔR) are the output by VI-Rail (and unknown). The determined slip shows an error compared to the actual slip (i.e. $S_{LR,x}-S$).

The fluctuation of the estimation of rotational velocities is attenuated, compared to the ‘dry’ traction curve case, as can be seen in figure 5-15.

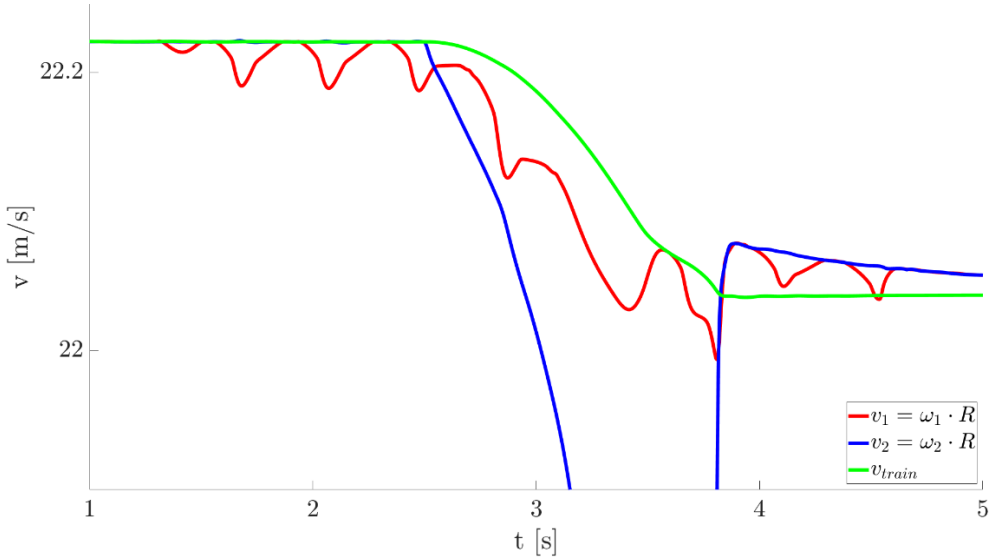


Figure 5-15. The estimated rotational velocities of the non-braked wheelset v_1 and braked wheelset v_2 , and the train speed v_{train} , corresponding to figure 5-14.

In figures 5-16 and 5-17, the dry and third body traction curve estimations are shown, corresponding to the two simulations in this section. As one can see, the slip estimation error in the third body traction curve is less significant in absolute terms. Also, the third body traction curve has a lower creep coefficient, which would make such an slip estimation error less severe. This lower creep coefficient is probably the reason why the wheelset is hunting less intense compared to the ‘dry’ traction curve simulation. The CoF estimation error, $\Delta\mu$, will be discussed in section 5.4.

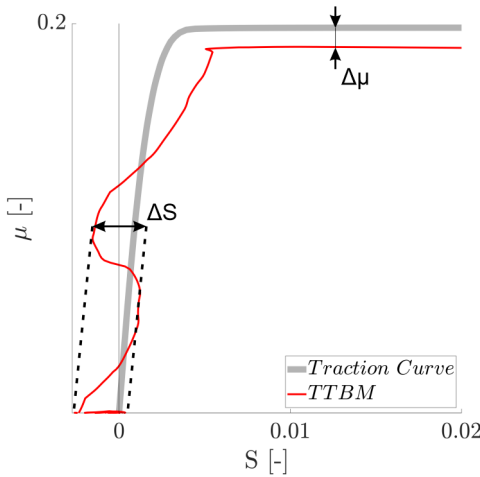


Figure 5-16. 'Dry' traction curve estimation, $\Delta S=0.3\%$ and $\Delta\mu=0.01$.

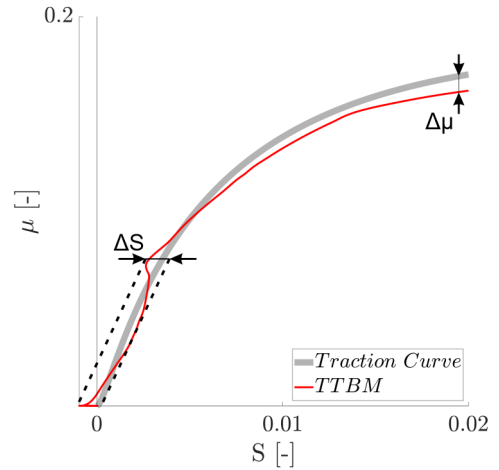


Figure 5-17. 'Third body' traction curve estimation, $\Delta S=0.1\%$ and $\Delta\mu=0.009$.

Comparing the lateral sine (track irregularity, shift) to the track gauge case in previous section, the slip estimation error is higher. But there is a similarity, namely instantaneous lateral displacement of the track (shift or track gauge) leads to a different contact point between wheel and rail. This leads to a mean change in rolling radii between leading and trailing wheelset, resulting in a slip estimation error. Track irregularities co-exist and are not perfectly isolated. Finding the exact cause of the slip error at a certain moment will be hard to retrieve.

Within a bogie, the leading wheelset 'steers' when the train passes a track irregularity (or a curve). When the track irregularity, or sudden lateral displacement of the contact point, is high, then one of the wheels of the leading wheelset is most likely in flange contact. This causes a sudden increase in mean rolling radii. The trailing wheelset already steers a bit, hence the ΔR_1 error in the leading wheelset is higher than the ΔR_2 error in the trailing wheelset.

A note about equation 5.1. Suppose that the wheels are smaller (lower nominal radii R_0), the ΔR error remains more or less the same due to the same wheel profile, but the accompanying slip estimation error increases.

5.3.3 Cant on straight track

The third track irregularity that will be discussed is the cant on a straight track, as shown in figure 5-4. The right rail will remain unaltered while the left rail will have a periodical cant irregularity with wavelength of 48 m and an amplitude of 20 mm. In figure 5-18, one can see the slip error estimation. Note, actual slip is present when traversing the track irregularity, which is shown in Appendix D.

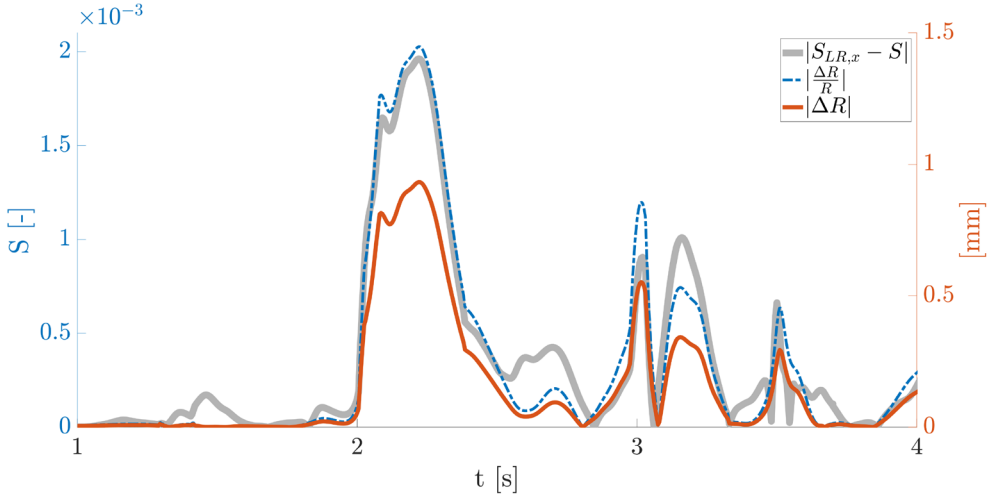


Figure 5-18. The actual slip $S_{LR,x}$ and the change in rolling radii difference ΔR are the output by VI-Rail (and unknown). The determined slip shows an error compared to the actual slip (i.e. $S_{LR,x} - S$).

Note that the contact point of the wheel and rail changes laterally when traversing the cant track irregularity as for instance shown in figure 5-10. This can sometimes lead to flange contact, most often in the leading wheelset, as shown in figure 5-19. The wheel and rail profiles have a different local curvature when the contact point changes, resulting in a different shape of the contact patch. This change in semi-axes of the contact patch influences the creep coefficient of the traction curve, which is shown in Appendix F.

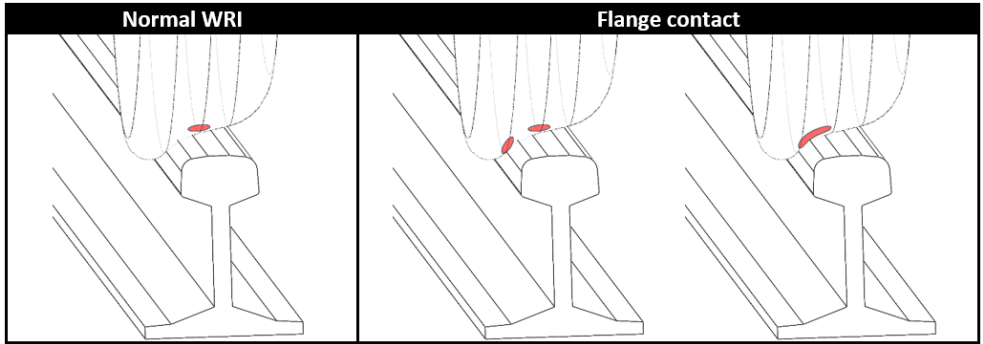


Figure 5-19. Normal WRI in which the contact is on the wheel tread and top of rail versus a wheel in flange contact.

Besides the slip estimation error, a CoF estimation error ($\Delta\mu$) is present as well. The cant on a straight track causes vertical displacement of the train, resulting in varying normal forces acting on the wheels. The left and right normal forces of the braked wheelset are shown in figure 5-20, as well as the mean value. As can be observed, the cant has a significant influence on the normal load.

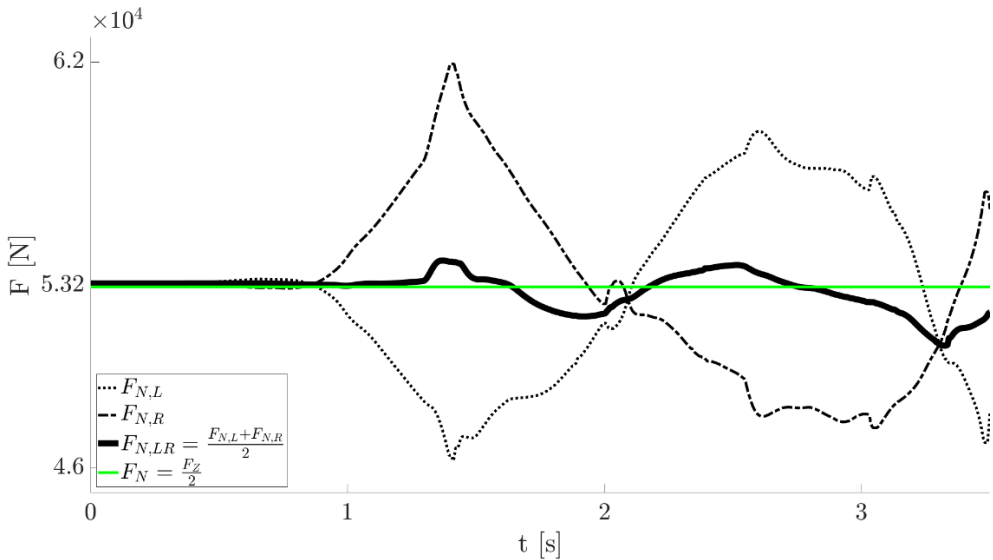


Figure 5-20. Normal force of the left and right wheel, $F_{N,L}$ and $F_{N,R}$ respectively, when traversing the cant irregularity and its mean value $F_{N,LR}$ over time.

Normal force variations are also present in other track irregularities, such as the lateral shift scenario in section 5.3.2. In addition, train operating conditions, such

as de- and acceleration of the train, influence the normal forces among its wheelsets as well. This will be discussed in the next section.

5.4 Normal force variations

Various types of dynamic normal force variations are summarized here and are explained in more detail in Appendix D. First, the change in normal force due to the TTBM brake will be discussed, as already mentioned in section 5.2 and shown in figure 5-5. The normal force variation depends on the brake intensity, thus how high one wants to measure the CoF (μ_{\max}). The change in normal force by the TTBM brake on one wheelset is (derivation in Appendix D):

$$\Delta F_N = -\frac{c}{L} F_R = -\frac{R_0}{L} \mu_{\max} F_Z \quad (5.2)$$

In which L is the wheelbase of the bogie. In the simulation in section 5.2, μ_{\max} is set to 0.2, $R_0=0.46$ m and $L=2.56$ m, the $\Delta F_N/F_Z$ ratio is then around 4%. Due to additional dynamic effects within the simulation in section 5.2, the actual $\Delta F_N/F_Z$ ratio is around 5% (see figure 5-16, $\Delta\mu=0.01$). This results in a relative CoF error of $\frac{\Delta\mu}{\mu} = \frac{\Delta F_N}{F_Z + \Delta F_N} \approx -5\%$ (equation from Table 4-2), while the absolute CoF estimation error is roughly 0.01 (the actual peak CoF is 0.2).

Depending on the driving direction, the brake forces by the brake pads acting on the brake discs are directed up or downward. In most scenarios in this chapter, the TTBM wheelset is trailing, resulting in an upward brake force, which relieves slightly the normal force (a negative ΔF_N).

Vertical track irregularities exist as well, as shown in figure 5-21, leading to vertical acceleration of the train. This leads to increased normal forces when traversing the valleys of the track and decreased normal forces when traversing the peaks.

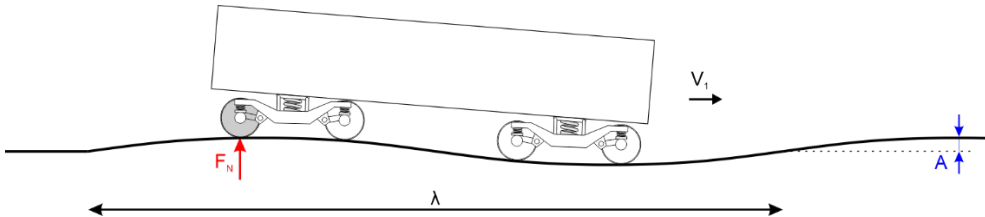


Figure 5-21. Track with a periodically vertical irregularity with a wavelength λ and amplitude A .

Two wavelengths with a certain amplitude at different train speeds have been tested and their influence on the normal force are shown in figure 5-22. Note that at a lower wavelength track irregularity, the time to traverse a full wave track irregularity decreases when the train speed is held constant.

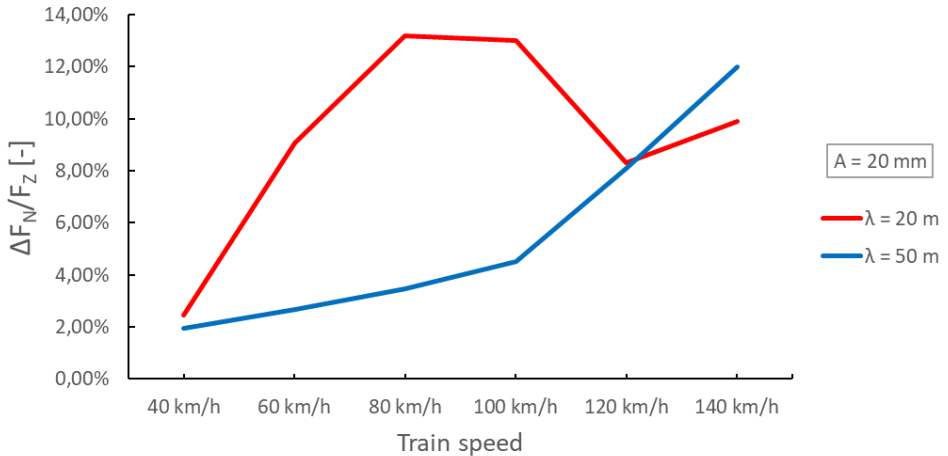


Figure 5-22. Vertical track irregularity with two wavelengths at various train speeds and the relative change in normal force ($\Delta F_N/F_z$).

The high frequent, short wavelength vertical track irregularity is expected to cause higher variations in normal forces compared to the long wavelength vertical track irregularity. However, this is not the case at higher train speeds, as shown in figure 5-22. The suspension system absorbs the vertical displacements. Still, up to 13% in normal force variations do occur. In Appendix D, five wavelengths from 20 m to 60 m and their influence on the normal force variation are presented.

Besides the change in normal forces among wheelsets, a change in the left and right normal force in the left and right wheels happens as well. On straight tracks with irregularities, such as the lateral shift case in section 5.3.2 or the cant case in section 5.3.3, a difference in normal force between left and right wheel is present. Considering the cant case, the change in normal force in the right wheel ($\Delta F_{N,R}$) compared to the expected mean normal force ($F_z/2$) is at maximum around 0.9 kN. While at the same time the left wheel is relieved by $\Delta F_{N,L}=0.7$ kN. The periodical lateral shift case in section 5.3.2 shows a $\Delta F_{N,L}$ and a $\Delta F_{N,R}$ around 0.3 kN (shown in Appendix D). This might become relevant when WRI conditions within the left and right wheel are not equal. Also, one might measure the left and right normal force

independently as a measure of track irregularity intensity, which will be discussed in chapter 6.

Furthermore, there are more scenarios that influence the normal force. De- and acceleration of the train itself by the driven wheelsets, as shown in figure 5-23, cause a dive and lift behaviour of the wagons, respectively. Depending on the bogie and wheelset location, this results in a certain normal force variation.

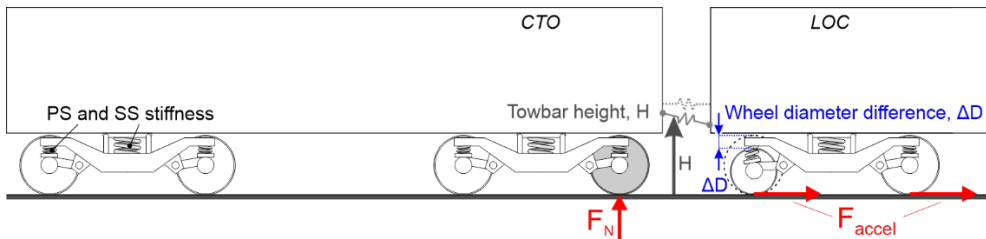


Figure 5-23. Changing suspension stiffness, wheel diameter, tow bar height or acceleration of the train induces a change in the normal force distribution among its wheelsets.

The total weight of the train is carried by the primary suspensions (PS), which are basically in a parallel configuration with respect to the track, as shown in figure 5-23. Now if the wheel diameter changes or different suspension values among the bogies are present, then the normal force distribution changes among the wheelsets. Note, when the train configuration changes (by e.g., shunting), possibly different suspensions and wheel diameter combinations will follow, which could lead to a different normal force distribution. In Appendix D, a simulation on a perfect straight track while the train is accelerating (the four driven wheelsets of the LOC are engaged) has been carried out and normal force variations among the wheelsets vary between 1.5% to 8.5%.

Keep in mind that one finds the same type of normal force variation but different values when looking for instance at different train configurations, suspension values and train parameters (i.e., weight and size of the wheels, bogie and wagon). Also, the normal force variations were investigated separately, but just as with the track irregularities, these normal force variations co-exist, potentially adding up all the normal force variations (or cancel each other out).

5.5 Operating conditions

5.5.1 TTBM leading wheelset and drive direction

When the drive direction is altered and the train configuration has not changed, the TTBM wheelset becomes the leading wheelset, as shown in figure 5-24.

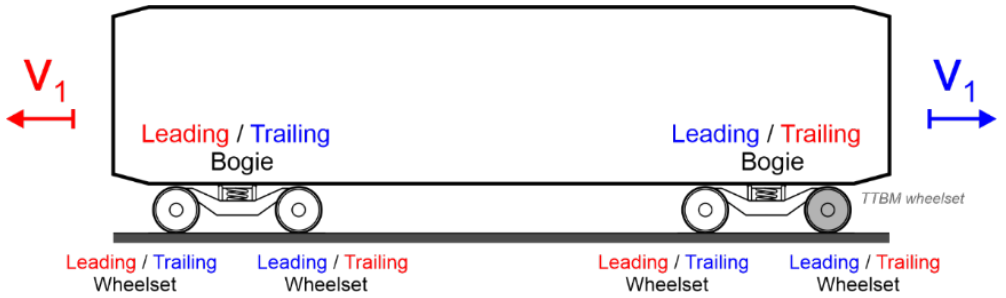


Figure 5-24. Different drive direction leads to different roles (leading or trailing) of the bogies and wheelsets.

Similar simulations have been carried out in which the TTBM wheelset is the leading wheelset, the estimated slip error and normal force variations when traversing track irregularities are overall larger. A simulation has been carried out under the same conditions as in section 5.3.2 (straight track, lateral track irregularity, 'dry' traction curve), but the leading wheelset in the bogie has been used as the TTBM wheelset instead of the trailing wheelset.

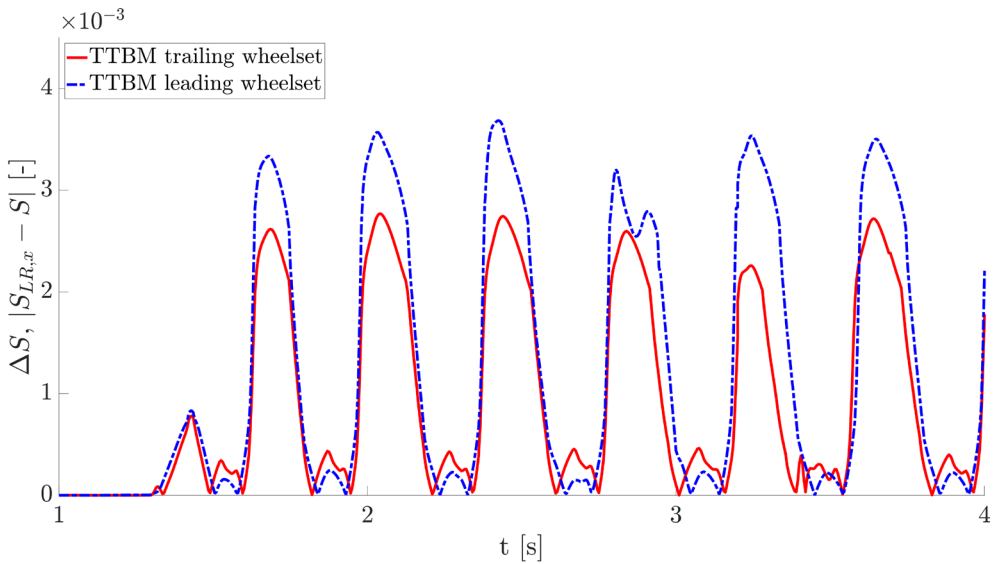


Figure 5-25. Two separate simulations under the same simulation conditions as presented in section 5.3.2 ('dry' traction curve). One simulation uses the leading wheelset for the TTBM system while the other uses the trailing wheelset. The slip estimation error (ΔS) for both simulations over time are shown.

As can be seen in figure 5-25, the slip estimation error is larger when using the leading wheelset, because the actual occurring slip is larger. The leading wheelset

steers when negotiating curves or when traversing a track irregularity, as mentioned in section 5.3.2. This leads to a larger lateral displacement in the contact point on the wheel profile (more often into a flange contact) and a larger AoA, which congests the measured traction curve by the TTBM and increases the difficulty to analyse it.

5.5.2 Comfort

Suppose the train has a constant speed and at a certain moment the TTBM brake is carried out. For simplicity, the only acting force in longitudinal direction (neglect air resistance) is the generated friction force in the TTBM wheelset. If one rewrites the Newton's second law in longitudinal direction ($F_f = M_{train} \cdot a_x$) and solve for the acceleration (deceleration in this case, hence the minus sign), one would get:

$$a_x = -\frac{F_Z}{F_{Z,train}} \cdot \mu \cdot g \quad (5.3)$$

The deceleration depends on the ratio of the weight felt on the TTBM wheelset (F_Z) over the whole train weight ($F_{Z,train}$). Also, the higher one wants to measure μ (a higher μ_{max}), the higher the deceleration will be. If the TTBM were to be installed within a passenger train, the deceleration during a TTBM brake might also be felt by the passengers, as shown in figure 5-26. When carrying out the VI-Rail simulations, the acceleration of the wagon is measured, in which one simulation is shown in figure 5-27, which corresponds to the simulation in section 5.3.2. Note, in this simulation, the traction curve had a $\mu_{peak}=0.2$ ($\mu_{max}=0.2$, hence the value of $\mu=0.2$ has been reached). If one considers the LOC and CTO weights in Table 5-1, $g=9,81 \text{ m/s}^2$ and substitutes these values into equation 5.2, one gets a deceleration value of roughly 0.18 m/s^2 .

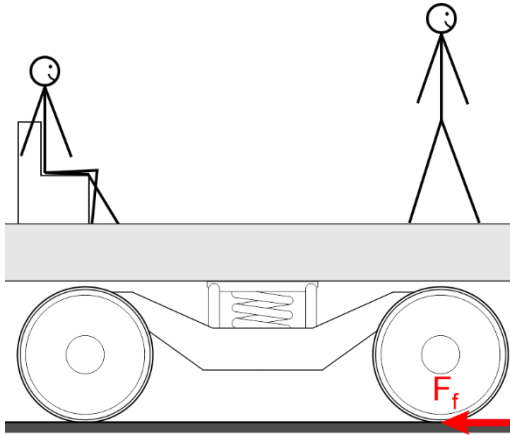


Figure 5-26. Friction force induced by the TTBM brake.

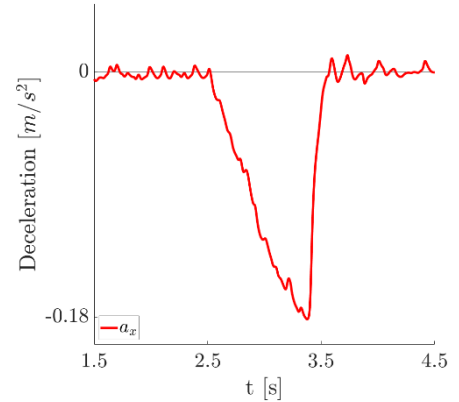


Figure 5-27. The acceleration within the LOC wagon during a TTBM brake.

Besides keeping the deceleration small, one wants to attenuate the jerk ($J = \frac{da}{dt}$) as well. The higher the sudden changes in deceleration, the more it feels as a shock, which is unwanted. This is an extra reason to use a ramp function for the applied brake force.

One could increase the time to apply the ramp brake force, but, as mentioned in chapter 4, one wants to keep the time to carry out the TTBM brake small, to keep the covered track distance low over which the TTBM brake is carried out. Also, the overall brake intensity increases, which is unwanted as well, because maintenance is then required faster.

The passenger comfort must not be affected by the TTBM system, hence one must consider this as well upon further designing the TTBM system and its brake force profile. Depending on the use case of the TTBM, a different brake strategy might be considered, such as measuring up to a lower μ_{\max} or measure only the creep coefficient. The latter will be discussed further in the following chapter.

5.5.3 TTBM brake during curve negotiation

The track has, besides straight track, curves as well. A single wheelset has a certain radial alignment, the outer wheel will roll on a larger radius than the inner wheel, as shown in figure 5-28. But within a bogie frame consisting of two wheelsets, the wheelsets are constrained by the suspension of the bogie and thus not able to radially align properly, as shown in figure 5-29.

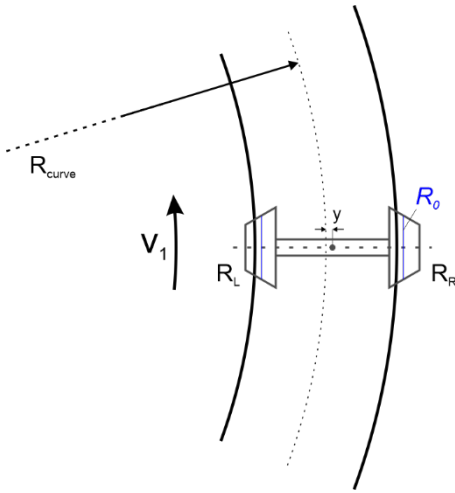


Figure 5-28. Single wheelset negotiating a curve, with the lateral displacement y .

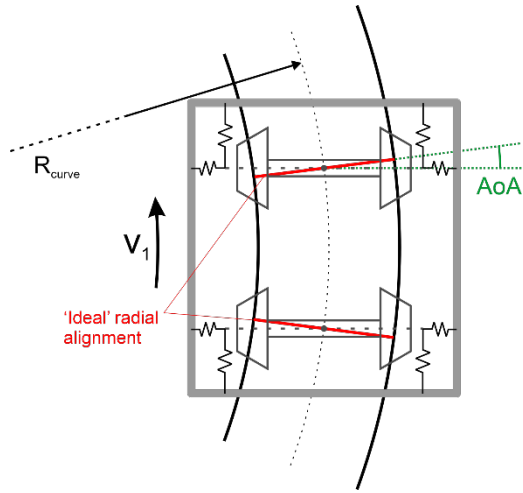


Figure 5-29. A bogie with two wheelsets suspended negotiating a curve.

The radius of the curve (R_{curve} in figure 5-28) and the amount of cant have to meet certain requirements set by ProRail [43]. A sharp curve (low R_{curve}) is only allowed at lower train speeds, whereas at higher train speeds the curve is gentle (high R_{curve}). These two scenarios will be compared, and the used parameters are shown in Table 5-3.

Train speed	R_{curve}	Cant
80 km/h	2000 m	70 mm
40 km/h	190 m	0 mm

Table 5-3. Used parameters for the TTBM brake test when negotiating a curve.

In Table 5-4, the change in rolling radii of the front and rear wheelset are shown (relative to $R_0=0.4602$ m), as well as the difference between them (ΔR). One can see the leading wheelset increasing the most in mean rolling radii, due to the flange contact, especially in the sharper curve, compared to the trailing wheelset. The slip estimation error is shown as well (keep in mind that equation 5.1 is an estimation of it).

Simulation	ΔR_1	ΔR_2	ΔR	ΔS	AoA_1	AoA_2
$R_{\text{curve}}=2000$ m	0.25 mm	0.05 mm	0.2 mm	0.02%	0.064°	0.008°
$R_{\text{curve}}=190$ m	3 mm	0.25 mm	2.75 mm	0.43%	0.423°	0.358°

Table 5-4. Results of the simulations mentioned in table 5-3.

The leading and trailing AoA, denoted with AoA_1 and AoA_2 , respectively, when negotiating the corresponding curve are shown in Table 5-4. In Appendix D, the AoA of the leading and trailing wheelset are shown over time. For the sharp curve, the AoA in both wheelsets are large compared to the lower radius curve. The AoA induces a certain lateral slip and lateral friction force within the WRI. During the TTBM brake test, when measuring low longitudinal slip, the lateral slip and lateral friction force may influence the longitudinal friction force (when measuring high longitudinal slip, thus high slip generated by the TTBM, the lateral effects are attenuated).

Flange contact and the presence of high lateral creepage, which are present in sharp curves, may intervene with the TTBM measurement. Note, within a curve, the PS constrains the wheelsets within a bogie and the SS constrains the two bogies relative to the wagon. Different train suspensions (SS and PS) lead to different wheelset alignment relative to the track, which result in different values found in Table 5-4.

5.6 Conclusion

The TTBM has a certain error in measuring traction curves. Within the VI-Rail simulations of the LOC-CTO train model on straight track with certain track irregularities, a slip estimation error (ΔS) of roughly 0.5% has been found. This slip error is mainly caused by the difference in change in rolling radii of the leading wheelset (ΔR_1) and trailing wheelset (ΔR_2), i.e., $\Delta R = \Delta R_2 - \Delta R_1$.

Regarding the coefficient of friction, normal force variations are present as well due to various causes, which compound to the total change in normal force of approximately 15%. This leads to roughly 15% CoF estimation error ($\Delta \mu$). For measuring the friction force, it is desired to have the WRI within the wheel tread and rail top of head. When this is not the case, such as a flange contact when negotiating a curve or facing severe track irregularities, then interpreting the data becomes more difficult and needs more research.

Chapter 6 – Detailed design considerations

The initial TTBM concept was presented in chapter 4 and simulated in chapter 5. Chapter 2 mentioned various use cases in which the TTBM could be used for, but the requirements may differ among the use cases. Various options for the TTBM design by identifying certain sensor locations of the TTBM on TRL 5-7 (for field tests) are proposed in section 6.1. The TTBM sub-systems will be investigated separately (brake force system, normal force system and the slip detection system). Then, two main TTBM brake strategies are shown in section 6.2. Depending on the use cases in combination with the TTBM brake strategies, a different TTBM design may be chosen instead, i.e., different options for the subsystem combinations, which will be evaluated in section 6.3. Finally, a TTBM design is proposed.

6.1 Design of the TTBM calibration system

Certain design options are proposed for the three sub-systems (brake force-, normal force- and slip measurement system). Within section 6.3, a TTBM design is proposed.

6.1.1 Brake force measurement system concepts

6.1.1.1 Built-in brake force sensor

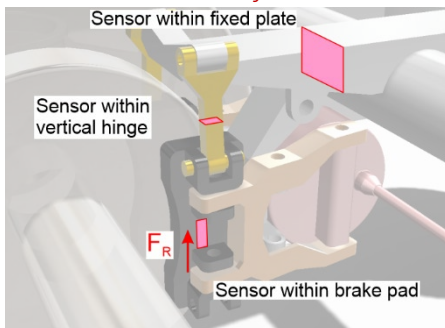


Figure 6-1. Placement of the possible brake force sensors.

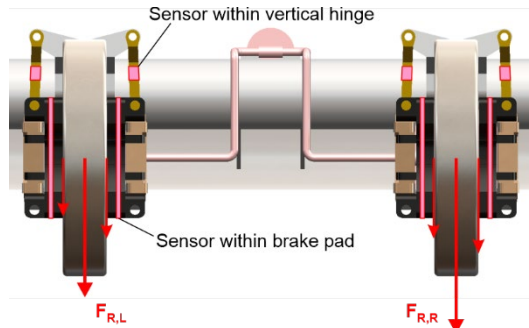


Figure 6-2. Two pinch and brake forces acting on one brake disc, adding up to a left and right brake force, $F_{R,L}$ and $F_{R,R}$.

By integrating force transducers somewhere within the brake system, one can use most of the existing parts already there, no extra modules are needed. There are a few points to consider:

Integrating the force transducers within the four brake pads, as shown in figure 6-2, would be the closest location to the applied brake force. However, braking induces wear and an increase of temperature, which most transducers are susceptible to.

The brake shoes are connected by horizontal and vertical hinges, as can be seen in figure 6-1. The vertical hinge will endure the most and one might consider placing a transducer over there, as shown in figure 6-2 as well. A fraction of the reaction force might be present within the horizontal hinge, meaning one might not capture all the brake forces by placing the sensor in the vertical hinge only and thus needs to be tested and validated.

Integrating the brake force sensors further away from the applied brake force might measure all the brake forces, e.g., 'within the fixed plate' (see figure 6-1). However, the further away the sensors are, the larger the error becomes (a larger load on the sensor, leading to dynamic errors). Also, one needs to safeguard the safety of the brake system construction.

Furthermore, when integrating the sensors in the existing brake system, one separate brake system needs to be activated only (which engages only one wheelset). This means one brake system needs to be decoupled of the global brake system of the train, resulting in lowering the overall braking power of the train. For carrying out experiments on a measurement train, that is manageable. However, within a passenger train, decoupling one brake system is unacceptable. It needs to be integrated such that the TTBM brake can carry out a measurement while not intervening with normal braking operations (e.g., by designing the control of the TTBM brake system to participate during normal braking as well).

6.1.1.2 Separate brake system module

To maintain the integrity of the global brake system and without decoupling a single brake system, a separate brake system module for a single wheelset should be designed, as shown in figure 6-3. This is needed to make sure that the braking power of the global braking system of the train is not affected.

For TRL 5-7, within the CTO measurement train of the TU Delft, it is possible to decouple a single brake system, which makes the first method (the built-in brake force sensor) the easier option. However, one should keep the separate brake module in mind if the built-in brake force system becomes too complex.

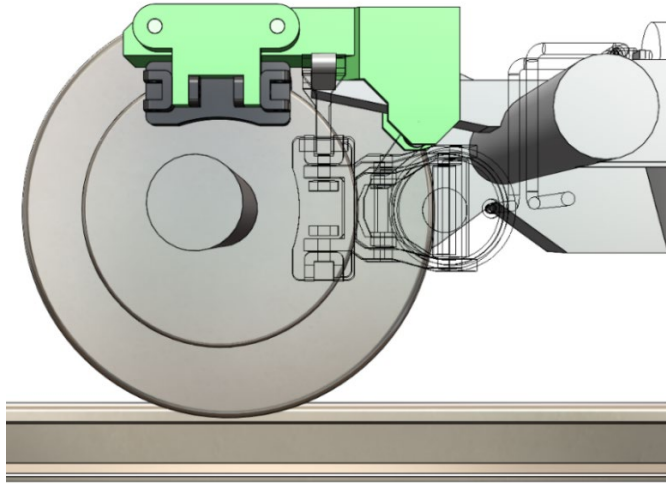


Figure 6-3. Separate, additional brake module, shown in green.

6.1.2 Normal force measurement system concepts

As mentioned in the previous chapter, various scenarios influence the normal force within the wheelsets: train de- and acceleration, braking of one wheelset within an undercarriage containing two wheelsets. This leads to variations in the left and right wheel normal forces and the normal forces among the wheelsets themselves.

The simplest way by estimating the static normal force of the braked wheelset is by simply weighting the train, see equation 4.6. All normal force deviations just mentioned will be neglected, resulting in a certain normal force estimation error at the wheel-rail contact. Two other ways to estimate the normal force are presented here.

6.1.2.1 Normal force transducer within the Secondary Suspension (SS)

The normal force transducer will be installed within the SS, between bogie and wagon, as shown in figure 6-4. However, this measures the normal forces of both wheelsets in the bogie. For measuring friction, the normal force on one wheelset needs to be measured. Also, the normal force sensor within the SS can only measure normal force variations within one bogie, i.e. the combined normal force of both wheelsets. measured normal force variations are hard to account to which wheelset experiences this change. The transducer would then mostly be used to estimate the static expected normal force.

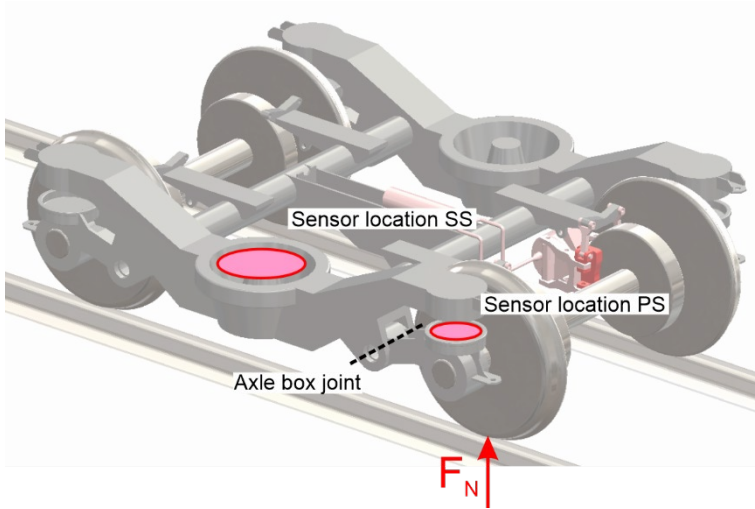


Figure 6-4. Normal force transducer located within the primary suspension (PS) or secondary suspension (SS) of the bogie.

6.1.2.2 Normal force transducer within the Primary Suspension (PS)

One could also place the normal force transducer between the wheelset and bogie frame, thus within the PS, as shown in figure 6-5.

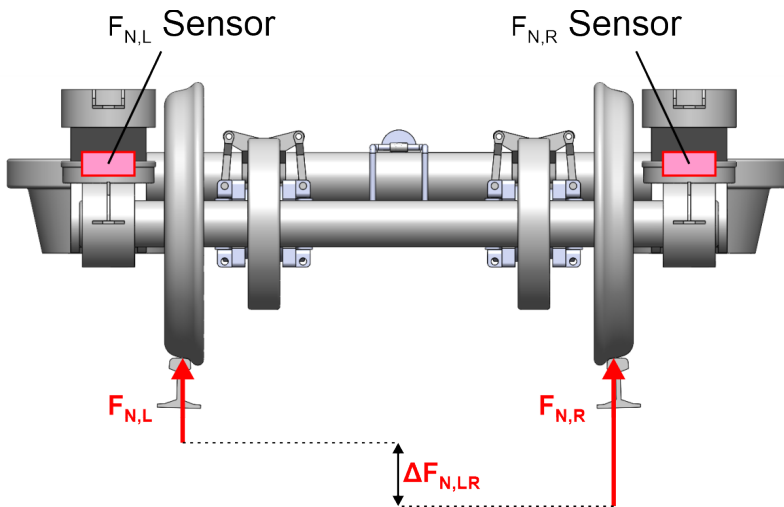


Figure 6-5. Normal force transducers placed within the PS.

By integrating the normal force transducers within the PS on the left and right side, as depicted in figure 6-5, one only measures the normal force of one wheelset and thus the normal force variations can be measured directly. Normal force variations

between the left and right wheel could be measured as well to a certain degree, which might indicate if a certain track irregularity is present.

However, the elbow joint between bogie and the axle box, as shown in figure 6-4, has a certain rotational stiffness which could account for the normal force of the wheelset. This means that the normal force transducer in the PS location might not measure the complete acting normal force, hence this needs to be validated.

6.1.3 Slip measurement system

Using a tachometer for the braked wheelset (v_2) and a tachometer for the non-braked wheelset tachometer (v_1) is the initial TTBM concept, used in the MBD simulations of chapter 5. A few other methods to estimate v_1 of the braked wheelsets have been tested as well, such as directly using the train speed itself (e.g., by GPS) or the circumferential speed of the braked wheelset just before applying the TTBM brake as estimation for v_1 . However, both methods introduce errors as well and are not more accurate, as shown in Appendix D.

One could consider improving the accuracy of the slip measurement by using accelerometers on both sides of the braked wheelset to measure the v_1 velocity. One might consider using axle box accelerometers, which can measure the longitudinal and vertical accelerations [44]. This might be used to improve the normal force measurement system as well. The longitudinal and vertical channel may enhance the slip measurement and normal force measurement accuracies. The longitudinal channel can be used to monitor the yawing of the wheelset, whereas the vertical channel could monitor the dive and lift behaviour of both sides of the wheelsets. However, this should only be considered when the accuracy needs to be improved, since it brings extra complexity to the TTBM system.

For now, the initial TTBM concept will be considered only, how accurate one wants to measure the slip and whether one wants to measure with a high or low resolution depends on the use case of the TTBM, as measuring slip accurately is going to be critical in certain scenarios.

The TTBM system has a certain slip estimation error as mentioned in the preceding chapter. If one is only interested in the maximum CoF, excessive slip detection may be enough, which requires the lowest slip resolution (an absolute slip resolution of 1-2%) since it only needs to check whether the peak value has been reached.

However, there are two main reasons to measure with a higher slip resolution:

- First, a traction curve contains more information than only its CoF peak value. If one can capture the shape of the traction curve, the creep coefficient and the behaviour at excessive slip can be investigated. This can be used to e.g., distinguish the friction conditions in the WRI, whether a 'dry' or 'third body' traction curve is present.
- Second, the TTBM brake input force profile, thus the design parameters in chapter 4 and the shape of the brake force profile, can be properly designed. Depending on the friction conditions within the WRI and different track conditions, the output (such as wheelset deceleration) behaves differently with the same input. Monitoring the slip properly and thus better rotational velocity measurement, gives valuable insight in the accompanying dynamic effects, which can be used within the iteration steps to improve.

if one wants to measure creep coefficients, which will be discussed in the next section, a high slip resolution is required (an absolute slip resolution of 0.1-0.2%), especially for dry traction curves (high creep coefficient). One could consider something in between the two extremes, the least and most accurate slip measurement. By measuring slip with an absolute slip resolution of 0.5% instead of 0.1%. This may result in a less refined measured traction curve, but it is sufficient to distinguish the traction curve type ('dry' or 'third body').

6.2 TTBM brake strategy

Two main TTBM brake strategies will be discussed in this section.

6.2.1 'Peak and beyond' traction curve measurement

This brake strategy has been mainly used within the MDB simulations in chapter 5. The peak value of the traction curve will be measured, which is easy to interpret. If the peak value of the traction curve is not reached (the braked wheelset is at μ_{\max} , but no excessive slip occurs), then sufficient friction is present as well. However, too high friction may then be present which will not be detected if μ_{\max} is set too low. Even if slip is not measured accurately and the tachometers are only capable of detecting whether excessive slip occurs, then one can still use the TTBM brake to measure the peak CoF value as a result.

By measuring slip accurately and with a high resolution (as well as the accompanying CoF), the traction curves are measured accurately, which can be used as a basis for the next TTBM brake strategy.

6.2.2 'Creep coefficient' traction curve measurement

The used TTBM brake strategy for the simulations (measure up to and beyond the peak of the traction curve) is one way to utilize the TTBM. Another way to use the TTBM is by measuring only a part of the slope of the traction curve, to determine the creep coefficient. In Appendix E, two traction curve measurement results on a twin-disc machine are presented, in which one test was conducted under 'dry' conditions while the other test was carried out with oil within the WRI, thus 'third body' friction conditions, resulting in a lower creep coefficient. If enough data is gathered about traction curves, one could use this to estimate the peak CoF by extrapolating the creep coefficient, as shown in figure 6-6.

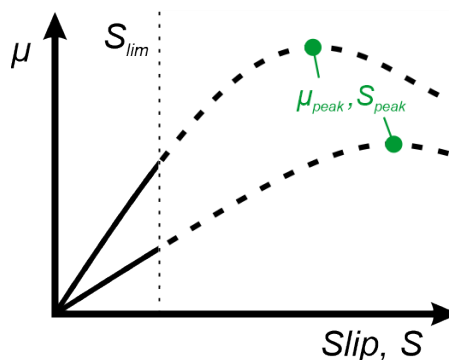


Figure 6-6. Measuring up to a certain low slip limit (S_{lim}) to determine the creep coefficient.

There are advantages of the creep coefficient measurement strategy over the peak traction curve measurement strategy. Significant lower brake forces can be used during the TTBM brake test to measure the friction. This will result in a lower jerk motion, removing the possible impairment of passenger comfort. A lower brake force and consequently a lower friction force result also in a lower wear and tear of the brakes, wheel tread and rail top of head.

In addition, since one is only interested in the creep coefficient, no excessive slip occurs and thus the dynamic effects become minimal. This means that the effect of the second term in the RHS of equation 4.15 ($F_f = \frac{c}{R} F_R + \frac{I}{R} \alpha$) attenuates. The rotational acceleration will be determined by the time derivative of the tachometer, resulting in noise caused by taking the derivatives. Not needing to measure this term would make it much simpler and more accurate to estimate the friction force.

The design of the TTBM and its subsystems depend heavily on the brake strategy. Suppose one is able to measure the creep coefficient and estimate accurately the available friction (by extrapolating), then the applied brake force by the TTBM would be low. If one chooses the separate brake module to carry out the TTBM test, as shown in figure 6-3, then this module does not have to be large and clunky due to the lower applied brake force. The brake system does not have to be designed to apply large brake forces and the brake force sensors do not have to measure within a large brake force range that reach high friction levels, but only a fraction of it.

There are however some points to consider regarding the creep coefficient measurement strategy. One needs good knowledge of traction curves within the WRI, in order to extrapolate to peak value traction curve by measuring only the creep coefficient.

As shown in the preceding chapter, a certain amount of slip is naturally present within the wheelsets due to track irregularities and the hunting motion. The presence of slip noise causes a certain error in the determination of the creep coefficient. Hence, a certain amount of slip needs to be measured to estimate the creep coefficient with a certain accuracy. Also, since one measures in low slip ranges, an accurate and a high resolution slip sensor is needed in order to have a decent creep coefficient resolution.

Nevertheless, the creep coefficient measurement strategy has certain major advantages which are worth testing it.

6.3 TTBM design cycle

As shown in section 6.1, for each sub-systems of the TTBM (brake-, normal force- and slip measurement sub-system), multiple options exist. Choosing the right design for each sub-system depends on the given requirements, which on their turn are based on the use case (chapter 2, ERTMS, ATO, WRC, etc.). This design pattern is shown in figure 6-7. Normally for a design process, a certain problem exists, i.e., a certain use case, from which requirements follow and a certain design emerges. In figure 6-7 this pattern for the TTBM is then $A \rightarrow B \rightarrow C$.

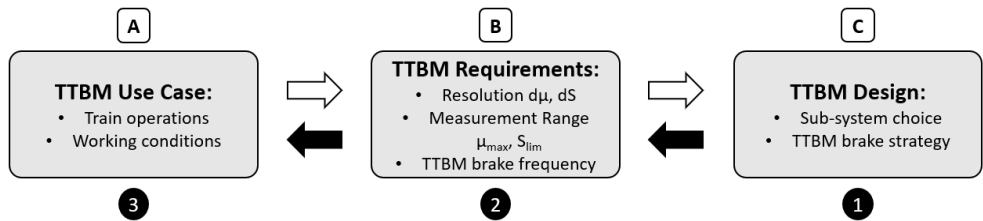


Figure 6-7. TTBM Design steps. Note, iteration occurs between the three levels.

To conclude, two use cases (ERTMS and WRC, see chapter 2) will be compared, by using the approach $A \rightarrow B \rightarrow C$ from figure 6-7. It is assumed that for ERTMS the TTBM needs to be accurate within the low friction regime (CoF up to 0.15). The WRC use case is, in addition to the low friction regime, interested in the high friction regime as well (CoF up to 0.25). For the WRC use case, the traction curve measurement accuracy ($d\mu$ and dS) is lower compared to the ERTMS case. Table 6-1 shows the requirements and accompanying TTBM sub-system design choices for both use cases.

Note, this is only an example to illustrate that two distinct use cases lead to different requirements and ultimately one may choose an alternative TTBM design. Over time, requirements will change, if more is known about the TTBM regarding measuring traction curves by simulations, lab-experiments, and field tests.

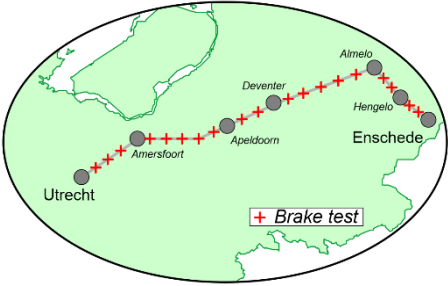
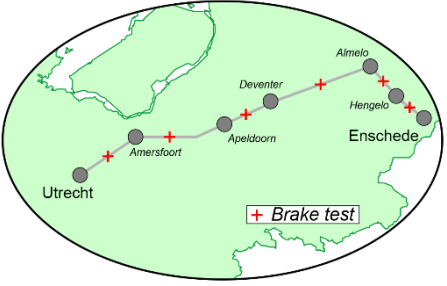
<u>TTBM Use Case</u>	
ERTMS	WRC
Increase (passenger) train density	(Predictive) maintenance
TTBM within passenger train	TTBM within maintenance train
Preferably on all tracks	Mainly measure track on critical points (e.g. track before station)
<u>TTBM Requirements</u>	
$\mu_{\max} = 0.15, S_{\lim} = 0.02$	$\mu_{\max} = 0.25, S_{\lim} = 0.05$
$d\mu = 0.01, dS = 0.001-0.002$	$d\mu = 0.02, dS = 0.005$
High frequent TTBM measurement to safeguard the distance between trains	Low frequent TTBM measurement to check low/high adhesion per track
	
Additional requirements, e.g., regarding passenger comfort	Less demanding additional requirements
<u>TTBM Design</u>	
Separate brake force module OR Built-in brake force system without decoupling of central brake system	Built-in brake force system
Normal force sensor within PS	Expected static normal force
'Creep coefficient' traction curve measurement	'Peak and beyond' traction curve measurement

Table 6-1. Illustrative example of the ERTMS and WRC use cases, leading to different requirements and TTBM design.

However, in the case of the TTBM design, even though there are multiple use cases, the requirements are not strictly defined, especially regarding to how accurate the traction curves need to be measured. This also has to do with traction curves being relatively unknown within the railway industry. To give more insight for what the TTBM can be used for, one could also start with a certain TTBM design by choosing the options of the sub-systems and accompanying sensors that lead to the best traction curve measurement. This will result in a certain resolution and accuracy in measuring the traction curves, which is then applicable for various use cases. In figure 6-7, this pattern is shown as 1→2→3. One can always simplify the design later if certain sub-systems are over-qualified for certain use cases.

Because of this, the design pattern 1→2→3 in figure 6-7 will be recommended and by realising the most accurate TTBM design for the measurement train of the TU Delft, the TTBM will be the most versatile and applicable in many use cases.

Hence, the recommendation for the TTBM design will be: regarding the sub-systems of the TTBM, for the brake measurement system, the separate brake module will be recommended, it does not require to decouple a single brake system, as shown in figure 6-3. To measure the applied brake force as close as possible, integrate the force transducers within the brake pad holders of the separate module. For the normal force measurement system, by placing force transducers within the primary suspension, one captures the normal force of the wheelset and varying normal forces among the left and right wheel. Regarding the slip measurement system, two tachometers will be used to measure the rotational velocity of the braked and non-braked wheelset. Regarding the drive direction of the train, carry out the TTBM brake test on the trailing wheelset of a bogie, due to the lower traction curve estimation errors as mentioned in chapter 5. As for the brake strategy, measuring traction curve peak values and beyond accurately will be endorsed. This gives proper feedback regarding the further development of the TTBM brake and potentially form the basis to measure creep coefficients instead. Before carrying out field tests, lab test validation of the sub-systems of the TTBM design need to be carried out first, which will be discussed in the next chapter.

6.4 Conclusion

Regarding the sub-systems of the TTBM (brake-, normal force- and slip measurement sub-system), multiple design options are possible and were presented. Additionally, two main TTBM brake strategies were discussed. The first strategy is to measure the peak values and the second strategy is to focus on measuring the creep coefficient of traction curves. Depending on the use case and the accompanying requirements, different sub-system design combinations will comply with the requirements.

A TTBM design recommendation is given. Within the TTBM bogie, the TTBM brake should be applied to the trailing wheelset. For the brake measurement system, it is advised to add the separate brake module (see figure 6.3) and integrate the force transducers within the brake pad holders. For the normal force measurement system, place force transducers within the primary suspension and for the slip measurement system, two tachometers will be used to measure the rotational velocity of the braked and non-braked wheelset. Measuring accurately traction curve peak values and beyond will be recommended to be used as brake strategy.

Chapter 7 – Conclusions and recommendations

7.1 Conclusions

This report investigated, by means of multibody-dynamics (MBD) simulations, the feasibility of the TTBM concept. Regarding the MBD simulations of the TTBM on a straight track with track irregularities, using the scenarios and conditions set in chapter 5, the following can be concluded:

- In chapter 6 the design cycle is shown, in which the TTBM could be designed to accommodate certain use cases and requirements. The use cases are known, however the accompanying requirements are inexact. If this problem is approached by starting at the TTBM design and one would go for the most accurate version of the TTBM, it will then also be the most versatile version and applicable in the most use cases.
- The TTBM brake force profile (input of the system, to be applied on the wheelset) has the following TTBM brake design parameters: The traction curve measurement range is determined by the slip limit and the maximum CoF one wants to measure (S_{lim} , μ_{max}), and the TTBM brake is carried out within a certain amount of time (duration, T). These design parameters can be altered to meet requirements of certain use cases.
- As for the location of the TTBM within the bogie, the trailing wheelset is preferred, since the leading wheelset is more often in flange contact upon entering track irregularities or when traversing a curve, which results in larger slip and CoF estimation errors.
- The absolute slip estimation error varies up to roughly 0.6%. Track irregularities, in combination with hunting of the train, see figure 7-1, causes a change in rolling radii in both the leading and trailing wheelset, ΔR_1 and ΔR_2 respectively, as shown in figure 7-2. The difference in change in rolling radii between the leading and trailing wheelset, ΔR , causes a slip estimation error in the TTBM.

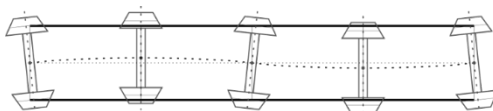


Figure 7-1. Hunting motion of the wheelset.



Figure 7-2. Change in rolling radii due to track irregularities.

- Using only the estimated static normal force, the relative CoF estimation error is about 15-20%. This is mainly caused by varying normal forces by track irregularities, the induced change in normal force by the TTBM brake itself and other dynamic effects (e.g. de- or acceleration of the train itself).
- Note, these values for the estimation errors should not be taken over blindly, as the influence of the various track irregularities and train dynamics vary a lot. Not always do these errors present themselves, there is a certain probability of occurrence of the slip and CoF estimation errors.

Based on the results of the MBD simulations of chapter 5 and the design considerations in chapter 6, it can be concluded that the TTBM is a feasible method to measure traction curves.

7.2 Discussion

There are multiple ways to measure adhesion, or traction curves, within the Wheel-Rail Interface (WRI). The Train Tribometer (TTBM) concept is such an adhesion sensor and has been designed and investigated. Within the TTBM concept, multiple design options are available with certain slip and CoF resolution and accuracy, as shown in the previous chapter. In section 7.3.1, a recommendation is given.

For the multibody dynamics (MBD) simulations, certain scenarios were chosen above others (specific train and track conditions as shown in chapter 5). One might get different results when looking at a different set of scenarios. E.g., at different track speeds, alternative track irregularities requirements are set. Dynamic effects increase as well at higher train speeds, which result in different slip and CoF estimation errors.

A wheelset in a train consists of two wheels both in contact with the rail, which are rigidly fixed together. The wheelset has two WRI. Within the MBD simulations, one is limited to equal friction conditions in the left and right contact. The friction conditions do not have to be equal for the left and right WRI, which could lead to a different readout and interpretation of the TTBM, as shown in figure 7-3.

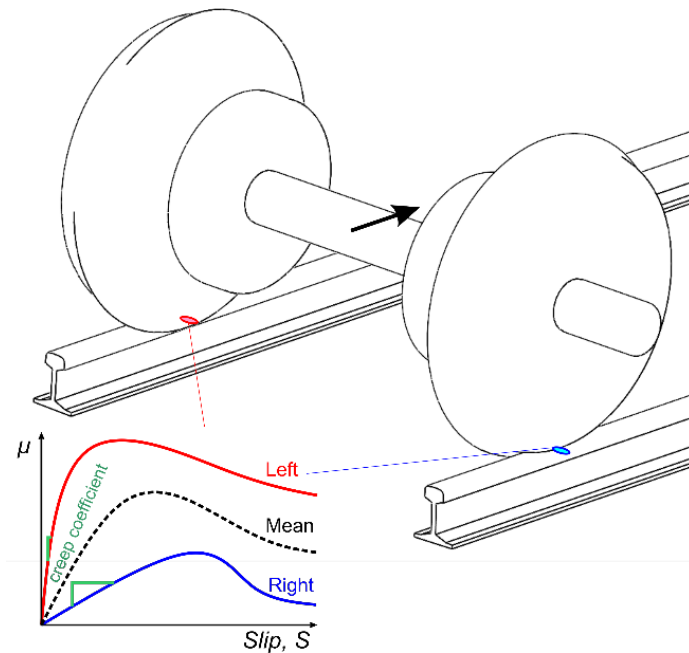


Figure 7-3. Different friction conditions for the left and right WRI of a wheelset.

7.3 Recommendations

7.3.1 TTBM Design

To design the most accurate and therefore most versatile version of the TTBM, it is desirable to take the TTBM design as a starting point (as mentioned in section 7.1).

Therefore, the TTBM design with the highest resolution and accuracy for the first field tests of the TTBM in an actual measurement train (TRL 5-6) will be recommended and is shown in figure 7-4. For the brake force measurement system, instead of decoupling one brake system of one wheelset, a separate brake module should be designed instead. The brake force sensors are integrated within the brake pads of this separate brake module. As for the normal force measurement system, to determine the normal force of the braked wheelset and variations between the left and right wheel of the braked wheelset, force transducers need to be integrated within the primary suspension. For the slip measurement system, the braked and non-braked wheelset will be equipped with a tachometer. The TTBM design and its sub-systems need to be validated.

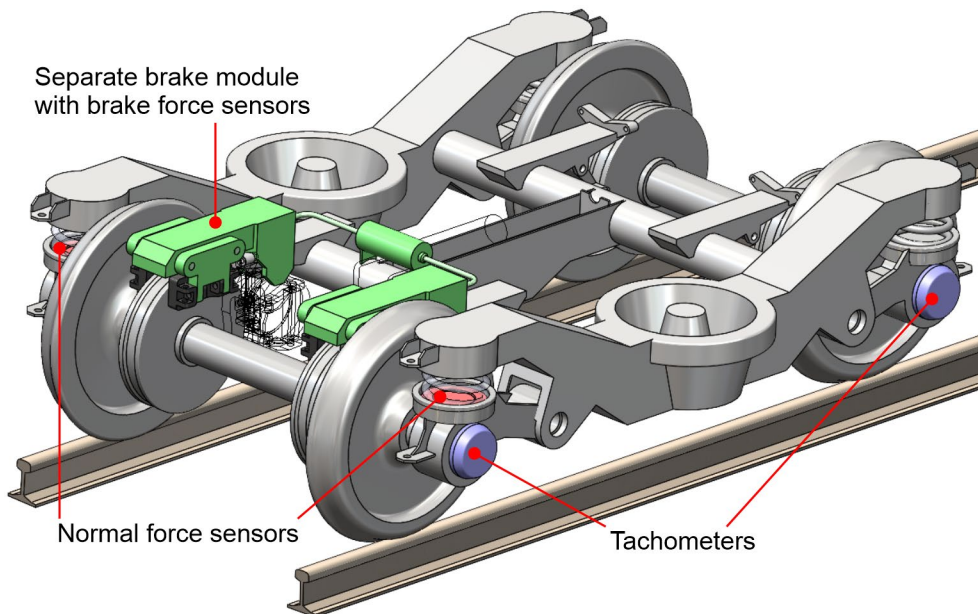


Figure 7-4. Proposed TTBM design.

7.3.2 Validation by lab experiments

Most results so far are largely obtained by simulations. Lab experiments are needed to validate the sub-systems of the TTBM brake system. One could start with a twin disc machine, that is able to brake only one disc and adapt the normal force when the discs are up and running. By testing different TTBM brake design parameters (such as S_{lim} , μ_{max} and T), one can assess various brake strategies. E.g., by shortening the TTBM brake time (T), the significance of the dynamic part (the rotational inertia and rotational deceleration) can be measured.

The next step, after carrying out tests on a single twin disc machine, would be to test a wheelset on a double twin disc machine. This way, different conditions for the left and right WRI can be tested and its influence on the TTBM measurement analysed (such as friction conditions as shown in figure 7-3, but normal force or even different wheel profiles as well).

7.3.3 Validation by field tests

Not everything can be tested with lab setups, eventually field tests are required as well. For now, this seems to be far away, and the focus should be on validating the TTBM on lab setups, but one might already carry out certain field tests. One does

not need to directly build a complete TTBM system within a train to do so, some subsystems can be tested individually.

For the slip measurement system, if a certain track is exactly known (the exact track irregularities are known over the whole track distance), one can monitor the tachometer readout when traversing certain track irregularities and its influence on the slip measurement.

One can also gradually test the TTBM design by first only testing the normal force measurement system and monitor the normal force transducer readout when traversing a track with specific irregularities or curves and during de- and acceleration of the train. As for the brake system, considering comfort, one might want to measure the accompanying deceleration and jerk (time derivative of the deceleration) when carrying out a short brake.

7.4 Closure

In the end, one wants to use such an adhesion sensor to know the actual adhesion levels on the tracks. The TTBM is a promising concept for the 'live and on-board' adhesion sensor, which measures traction curves, to be used for train operations and (predictive) maintenance. Braking distances of trains can be estimated (relevant for ATO/ERTMS), which increase train capacity by decreasing the distance between trains. Also, by knowing the location of too slippery or too dry tracks (too low or high adhesion, respectively), the right precautions can be applied (usage of friction modifier such as Sandite, adjust the drive behaviour), which lead to less downtime of assets and reduce the overall costs.

Sooner or later, *not* knowing the actual adhesion levels is going to be the bottleneck in increasing train capacity, hence the TTBM is needed. Understanding how one could translate any 'live and on-board' adhesion sensor to the amount of grip a train has between its wheels and track is therefore essential.

A.2 LOC-CTO system parameters

But also dimensions of the LOC and CTO combination used in the VI-Rail simulations are shown in figure A-3.

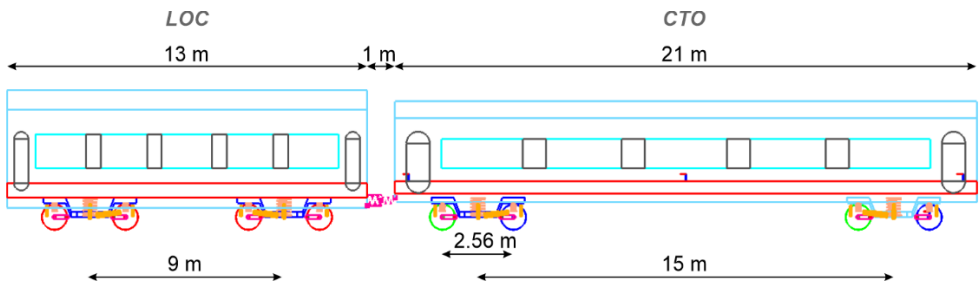


Figure A-3. The dimensions of the LOC and CTO wagon.

The accompanying weight values and system parameters are shown in Table A-1.

Parameter	Value
M_{LOC}	72.5 ton
$M_{CTO, wagon}$	31 ton
M_{bogie}	2.6 ton
$M_{wheelset}$	1.5 ton
$M_{axle\ box}$	0.15 ton
M_{CTO}	43.5 ton
$I_{wheelset}$	122 kg m ²
R_0	0.46 m
c	0.22 m

Table A-1. Used train parameters for the simulations.

Appendix B – TTBM brake strategy

B.1 Deceleration

TTBM brake design variables		
Parameter	Value [unit]	Description
T	1 [s]	TTBM measurement duration
μ_{max}	0.2 [-]	Want to measure up to this level of friction
S_{lim}	0.05 [-] 5 [%]	Slip limit, if slip reaches this value, then release the brake force
Train parameters		
Parameter	Value [unit]	Description
R [m]	0.46	Radius wheel
c [m]	0.22	Distance brake to center wheelset
I [kg m ²]	122	Inertia of the wheelset
F_N [kN]	109	Normal force
V_1 [m/s]	40	Train speed

Table B-1. TTBM brake design and train parameters.

The required brake force is:

$$F_R = \frac{R}{c} \mu_{max} F_N - \frac{I}{c} \alpha \quad (B.1)$$

The circumferential velocity of the braked wheelset at the slip limit can be simplified:

$$v_{2,lim} = \frac{2 - S_{lim}}{2 + S_{lim}} \cdot v_1 \approx (1 - S_{lim}) \cdot v_1 \quad (B.2)$$

The mean deceleration value of the braked wheelset during the TTBM brake, which has a duration of T seconds, can be found in the following way, by substituting equation B.2 into equation B.3:

$$\alpha = \frac{(v_{2,lim} - v_1)}{R \cdot T} = -\frac{v_1 S_{lim}}{R \cdot T} \quad (B.3)$$

Substituting equation B.3 into equation B.1 gives:

$$F_R = \frac{R}{c} \mu_{max} F_N + \frac{I}{c} \frac{v_1 S_{lim}}{R \cdot T} = F_{R,static} + F_{R,dynamic} \quad (B.4)$$

The first term on the RHS will be referred to as the static part, the second term the dynamic part. When using the values in Table B-1, $F_{R,static} = 45,5$ kN and for changing duration T, the dynamic part changes and is shown in Table B-2.

T	0.1 s	0.5 s	1 s
$F_{R,dynamic}$	24,1 kN	4,82 kN	2,41 kN

Table B-2. Increased dynamic part of the brake force when decreasing T .

For this reason, the duration is set to 1 second. Two things need to be considered, the profile of the input brake force and the actual friction force, or traction curve, that is present.

Suppose a brake profile is determined for the design parameters as shown in Table B-1, μ_{max} is 0.2 at $S_{lim} = 5\%$. When a TTBM brake is carried out and when in presence of such a traction curve, it should be able to measure that part of the traction curve.

Now suppose the same brake profile is fixed for all TTBM brakes and is applied in presence of extreme low friction ($\mu_{peak} \approx 0$). Almost no friction torque is present, hence all the brake torque will rotationally decelerate the wheelset and will reach the slip limit earlier than the brake force profile is designed for (in presence of a traction curve with $\mu_{peak} = 0.2$). The brake force needs to be relieved when the slip limit is reached. This brake force relieve needs to be fast, otherwise the wheelset will freeze, i.e., reaching high slip, and will result in flat spots.

In case of extreme high friction, the traction curve has a higher creep coefficient (e.g., $\mu_{peak} \approx 0.4$ at 5% slip), enough friction is present even to account for the peak applied brake force, leading to a slip limit not being reached within the duration of the TTBM brake.

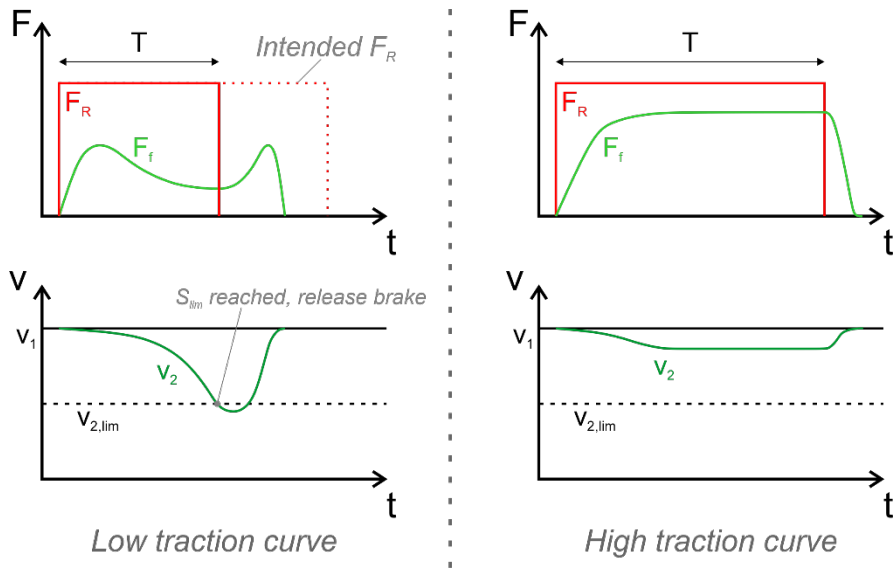


Figure B-1. Same Brake profile under low and high traction curve conditions. Note, $v_{2,lim} = (1 - S_{lim})v_1$.

If one wants to measure slip values above 5%, say $S_{lim} = 10\%$ or so, then most traction curves tend to flatten or drop after reaching the peak value (see chapter 3). This non-linear, hard to predict behaviour of traction curves makes it hard to design a proper brake force profile.

B.2 Brake force profile

Two input profiles will be considered, the ramp and step function, see figure B-2.

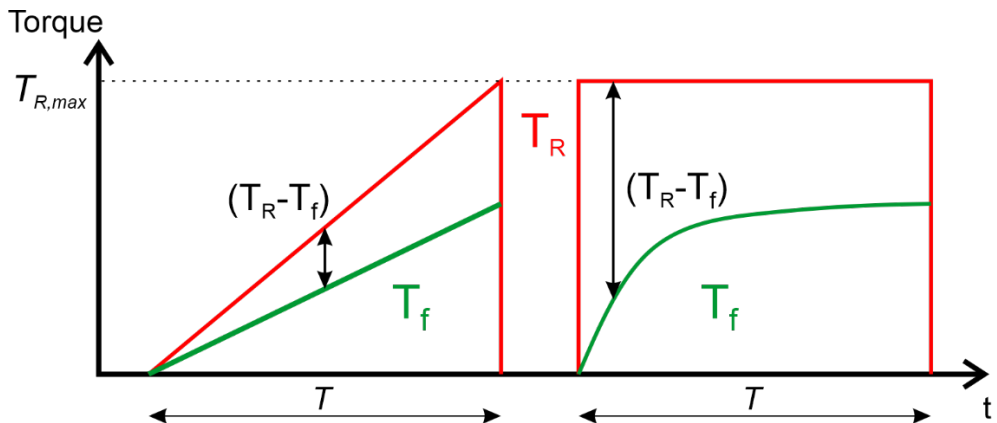


Figure B-2. Brake torque (T_R) ramp profile on the left and the step function on the right, causing a different response in friction torque (T_f).

Note, the brake torque is $T_R = c \cdot F_R$ and the friction torque is $T_f = R \cdot F_f$. The remainder of the two torques divided by the inertia of the wheelset determines the instantaneous deceleration:

$$\alpha = \frac{T_R - T_f}{I} \quad (\text{B.5})$$

The ramp function leads to a lower rotational deceleration and a more fluent increase of friction force. This generated friction force is also felt in the wagon/train since it slows down the train. A larger friction force leads to a larger deceleration, but a faster changing friction force leads to a larger jerk $\left(\frac{da}{dt} \left[\frac{m}{s^3}\right]\right)$. The step function is easier to apply as well to analyse, more data points are acquired at the height of the brake force. One might consider combining the two types, this would lead to a shape as in figure B-3.

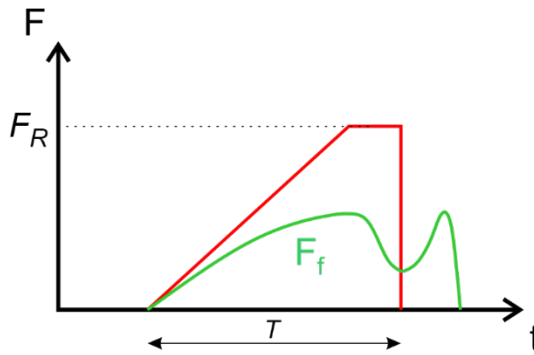


Figure B-3. A ramp and step function combined.

B.3 Work wheelset within TTBM brake and normal braking

A comparison regarding brake intensity or energy between TTBM braking and normal braking has been made. Sufficient friction is present, no overshoot (high slip) occurs. Over a certain route, N brake tests will be carried out, as shown in figure B-4.

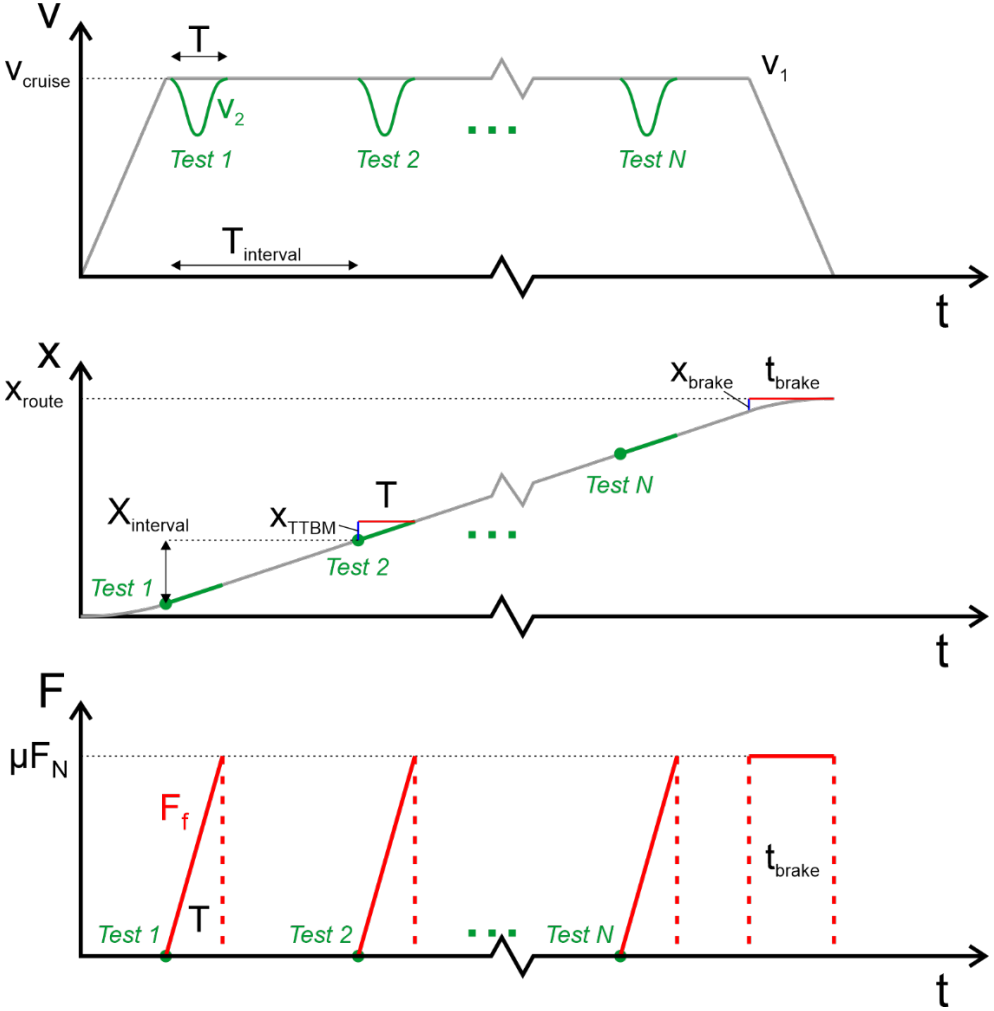


Figure B-4. The velocity, distance and force profile over time.

The amount of work done by a TTBM brake within the WRI is:

$$W_{f,TTBM} = F_{f,TTBM} \cdot x_{TTBM} = \frac{1}{2} \mu F_N \cdot v_{train} \cdot T \quad (B.6)$$

Note, the $\frac{1}{2}$ factor is due to the ramp profile of the friction force. For a normal train brake operation, the deceleration, time to brake and the braking distance are:

$$a_{brake} = \mu g; \quad t_{brake} = \frac{v_{train}}{a_{brake}}; \quad x_{brake} = \frac{1}{2} \frac{v_{train}^2}{\mu g} \quad (B.6)$$

The amount of work done by the normal brake within the WRI is:

$$W_{f,brake} = F_{f,brake} \cdot x_{brake} = \mu F_N \cdot \frac{1}{2} \frac{v_{train}^2}{\mu g} \quad (B.8)$$

The train parameters are shown in Table B-1. The input as well as the output parameters are shown in Table B-3.

Input		Output	
V_1 [m/s]	30	X_{route} [km]	20
μ [-]	0.2	X_{TTBM} [m]	30
T [s]	1	X_{brake} [m]	450
x_{route} [km]	20	$W_{f,brake}$ [kJ]	5625
$x_{interval}$ [km]	2	$W_{f,TTBM}$ [kJ]	187.5
N [-]	10	$W_{f,TTBM,N}$ [kJ]	1875

Table B-3. Input and output values regarding work done by TTBM braking and normal braking.

Now the work done by the brake pad will be investigated. The rotational velocity is:

$$\omega = \frac{2 - S}{2 + S} \cdot \frac{v_{train}}{R} \quad (B.9)$$

The distance covered by the brake pad, as shown in figure B-5, on the brake disc depends on the amount of slip:

$$x_R = \omega \cdot c \cdot T = \frac{2 - S}{2 + S} \cdot \frac{c}{R} \cdot v_{train} \cdot T \quad (B.10)$$

Suppose wheel locking occurs during braking, i.e., $S=2$. That means that the rotational velocity of the wheel drops to zero and no distance is covered by the brake pad onto the brake disc. It only holds the wheel, the brake force is there, but no work is done once the wheel is in full slip by the brake pad in this scenario. The train still has a translational velocity and so does the wheel, leading to distance covered in the WRI leading to work done by the friction force. If no overshoot happens ($S < 5\%$), then the braking distance by the brake pad becomes:

$$x_R \approx \frac{c}{R} \cdot v_{train} \cdot T \quad (B.11)$$

The work done by braking is then:

$$W_R = F_R \cdot x_R = \frac{R}{c} F_f \cdot \frac{c}{R} \cdot v_{train} \cdot T = F_f \cdot v_{train} \cdot T \quad (B.12)$$

Which is the same as the work done within the WRI in equation B-6.

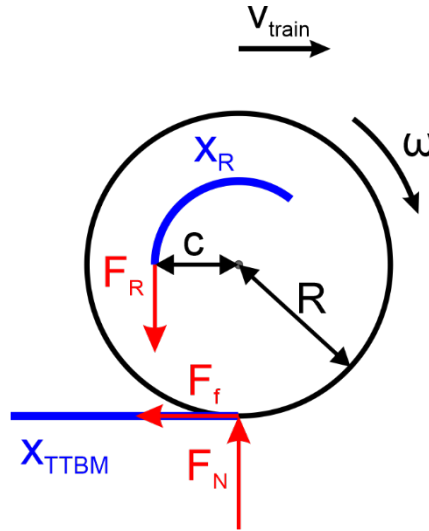


Figure B-5. Work done by the friction force and brake force.

Appendix C – Sensor resolution

The following TTBM brake and train parameters will be used:

TTBM brake design variables		
Parameter	Value	Description
T	1 [s]	TTBM measurement duration
μ_{\max}	0.2 [-]	Want to measure up to this level of friction
S_{\lim}	0.05 [-] 5 [%]	Slip limit, if slip reaches this value, then release the brake force
Train parameters		
Parameter	Value	Description
R [m]	0.46	Radius wheel
c [m]	0.22	Distance brake to center wheelset
I [kg m ²]	122	Inertia of the wheelset
F_N [kN]	109	Normal force
V_1 [m/s]	40	Train speed
Desired resolution steps		
$d\mu$ [-]	0.01	CoF resolution
dS [-]	0.001	Slip resolution

Table C-1. TTBM brake design and train parameters as well as desired resolution steps.

An overview of the resolution formulas is given in Table C-2. The derivations of these formulas are given in the sections C.1 and C.2.

An overview of the calibration errors of certain train parameters and its effects on determining the CoF and slip is shown in Table C-3. The derivations of these formulas are given in section C.3.

CoF ($d\mu = 0.01$)	
Friction force resolution	$dF_f = F_N d\mu = 1.09 \text{ kN}$
Brake force resolution	$dF_R = \frac{R}{c} F_N d\mu = 2.28 \text{ kN}$
Four sensors in four brake pads	$\frac{dF_R}{4} = 0.57 \text{ kN}$
Normal force resolution (at $\mu=0.2$)	$dF_N = -F_N \frac{d\mu}{\mu} = 5.45 \text{ kN}$
Two normal forces within PS (left and right side wheelset)	$\frac{dF_N}{2} = 2.73 \text{ kN}$
Slip ($dS = 0.001$)	
Braked wheelset tachometer resolution (at $v_1=40 \text{ m/s} = 144 \text{ km/h}$)	$dv_2 = -v_1 dS = 0.04 \text{ m/s}$
	$dRPM = \frac{dv_2}{2\pi \cdot R} \cdot 60 = 0.83 \text{ RPM}$
Braked wheelset tachometer resolution (at $v_1=10 \text{ m/s} = 36 \text{ km/h}$)	$dv_2 = -v_1 dS = 0.01 \text{ m/s}$
	$dRPM = \frac{dv_2}{2\pi \cdot R} \cdot 60 = 0.21 \text{ RPM}$

Table C-2. The required resolutions of sensors for a certain slip and CoF resolution.

CoF error, $\Delta\mu$	
Error in brake force estimation	$\Delta_c \mu = \frac{\frac{\Delta_c c}{R} F_R}{F_Z}; \quad \frac{\Delta_c \mu}{\mu} = \frac{\Delta_c c}{c}$
Error in expected static normal force F_Z	$\frac{\Delta_c \mu}{\mu} = -\frac{\Delta_c F_Z}{F_Z + \Delta_c F_Z}$
Slip error, ΔS	
Slip error (for $S < 10\%$), due to change in rolling radius R_2 (same formula if only R_1 has an error $\Delta_c R$ in wheel radius)	$\Delta_c S = \frac{\Delta_c R}{R_2}$

Table C-3. Errors in parameters leading to certain CoF and slip errors.

C.1 CoF

Suppose one wants to measure a traction curve with an accuracy of $d\mu$. Change of CoF due to change of F_f or F_N :

$$\mu = \frac{F_f}{F_N}; \quad d\mu = \frac{\delta\mu}{\delta F_f} dF_f + \frac{\delta\mu}{\delta F_N} dF_N = \frac{1}{F_N} dF_f - \frac{F_f}{F_N^2} dF_N \quad (C.1)$$

C.1.1 Friction force sensor

Change in friction force F_f (fixed F_N):

$$d\mu = \frac{\delta\mu}{\delta F_f} dF_f = \frac{dF_f}{F_N} \rightarrow dF_f = F_N d\mu \quad (C.2)$$

This part is rather straightforward, since the (change in) friction force and (change in) CoF are linearly proportional.

$$cF_R - RF_f = I\alpha \xrightarrow{\text{neglect } \alpha} F_R = \frac{R}{c} F_f \quad (C.3)$$

This would lead to the accuracy of the brake force sensor (i.e., friction force sensor):

$$dF_f = F_N d\mu \rightarrow dF_R = \frac{R}{c} F_N d\mu \quad (C.4)$$

C.1.2 Normal force sensor

Change in normal force F_N (fixed F_f):

$$d\mu = \frac{\delta\mu}{\delta F_N} dF_N = -\frac{F_f}{F_N^2} dF_N = -\mu \frac{dF_N}{F_N} \rightarrow dF_N = -F_N \frac{d\mu}{\mu} \quad (C.5)$$

This part is harder to grasp. Suppose there is no friction force, meaning F_f and CoF are zero. Then no matter how much the normal force changes, the CoF remains zero. When a certain friction force is present and is fixed (thus, there is a certain CoF) then a small drop in normal force would lead to a small increase in CoF. This small increase in CoF is higher at a higher CoF.

Note, one could also introduce a normal force resolution to measure changes in normal forces due to all kinds of effects as mentioned in section 5.4, instead of $\Delta_c\mu$.

C.1.3 Braking distance

Perhaps one wants to have a certain dx (say, 50 m or 100 m so at a train speed of 144 km/h = 40 m/s) in braking distance resolution, what should the resolution of $d\mu$ be at $\mu = 0.01$, $\mu = 0.1$ or $\mu = 0.2$?

$$x_{brake} = \frac{1}{2} \frac{v_{train}^2}{\mu g} \quad (C.6)$$

The change in braking distance due to change of μ :

$$dx_{brake} = \frac{\delta x_{brake}}{\delta \mu} d\mu = -\frac{1}{2} \frac{v_{train}^2}{\mu^2 g} d\mu \quad (C.7)$$

Now suppose one is able to measure with an accuracy of $d\mu$ (value in Table C.1), Table C-4 shows the braking distance resolution for two train speeds and available CoF options.

Train speed	$V_{train} = 10 \text{ m/s} = 36 \text{ km/h}$		$V_{train} = 40 \text{ m/s} = 144 \text{ km/h}$	
CoF	$\mu = 0.05$	$\mu = 0.15$	$\mu = 0.05$	$\mu = 0.15$
$dx_{brake} [\text{m}]$	20	2	320	36
$x_{brake} [\text{m}]$	100	33	1600	533

Table C-4. The braking distance as well as the resolution at certain train speeds and CoFs.

One could also set up a desired braking distance resolution at a given train speed and a certain CoF. Rewriting equation C.7 gives:

$$d\mu = -\frac{2\mu^2 g}{v_{train}^2} dx_{brake} \quad (C.8)$$

C.2 Slip

For the slip, a certain resolution is desired. Changes in v_1 and v_2 cause a change in S :

$$dS = \frac{\partial S}{\partial v_1} dv_1 + \frac{\partial S}{\partial v_2} dv_2 \quad (C.9)$$

This will be split in two parts, first the wheel velocity part v_2 since it changes the most during such a measurement. The second part is about changes in slip due to the change in wheel velocity of the non-braked wheelset v_1 .

$$S = 2 \cdot \frac{v_1 - v_2}{v_1 + v_2} = 2 \cdot \frac{u}{e} \quad (C.10)$$

Suppose v_1 is held constant, the change in slip due to a change in wheel velocity v_2 would then be:

$$dS = \frac{\partial S}{\partial v_2} dv_2 \quad (\text{C.11})$$

Using the chain and sum rule for the partial derivative on the RHS:

$$\begin{aligned} \frac{\partial S}{\partial v_2} &= \frac{dS}{du} \frac{du}{dv_2} + \frac{dS}{de} \frac{de}{dv_2} = \frac{2}{e} \cdot -1 + -\frac{2u}{e^2} \cdot 1 \\ \frac{\partial S}{\partial v_2} &= -\frac{2}{v_1 + v_2} - \frac{2(v_1 - v_2)}{(v_1 + v_2)^2} \end{aligned} \quad (\text{C.12})$$

Rewriting gives:

$$\frac{\partial S}{\partial v_2} = -\frac{2(v_1 + v_2)}{(v_1 + v_2)^2} - \frac{2(v_1 - v_2)}{(v_1 + v_2)^2} = -\frac{4v_1}{(v_1 + v_2)^2} \quad (\text{C.13})$$

One could rewrite the slip formula to find the wheel velocity v_2 :

$$v_2 = \frac{2 - S}{2 + S} \cdot v_1 \quad (\text{C.14})$$

Substituting this in the partial derivative equation gives:

$$\frac{\partial S}{\partial v_2} = -\frac{4v_1}{\left(v_1 + \frac{2 - S}{2 + S} \cdot v_1\right)^2} = -\frac{4}{v_1 \left(1 + \frac{2 - S}{2 + S}\right)^2} \quad (\text{C.15})$$

Substituting this in equation C.11 to find dS :

$$dS = \frac{\partial S}{\partial v_2} dv_2 = -\frac{4}{v_1 \left(1 + \frac{2 - S}{2 + S}\right)^2} dv_2 \quad (\text{C.16})$$

Rewrite to find the change in wheel velocity for a certain slip change:

$$dv_2 = -\frac{1}{4} v_1 \left(1 + \frac{2 - S}{2 + S}\right)^2 dS = -4v_1 \left(\frac{1}{2 + S}\right)^2 dS \quad (\text{C.17})$$

$$dv_2 = -4v_1 \left(\frac{1}{4 + 4S + S^2} \right) dS = -\frac{v_1}{1 + S + \frac{1}{4}S^2} dS \approx -\frac{v_1}{1 + S} dS$$

One could neglect the squared term of S, if S is low (if $S_{lim}=0.2$; $1+S_{lim}=1.2$; $0.25S_{lim}^2=0.01$, error 0.83%):

$$dv_2 \approx -\frac{v_1}{1 + S} dS \quad (C.18)$$

In a similar way, one could find the change in v_1 (while keeping v_2 fixed):

$$dv_1 \approx -\frac{v_2}{1 - S} dS \quad (C.19)$$

A simplified formula is given as well (for $S < 10\%$):

$$v_2 = (1 - S)v_1 \rightarrow S = 1 - \frac{v_2}{v_1} \quad (C.20)$$

Then:

$$dS = -\frac{dv_2}{v_1} \rightarrow dv_2 = -v_1 dS \quad (C.21)$$

Compared to equation C.18, around $S=0\%$ the resolution step is the same and the error is roughly 10% at $S=10\%$. For a rough estimation of the required resolution step of dv_2 of a desired resolution step dS , this simplification step is acceptable.

Note, in Appendix E, twin-disc experiments were carried out at 400 RPM, the radii of both discs were 27 mm. The used encoder is able to measure with a resolution of 0.1 RPM, using equation C.21 results in the following slip resolution:

$$dS = \frac{\frac{0.1}{60} \cdot 2\pi \cdot 0.027}{\frac{400}{60} \cdot 2\pi \cdot 0.027} = 0.00025 = 0.025\% \quad (C.22)$$

C.3 Parameter errors - Calibration

C.3.1 Slip error due to wheel radius error

Writing the slip equation in terms of rotational velocities and radii:

$$S = \frac{2 \cdot (\omega_1 R_1 - \omega_2 R_2)}{\omega_1 R_1 + \omega_2 R_2} \quad (C.23)$$

Suppose the train has a constant speed and the wheels roll without slip ($S=0$, $v_1=v_2$) and hunting/track irregularities are not considered. Two scenarios, in the first one the wheel radii are equal and perfectly calibrated (the wheel radii are 0.46 m). This leads to a perfect measurement of slip, namely $S=0$. In the second scenario, one of the two wheelsets is slightly smaller, but the original values are still used. While the actual slip is still 0, this induces an error in determining the slip. The slightly smaller wheel has a slightly increased rotational velocity.

Suppose one only remains within the low slip regime ($S<10\%$), by using equation C.21 and by using $v_1 = \omega_1 \cdot R_1$ and $v_2 = \omega_2 \cdot R_2$, one could find the changed rotational velocity:

$$\omega_2 R_2 = (1 - S) \omega_1 R_1 \quad (C.24)$$

If one looks around $S = 0$ and introduces the small error within the braked wheelset (however no braking and $R_2 = R_2 + \Delta_c R$), then one could express the rotational velocity of the non-braked wheelset as:

$$\omega_1 = \frac{R_2 + \Delta R}{R_1} \omega_2 \quad (C.25)$$

Substituting this within the slip equation gives:

$$\Delta_c S = \frac{2 \cdot ([R_2 + \Delta_c R] \omega_2 - \omega_2 R_2)}{[R_2 + \Delta_c R] \omega_2 + \omega_2 R_2} \quad (C.26)$$

Note, only ω_1 has been substituted in which the error is contained. If one would substitute all $R_2 = R_2 + \Delta R$ then the slip will simply be zero. But the idea is that one assumes no error in radii of the wheels. Equation C.26 can be reduced to:

$$\Delta_c S = \frac{2 \Delta_c R}{2 R_2 + \Delta_c R} \approx \frac{\Delta_c R}{R_2} \quad (C.27)$$

In a similar fashion, one gets the same formula when instead a change in R_1 occurs.

C.3.2 Friction force error due to brake pad-center to wheel distance error

When looking at a certain change in a parameter value and examine the change in CoF (note, the expected static weight F_z has been used to estimate F_N):

$$\Delta_c \mu = \mu_2 - \mu_1 = \frac{F_{f2}}{F_{Z2}} - \frac{F_{f1}}{F_{Z1}} \quad (C.28)$$

Now, look only at the change in friction force (assume constant F_z) due to a change in distance between brake pad and center wheel (i.e., a certain value of 'c' has been determined, but the actual value is $\Delta_c c$ off):

$$F_{f1} = \frac{c}{R} F_R; \quad F_{f2} = \frac{c + \Delta_c c}{R} F_R; \quad \Delta_c \mu = \frac{F_{f2} - F_{f1}}{F_z} \quad (C.29)$$

This would lead to a change in CoF in the following way:

$$\Delta \mu = \frac{\frac{c}{R} F_R + \frac{\Delta_c c}{R} F_R - \frac{c}{R} F_R}{F_z} = \frac{\frac{\Delta_c c}{R} F_R}{F_z} \quad (C.30)$$

If no brake force is applied, then the absolute change in CoF is zero as well. At higher brake forces, the change in CoF becomes larger as well. One may look at the relative change in CoF due to the 'c' error:

$$\mu = \frac{\frac{c}{R} F_R}{F_z}; \quad \frac{\Delta_c \mu}{\mu} = \frac{\Delta_c c}{c} \quad (C.31)$$

Suppose $c=0.22m$ and $\Delta c=-0.02m$, then the error in CoF is roughly -9% (e.g., the actual $\mu=0.2$, but one measures a CoF of 0.18).

C.3.3 Normal force error due to expected static normal force error

Again, looking at two scenarios of the WRI, but now look only at the change in expected static normal force F_z (and keep F_f fixed).

$$F_{Z1} = F_z; \quad F_{Z2} = F_z + \Delta_c F_z; \quad \Delta_c \mu = \frac{F_f}{F_{Z1}} - \frac{F_f}{F_{Z2}} = \frac{F_f (F_{Z1} - F_{Z2})}{F_{Z1} F_{Z2}} \quad (C.32)$$

This would lead to a change in CoF in the following way:

$$\Delta_c \mu = -\frac{F_f \Delta_c F_z}{F_z^2 + F_z \Delta_c F_z} = -\mu \frac{\Delta_c F_z}{F_z + \Delta_c F_z} \quad (C.33)$$

If no friction force is present within the WRI ($\mu=0$), then the change in expected normal force would not lead to a certain change in CoF.

$$\frac{\Delta\mu}{\mu} = -\frac{\Delta F_Z}{F_Z + \Delta F_Z} \quad (C.34)$$

Suppose $F_Z=109$ kN and the measured CoF is 0.2 (thus the measured $F_f=21.8$ kN). If the expected normal force error is $\Delta F_Z=-10.9$ kN (negative, thus the actual normal force is 98.1 kN), then the error in CoF is 11% (the actual CoF is 0.222). If the error were to be $\Delta F_Z=10.9$ kN (positive, thus the actual normal force is 119.9 kN), then the error in CoF is -9% (the actual CoF is 0.182).

Appendix D – VI-Rail simulations

D.1 change in rolling radii

Slip is estimated by the TTBM in the following way:

$$S = \frac{2 \cdot (\omega_1 R_1 - \omega_2 R_2)}{\omega_1 R_1 + \omega_2 R_2} \quad (D.1)$$

Assume that calibration is done perfectly and both wheelsets have the same nominal rolling radii ($R_1=R_2=R_0$, for simplicity it will be denoted here as R). Now Suppose, due to track irregularities etc., the actual rolling radii of both the leading and trailing wheelsets changes by ΔR_1 and ΔR_2 , respectively:

$$\Delta R_1 = R_1 - R; \quad \Delta R_2 = R_2 - R; \quad \Delta R = \Delta R_2 - \Delta R_1 \quad (D.2)$$

One uses a fixed value for radius in the slip estimation formula, but the rotational velocities of the wheelsets change due to a small change in actual rolling radii. Note that the train speed remains the same, the circumferential velocity is equal for both wheelsets and will be denoted as V :

$$\omega_1 = \frac{V}{R_1} = \frac{V}{R + \Delta R_1}; \quad \omega_2 = \frac{V}{R_2} = \frac{V}{R + \Delta R_2} \quad (D.3)$$

Substituting this into the slip equation and using $R_1=R_2=R$ gives:

$$\begin{aligned} \Delta S &= \frac{2 \cdot \left(\frac{1}{R + \Delta R_1} - \frac{1}{R + \Delta R_2} \right)}{\frac{1}{R + \Delta R_1} + \frac{1}{R + \Delta R_2}} \\ \Delta S &= \frac{2 \cdot (R + \Delta R_2 - R - \Delta R_1)}{R + \Delta R_2 + R + \Delta R_1} \\ \Delta S &= \frac{2 \cdot (\Delta R_2 - \Delta R_1)}{2R + \Delta R_1 + \Delta R_2} \\ \Delta S &= \frac{2 \cdot \Delta R}{2R + \Delta R_1 + \Delta R_2} \end{aligned} \quad (D.4)$$

In the denominator, the second and third term are small compared to the first one, hence one can use the following approximation for the slip error (use R_0 again instead of R):

$$\Delta S = \frac{\Delta R}{R_0} \quad (\text{D.5})$$

D.2 VI-Rail simulations

D.2.1 F_N variations

D.2.1.1 TTBM brake

The variation in normal force induced by the TTBM brake itself can be found by looking at the free body diagram (FBD) of the TTBM bogie, as shown in figure D-1. The axle pots are left out, since it would make the deviation cumbersome and if one would include them, the same result is obtained as well.

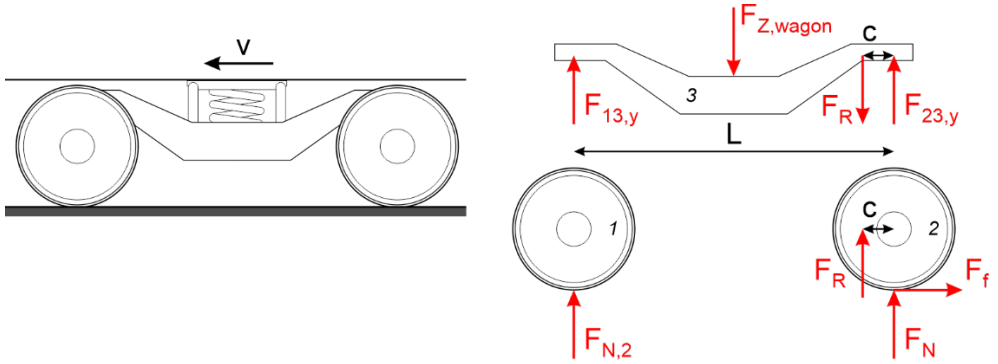


Figure D-1. FBD of the TTBM bogie. Note, some (reaction) forces are not shown for clarity.

Now if one looks at the moment equilibrium equation of body 3, and solve for $F_{23,y}$, one would get:

$$F_{23,y} = \frac{L-c}{L} F_R + \frac{1}{2} F_{Z,wagon} + \frac{1}{2} F_{Z,bogie} \quad (D.6)$$

Looking at the force equilibrium equation in vertical direction of body 2, use $F_Z = \frac{1}{2} F_{Z,wagon} + \frac{1}{2} F_{Z,bogie} + F_{Z,wheelset}$ and solve for F_N :

$$F_N = \frac{L-c}{L} F_R - F_R + F_Z = -\frac{c}{L} F_R + F_Z \quad (D.7)$$

Use $F_R = \frac{R}{c} \mu_{max} F_N$ (note, use here F_Z instead of F_N , which will give a good approximation) and $\Delta F_N = F_N - F_Z$. One could then find the change in normal force due to the TTBM brake as:

$$F_N = \left(1 - \frac{R}{L} \mu_{max}\right) F_Z; \quad \Delta F_N = -\frac{R}{c} \mu_{max} F_Z; \quad \frac{\Delta F_N}{F_Z} = -\frac{R}{c} \mu_{max} \quad (D.8)$$

Now one can find the change in normal force ($R=0.46\text{m}$, $c=0.22\text{m}$, $\mu_{max}=0.2$) roughly to be -3.5%. This corresponds to the simulation in section 5.2, however a -5% normal force error was found, leading to a roughly -5% error in estimating the CoF (i.e. at $\mu=0.2$, then $\Delta\mu=0.01$). Note, if the drive direction would be reversed, then

the brake force in figure D-1 would be flipped as well, leading to an increase in normal force.

D.2.1.2 Vertical track irregularities

Vertical sine simulations have been carried out for multiple wavelengths at different train speeds, which corresponds to the simulations carried out in section 5.4. The results are shown in figure D-2. Although the short wave vertical track irregularity might lead to the highest sudden change in normal force, at higher train speeds the change in normal force does not increase further. At higher train speeds, one should take roughly 10% change in normal force into account. Note, the variation in normal force can be both positive and negative, depending on when traversing the valley or peak of the track irregularity.

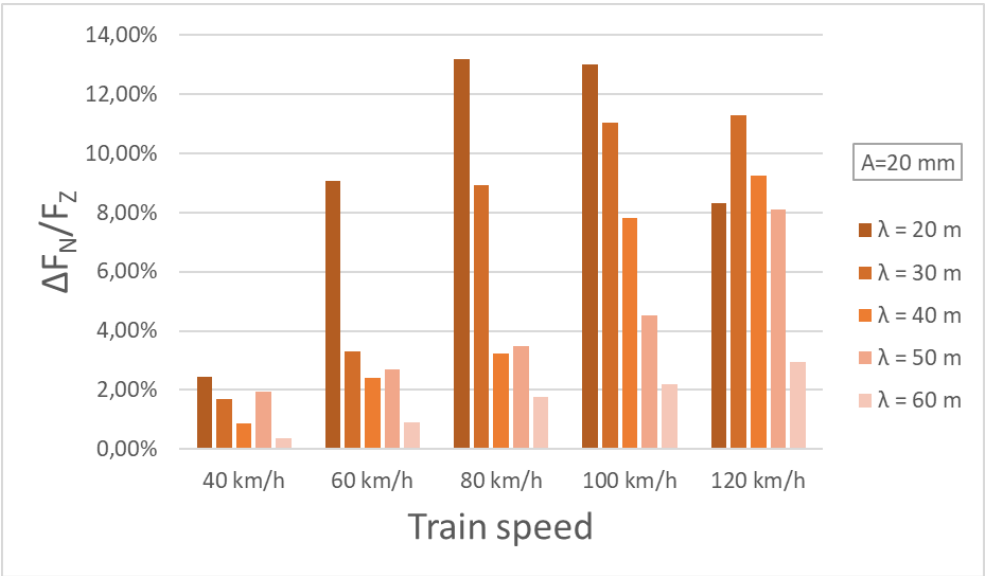


Figure D-2. A periodically vertical track irregularity with wavelength λ and amplitude $A = 20$ mm.

D.2.1.3 Normal force variation between two bogies and their wheelsets during train acceleration

The variations in normal forces among the four wheelsets of the CTO when accelerating are shown in figure D-3. N_1 and N_2 are the normal forces of the leading and trailing wheelset in the leading bogie and N_3 and N_4 of the leading and trailing wheelset of the trailing bogie. The mean normal force of the wheelsets in the leading and trailing bogies are denoted as N_{12} and N_{34} , respectively.

Two variations in normal force distribution among the wheelsets are recognizable. The wheelsets in the leading bogie experience a higher normal force than the ones in the trailing bogie, the difference is shown as ΔN_0 in figure D-3. In this case, it is roughly 0.7 kN (roughly 1.5%). This is due to the difference in suspension stiffness in the LOC and CTO. This may not be large, but in this scenario, all wheelsets have the same diameter. If those were not equal, then the normal force distribution among the wheelsets become more unbalanced as well (too large difference in wheel diameter among the wheelsets is not allowed within a train). Shunting of trains or varying train combinations with different wheel diameters and suspensions will add an additional uncertainty in the normal force estimation.

The second effect is when the train is accelerating. Within the simulation, the available friction is $\mu=0.25$. Due to the lift motion (or when decelerating, dive motion) of the bodies, the force distribution among the wheelsets changes. There is a difference in normal force between the wheelset and the mean wheelset normal force of a bogie, denoted as ΔN_1 (for simplicity, for all wheelsets roughly the same) in figure D-3, which is roughly 0.7 kN. The difference between the mean normal force in the leading and trailing bogie is shown as ΔN_2 .

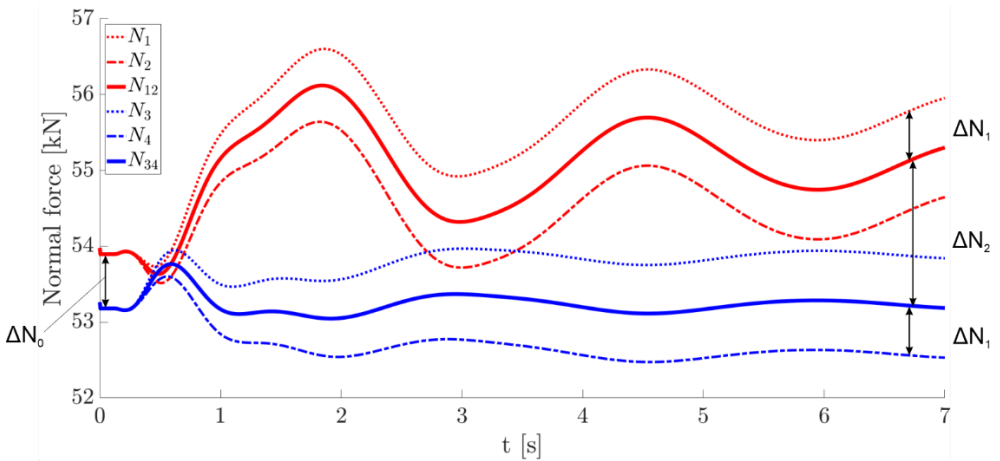


Figure D-3. Normal forces among the wheelsets of the CTO when the driven wheelsets are driven of the LOC, $a=1.45 \text{ m/s}^2$.

In most simulations in chapter 5, the TTBM wheelset is the trailing wheelset within the trailing bogie. In the scenario in figure D-3, this means roughly 1.5% change in normal force (compared to the expected normal force), which is not large. However if the drive direction is reverted and the TTBM wheelset becomes the leading

wheelset within the leading bogie, a larger normal force variation occurs, roughly 4.7%.

De- and acceleration of the LOC causes a change in normal force distribution among its wheelsets, the towbar height plays a role as well, more can be found in [41]. Note that the values found here are only for a certain train combination, one may find different values for different train combinations.

D.2.2 Additional VI-Rail simulation results of chapter 5

D.2.2.1 Straight track with lateral shift

The normal forces among the left and right wheel of the TTBM wheelset, when negotiating a periodical lateral shift track irregularity on straight track, are shown in figure D-4. This result corresponds to the simulation carried out in section 5.3.2.

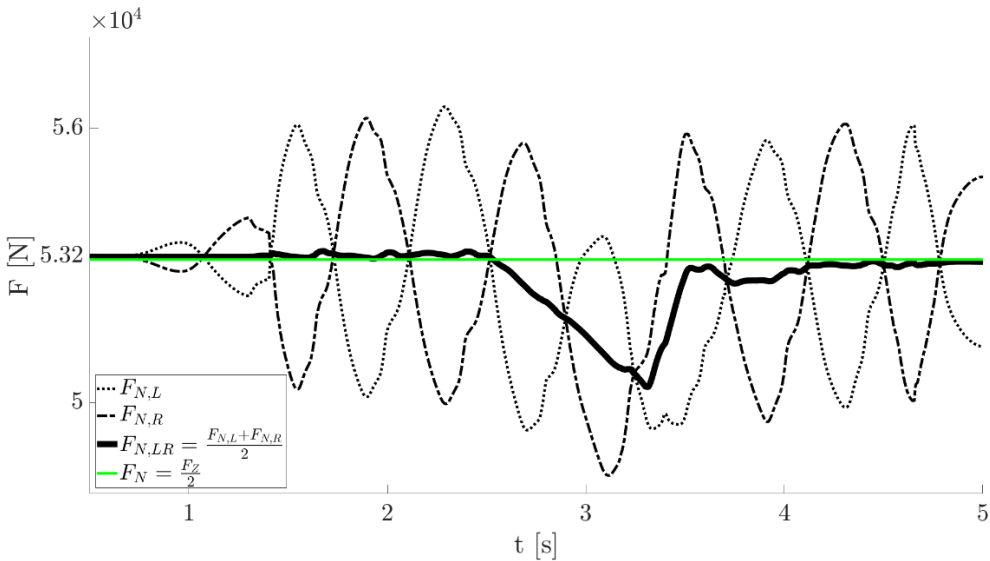


Figure D-4. Normal force of the left and right wheel, $F_{N,L}$ and $F_{N,R}$ respectively, when traversing the lateral shift irregularity and its mean value $F_{N,LR}$ over time.

D.2.2.2 Cant on straight track

The longitudinal slip within the left and right WRI of the TTB wheelset, when negotiating a periodical lateral shift track irregularity on straight track, are shown in figure D-5. This result corresponds to the simulation carried out in section 5.3.3.

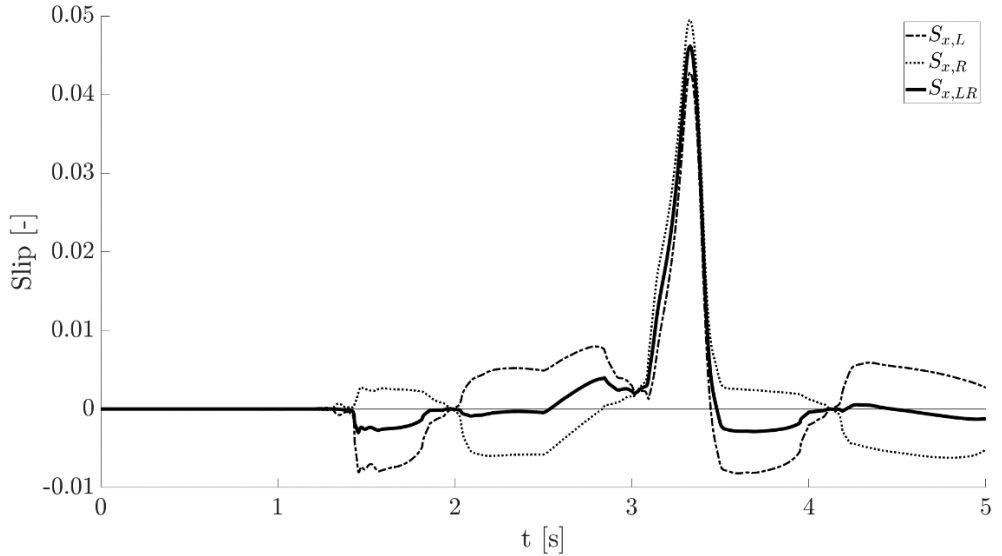


Figure D-5. Slip within the left and right wheel of the TTB wheelset and its mean value $S_{x,LR}$, when traversing the cant irregularity.

D.2.2.3 TTBM brake during curve negotiation

The AoA within the leading and trailing wheelset, AoA_1 and AoA_2 respectively, of the TTBM bogie (the trailing bogie of the CTO), when negotiating a curve with $R_{curve}=190m$ and $R_{curve}=2000m$, are shown in figure D-6. This result corresponds to the simulation carried out in section 5.5.3.

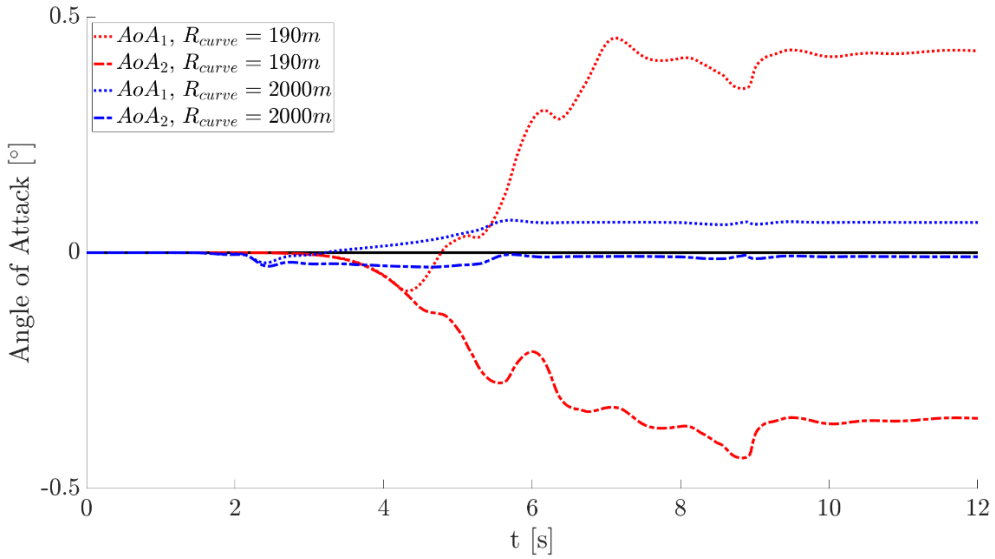


Figure D-6. The AoA of the leading and trailing wheelset within the TTBM bogie, corresponding to two curve negotiation simulations.

D.2.3 Slip estimation by train speed and braked-wheelset only

The initial TTBM concept measures the rotational velocities of both the braked and non-braked wheelset during a TTBM brake. Instead of measuring the non-braked wheelset rotational velocity (ω_1) to estimate the longitudinal velocity of the braked wheelset (the actual v_1), one may use instead the train speed (v_{train}) to estimate v_1 or use just before the TTBM brake the braked wheelset rotational velocity (ω_2) information to estimate v_1 .

The straight track with lateral track irregularity (shift) is considered from section 5.3.2. The TTBM brake was carried out between 2.5 s and 3.5 s. As can be seen, both other options, v_{train} and ω_2 , or not necessarily more accurate than the initial concept, i.e. ω_1 . The train speed is determined by the wagon speed, but due to the suspension between the wagon and wheelset, a certain lag exists. As for using the braked wheelset measurement only (ω_2), during the TTBM brake, the wheelset and the train decelerates and its longitudinal velocity drops slightly, which is not captured.

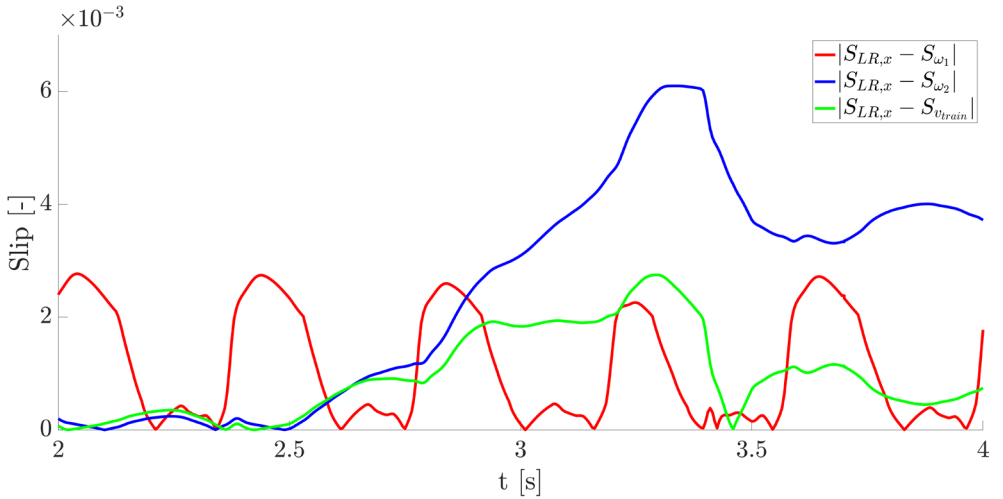


Figure D-7. Slip estimation by different V_1 estimations. Using the non-braked wheelset (the initial concept, S_{ω_1}), by using the braked wheelset only (S_{ω_2}) and by using the train speed ($S_{v_{\text{train}}}$).

Appendix E - Twin disc tests

The Surface Technology and Tribology (STT) group at the University of Twente features multiple twin disc machines. One of them can apply a brake torque on one disc while the other wheel is motorized and its rotational velocity is regulated, even when a brake torque is applied. This twin disc machine is shown in figure E-1 and explained in full detail in [45]. The two stainless steel discs are shown in figure E-2, in which a line contact is realised with a width of 4 mm (b in Table E-1).

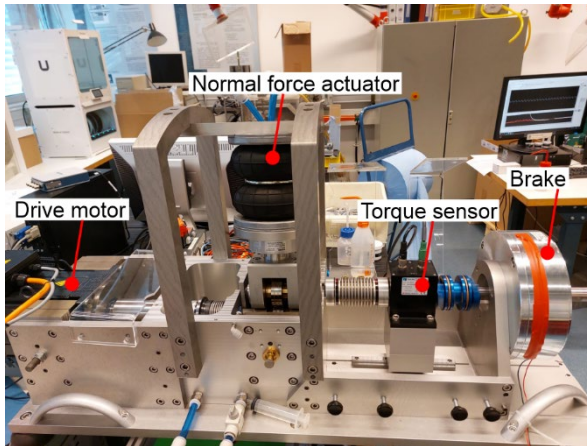


Figure E-1. Twin disc setup.

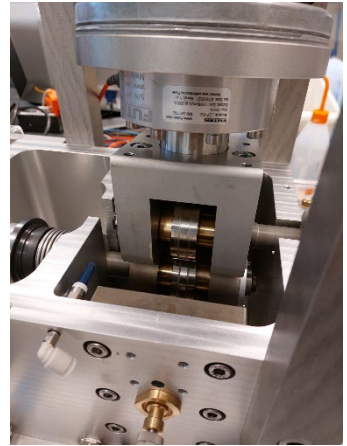


Figure E-2. Close-up of the two discs in the twin disc machine.

The drive motor drives the lower disc, the upper disc is pressed onto the lower disc by the normal force actuator (also measured) and rotates as well when the lower disc is set at a certain rotational speed. The brake torque is applied on the upper disc by the hysteresis brake, the brake torque is measured by the sensor and thus one can determine the friction force. Both the driven motor and the torque sensor are equipped with an encoder, to measure the rotational speed and thus to measure the slip.

Two tests were carried out under the conditions stated in Table E-1, the first test with a dry contact and the other test with oil within the contact (third body). The traction curve results are shown in figure E-3. The goal is to show how the traction curve changes when a bit of oil is present in the rolling contact (i.e., the difference between 'dry' and 'third body' conditions).

R_1	R_2	b	RPM	V_1	F_N	P_{\max}
27 mm	27 mm	4 mm	400	1.1 m/s	1.5 kN	1 GPa

Table E-1. Parameters of the twin disc machine corresponding to the tests in figure E-3. Note, v_1 is the circumferential velocity of the lower disc and P_{\max} is the maximum pressure according to Hertzian line contact theory.

Figure E-3 shows the raw measured data. The brake torque is slowly applied by increasing it stepwise, hence the clusters of datapoints. Compared to the dry case, when oil is applied a decrease in peak CoF is found. Also, the creep coefficient (the slope of the traction curve around $S=0$) is lower as well.

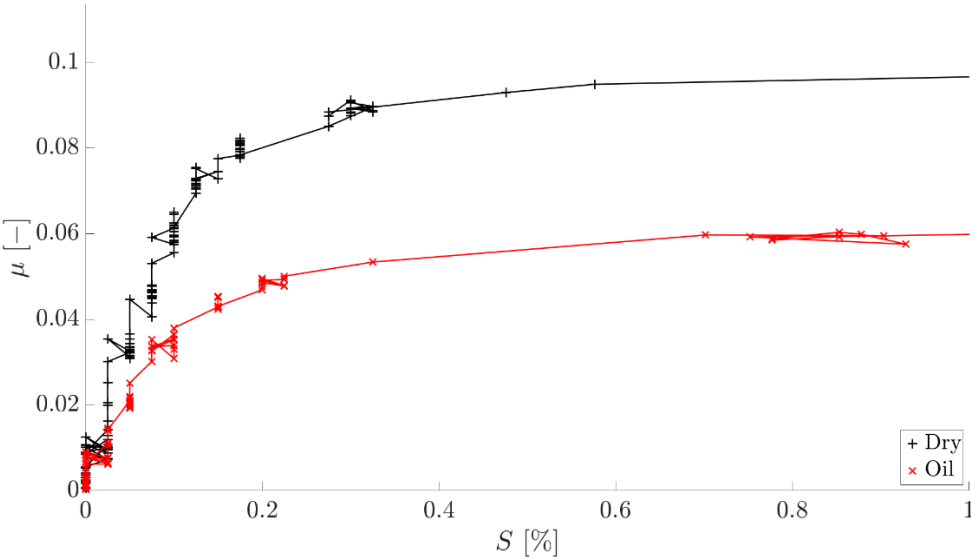


Figure E-3. Traction curves under dry conditions and when oil is applied to the two discs.

Appendix F – Traction curves

F.1 Third body traction curves

The following function has been used to describe the friction coefficient within the wheel-rail contact as function of slip:

$$\mu = c_1 \cdot \exp\left(-\frac{[\ln(S) - c_2]^2}{c_3}\right) \quad (\text{F.1})$$

The fit parameters c_1 , c_2 and c_3 are based on the results of the measurements conducted in [11] and are shown in Table F-1. The corresponding five traction curve classes are shown in figure 23.

Parameter	High 1	High 2	High 3	Medium	Low
c_1	0.37	0.30	0.18	0.11	0.065
c_2	0.98	1.03	1.28	1.05	0.83
c_3	7.58	4.98	6.19	5.94	5.16

Table F-1. The fit parameters corresponding to equation F.1 [11]

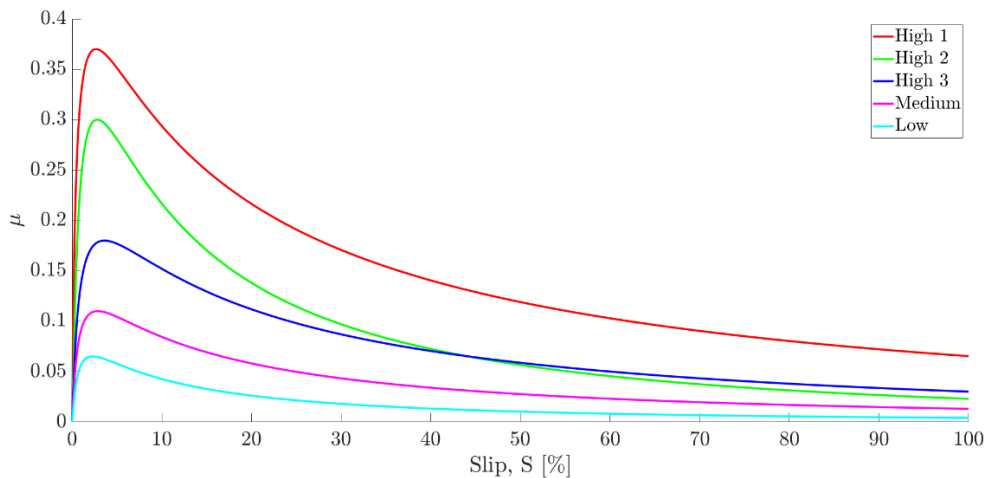


Figure F-1: The five traction curve classes [11].

F.2 Dry traction curves

The CONTACT programme can handle lateral slip and spin as well, besides longitudinal slip. However, if one only looks at longitudinal slip, the results are similar as of the Carter curve shown in equation 3.6, figure F-2 shows both results.

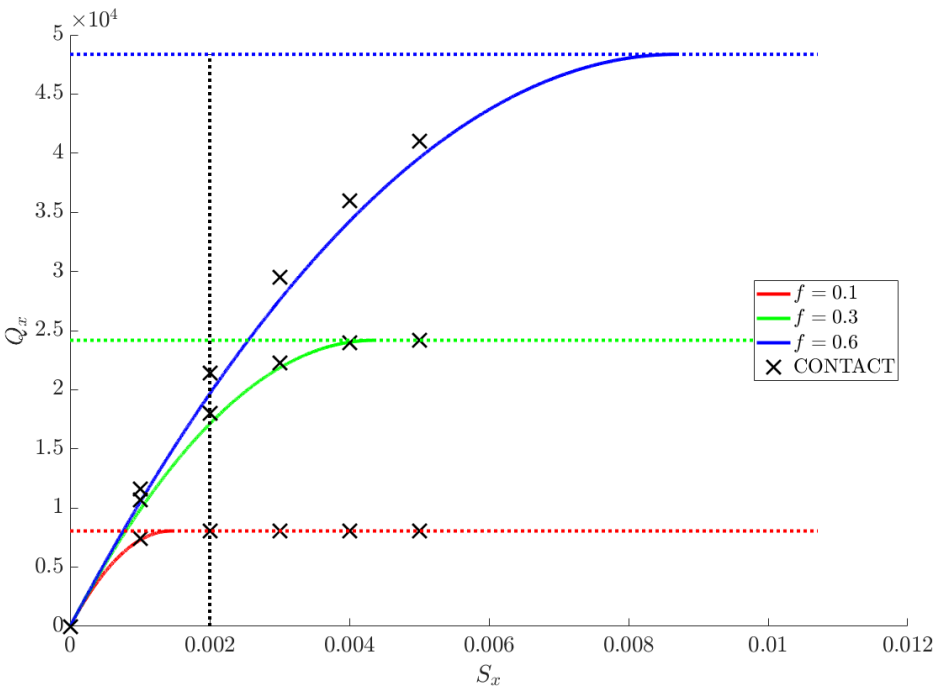


Figure F-2. Carter theory compared with CONTACT.

F.3 Different traction curve output under same friction conditions

In VI-Rail, three simulations of the TTBM brake test are carried out on a perfect straight track, only the track gauge is varied. The measured traction curves are shown in figure F-2.

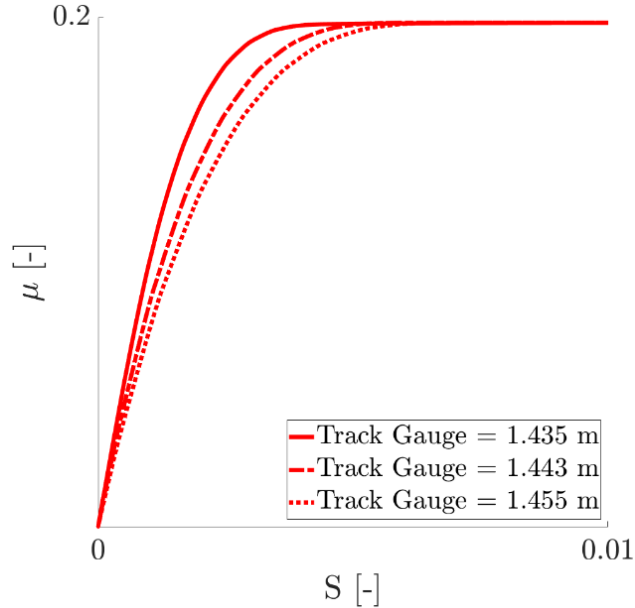


Figure F-3. Three simulated TTBM traction curves using three different track gauges.

One can see that the shape of the traction curve changes, even under the same friction conditions, only the track gauge has been changed. The creep coefficient and the slip value when full slip is reached is different.

The creep coefficient of the traction around $S=0$ of the Carter theory (note, 2D theory) is stated as [29]:

$$S_x = \frac{aF_f}{2RF_N} = \frac{a}{2R}\mu$$

The semi-axis a of the contact patch influences the creep coefficient. The size of the contact patch and the conicity of the three simulations in figure F-2 are different, as can be seen in Table F-2 which probably influence the traction curve behaviour within the WRI.

Simulation	Track Gauge [m]	a, b [mm]	γ [°]
1	1.435	5.7 , 8.2	2.87
2	1.443	5.6 , 5.7	0.72
3	1.455	5.9 , 4.3	0.61

Table F-2. Contact path sizes and conicity of the wheel corresponding to the simulations in figure F-3.

References

- [1] ProRail, “Jaarverslag 2021,” 2021.
<https://www.jaarverslagprorail.nl/jaarverslag-2021/profiel/organisatie-en-activiteiten> (accessed Jun. 17, 2022).
- [2] ProRail, “ERTMS: het digitale spoorplatform.”
<https://www.prorail.nl/programmas/ertms> (accessed May 25, 2022).
- [3] Treinreiziger, “NS kampt met personeelstekort,” 2022.
<https://www.treinreiziger.nl/ns-kampt-met-personeelstekort-treinen-vallen-uit/> (accessed May 25, 2022).
- [4] ProRail, “Automatisch bestuurdde treinen.”
<https://www.prorail.nl/toekomst/innoveren/automatisch-bestuurde-treinen> (accessed May 25, 2022).
- [5] ProRail, “Herfst in de ochtend,” 2015.
<https://www.prorail.nl/nieuws/herfst-in-de-ochtend> (accessed May 25, 2022).
- [6] ProRail, “Anti glijmiddel tegen doorslippen,” 2017.
<https://www.prorail.nl/nieuws/anti-glijmiddel-tegen-doorslippen> (accessed May 25, 2022).
- [7] A.F. Bower and K.L. Johnson, “Plastic flow and shakedown of the rail surface in repeated wheel-rail contact,” *Wear*, vol. 144, no. 1–2, pp. 1–18, Apr. 1991, doi: 10.1016/0043-1648(91)90003-D.
- [8] EN 15595, “Railway applications - Braking - Wheel slide protection,” 2018.
- [9] N.H. van Steenis, “Monitoring train performance in case of low adhesion,” PhD thesis, University of Twente, Enschede, The Netherlands, 2010. doi: 10.3990/1.9789036530125.
- [10] H. Harrison, T. McCanney, and J. Cotter, “Recent developments in coefficient of friction measurements at the rail/wheel interface,” *Wear*, vol. 253, no. 1, pp. 114–123, 2002, doi: [https://doi.org/10.1016/S0043-1648\(02\)00090-X](https://doi.org/10.1016/S0043-1648(02)00090-X).
- [11] R.I. Popovici, “Friction in wheel-rail contacts,” PhD thesis, University of Twente, Enschede, The Netherlands, 2010.

- [12] S.R. Lewis, R. Lewis, J. Cotter, X. Lu, and D.T. Eadie, "A new method for the assessment of traction enhancers and the generation of organic layers in a twin-disc machine," *Wear*, vol. 366–367, pp. 258–267, 2016, doi: <https://doi.org/10.1016/j.wear.2016.04.030>.
- [13] SpoorPro, "Thales demonstreert assentelsysteem voor ERTMS," May 26, 2022. <https://www.spoorpro.nl/partnerverhaal/2022/05/26/thales-demonstreert-assentelsysteem-voor-ertms/> (accessed Jun. 07, 2022).
- [14] Minister van Verkeer en Waterstaat, "Regeling spoorverkeer," 2020. <https://wetten.overheid.nl/BWBR0017707/2020-04-01#Hoofdstuk2> (accessed Jun. 07, 2022).
- [15] NEN-EN 16834, "Railway applications-Braking-Brake performance." Apr. 2019.
- [16] R. Lewis and R.S. Dwyer-Joyce, "Wheel-rail wear and surface damage caused by adhesion sanding," *Tribology Series*, vol. 43, pp. 731–741, Jan. 2003, doi: 10.1016/S0167-8922(03)80101-3.
- [17] ProRail, "Herfst," 2019. <https://www.prorail.nl/reizen/het-weer/herfst> (accessed Jun. 08, 2022).
- [18] A. van Beek, *Advanced Engineering Design - Lifetime performance and reliability*, Sixth. Delft: Delft University of Technology, 2015.
- [19] W.R. Tyfour, J.H. Beynon, and A. Kapoor, "Deterioration of rolling contact fatigue life of pearlitic rail steel due to dry-wet rolling-sliding line contact," *Wear*, vol. 197, no. 1–2, pp. 255–265, Sep. 1996, doi: 10.1016/0043-1648(96)06978-5.
- [20] A.F. Bower, "The Influence of Crack Face Friction and Trapped Fluid on Surface Initiated Rolling Contact Fatigue Cracks," *J Tribol*, vol. 110, no. 4, pp. 704–711, 1988.
- [21] ProRail, "Spooronderhoud," 2019. <https://www.prorail.nl/over-ons/wat-doet-prorail/spooronderhoud> (accessed Jun. 15, 2022).
- [22] DANOBAT, "Railway wheelset turning | DANOBAT DPL Lathe," Apr. 2019. <https://www.youtube.com/watch?v=H4eEjo-tKXs> (accessed Jun. 08, 2022).

- [23] Anne-Fleur Pel, "Die rotblaadjes op het spoor; waarom doen ze niets?," 2016. Accessed: Jun. 08, 2022. [Online]. Available: <https://www.metronieuws.nl/in-het-nieuws/2016/11/die-rot-blaadjes-op-het-spoor-waarom-doen-ze-niets/>
- [24] NASA, *NASA Systems Engineering Handbook*. Washington D.C., 2007. [Online]. Available: www.sti.nasa.gov
- [25] Europe's Rail, "Europe's Rail JU Members," 2022. <https://rail-research.europa.eu/about-europes-rail/europes-rail-ju-members/> (accessed Jun. 07, 2022).
- [26] "NEN-EN 15595: Railway applications-Braking-Wheel slide protection," 2018.
- [27] "NEN-EN 12299: Railway applications-Ride comfort for passengers-Measurement and evaluation," 2009.
- [28] "NEN-ISO 2631-1: Mechanische trillingen en schokken-Beoordeling van de invloed van trillingen op het menselijk lichaam-Deel 1: Algemene eisen," 1997.
- [29] K.L. Johnson, *Contact Mechanics*. Cambridge: Cambridge University Press, 1985.
- [30] VI-Grade, "VI-Rail 16.0 Documentation," Marburg, Germany, 2014.
- [31] H. Hertz, "Über die Berührung fester elastischer Körper (On the contact of elastic solids)," *Journal für die reine und angewandte Mathematik*, vol. 92, pp. 156–171, 1882.
- [32] M. Shahzamanian Sichani, "On Efficient Modelling of Wheel-Rail Contact in Vehicle Dynamics Simulation," 2016.
- [33] J.J. Kalker, "On the rolling contact of two elastic bodies in the presence of dry friction," PhD thesis, Delft University of Technology, Delft, The Netherlands, 1967.
- [34] F.W. Carter, "On the action of a locomotive driving wheel," *Proceedings of the Royal Society of London. Series A, Containing Papers of a Mathematical and Physical Character*, vol. 112, no. 760, pp. 151–157, 1926, doi: 10.1098/rspa.1926.0100.

- [35] A.E.W. Hobbs, "A survey of creep," *British Railway Department. DYN 52, Derby*, 1967.
- [36] O. Polach, "Creep forces in simulations of traction vehicles running on adhesion limit," *Wear*, vol. 258, no. 7, pp. 992–1000, 2005, doi: <https://doi.org/10.1016/j.wear.2004.03.046>.
- [37] "A survey of wheel/Rail Friction," Washington, DC, 2017. Accessed: Jun. 18, 2022. [Online]. Available: https://railroads.dot.gov/sites/fra.dot.gov/files/fra_net/17468/A%20Survey%20of%20Wheel-Rail%20Friction.pdf
- [38] E.R.M. Gelinck, *Mixed Lubrication of Line Contacts*, PhD thesis. Enschede, The Netherlands: University of Twente, 1999.
- [39] T.M. Beagley, "The rheological properties of solid rail contaminants and their effect on wheel/rail adhesion," *Proc. Inst. Mech. Eng.*, vol. 190, no. 1, pp. 419–428, 1976.
- [40] J.J. Kalker, "A Fast Algorithm for the Simplified Theory of Rolling Contact," *Vehicle System Dynamics*, vol. 11, no. 1, 1982, doi: 10.1080/00423118208968684.
- [41] C.P.; Keizer and P.K. Wiersma, *Railvoertuigtechniek*. Delft, The Netherlands: TU Delft, 1997.
- [42] ProRail, "Instandhoudingsspecificatie Spoor, Deel 1: Onderhoudswaarden, Interventiewaarden, Onmiddellijke actiewaarden," Utrecht, The Netherlands, 2021.
- [43] ProRail, "Ontwerpvoorschrift: Baan en Bovenbouw Deel 4.1 Alignement," Utrecht, The Netherlands, 2020.
- [44] A.; Nunez, A.; Hendriks, J.; Moraal, J. Ramirez Fonseca, I.; Dollevoet, and R.; Li, "Rail Condition Monitoring using Axle Box Acceleration Measurements: Defect detection in the Netherlands and Romania," 2018.
- [45] P.J. Amoroso Feijoo, "Tribological testing of CAM-roller follower systems: Design of the CRT-01," University of Twente, Netherlands, 2021.